



UNIVERSITÀ DEGLI STUDI DI PADOVA

Dipartimento di Fisica e Astronomia “Galileo Galilei”

Master Degree in Physics

Final Dissertation

How large can the light quark Yukawa couplings be?

Thesis supervisor

Prof. Ramona Gröber

Thesis co-supervisor

Dr. Nudžeim Selimović

Candidate

Barbara Anna Erdelyi

Academic Year 2023/2024

Abstract

The light quark Yukawa couplings are notoriously difficult to measure at the LHC. Current bounds and future projections for the HL-LHC (High-Luminosity Large Hadron Collider) foresee that the first generation couplings can be constrained to be a factor of several hundred times their Standard Model value.

This thesis aims at responding to the question on how large they actually can be in UV models. UV models that generate deviations in light quark Yukawa couplings via dimension-six effective operators at the tree level will be identified. A particularly good choice not studied yet in depth in literature is models with vector-like quarks.

The list of possible models is finite and can hence be studied systematically, taking into account potential bounds from direct searches, flavour physics, Higgs physics and electroweak precision tests.



Contents

1	Introduction	1
2	The Standard Model of Particle Physics	5
2.1	Gauge Group	5
2.2	Particle Content	6
2.3	The Lagrangian	7
2.4	Symmetry Breaking	8
2.4.1	Gauge and Higgs bosons masses	9
2.4.2	Fermion masses	10
2.4.3	Fermion interaction with the gauge bosons	10
2.4.4	CKM matrix	10
3	Effective Field Theories	13
3.1	Effective Theories	13
3.2	Effective Field Theories	14
3.2.1	Standard Model Effective Field Theory	15
4	Identifying the New Physics Model	19
4.1	SMEFT Operators	20
4.2	NP Model Choice	21
4.2.1	Motivation for the use of vector-like quarks	23
4.2.2	Lagrangian description	23
5	Matching	25
5.1	Model 1: $Q_1 + U$	26
5.1.1	$\phi^4 D^2$ class operators	27
5.1.2	$X^2 \phi^2$ class operators	32
5.1.2.1	Operator $\mathcal{O}_{\phi G}$	34
5.1.2.2	Operator $\mathcal{O}_{\phi B}$	36
5.1.2.3	Operator $\mathcal{O}_{\phi WB}$	37
5.1.2.4	Operator $\mathcal{O}_{\phi W}$	38
5.2	Model 2: $Q_1 + D$	39
5.3	Model 3: $Q_7 + U$	40
5.4	Model 4: $Q_5 + D$	41
5.5	Model 5: $Q_1 + T_1$	42
5.6	Model 6: $Q_5 + T_1$	43
5.7	Model 7: $Q_1 + T_2$	44

5.8	Model 8: $Q_7 + T_2$	45
6	Experimental Tests	47
6.1	ElectroWeak Physics	48
6.1.1	W^\pm and Z boson coupling to quarks	48
6.1.2	Application to Model 1	50
6.2	Higgs Fit	51
6.2.1	Modified Higgs production cross-section	52
6.2.2	Modified Higgs total width and branching ratios	53
6.2.3	Application to Model 1	53
6.3	Combined Fit	54
6.3.1	Models without Q_1	55
6.3.2	Models involving Q_1	56
6.4	Application to the Second Generation	58
7	Direct Searches	63
7.1	ATLAS Search	64
7.2	Decays in Model 1	64
7.2.1	Gauge and Higgs sector before and after Spontaneous Symmetry Breaking	64
7.2.2	Perturbative diagonalisation of the Mass matrices	65
7.2.3	Effects of the rotation on the interactions	66
7.2.4	Decay widths and branching ratios	66
7.3	Generalisation to all models	67
7.3.1	Generalised decay widths	69
8	Conclusions and Future Studies	73
A	Group Theory	75
A.1	Gell-Mann Matrices	75
A.2	Pauli Matrices	76
B	Triplet Interactions with the W^\pm and Z Bosons	77
C	Feynman Rules	79
C.1	VLQ Yukawa-like Interactions	79
C.2	Quark Interaction with the Gauge Bosons	81
C.3	$\psi^2\phi^2 D$ -class Operators	82
D	Flavour Physics	83
E	Additional Parameter Space Plots	85
F	Detector Schematics	91
G	Direct Searches	93
G.1	Model 1	93
G.2	Generalisation to all models	95
G.2.1	Generalised initial Lagrangian	95
G.2.2	Rotation to mass basis	96

G.2.3 After the rotation	98
H Bibliography	99

Chapter 1

Introduction

What we now call Higgs boson was first theorised in 1964 [1] in the context of developing a mechanism to describe how the massive Standard Model particles acquire their mass, since an explicit mass Lagrangian term would not be invariant under the Standard Model gauge group. Such mechanism is known as the Englert-Brout-Higgs mechanism [1–3], or simply the Higgs mechanism. Since then, the Higgs boson has been the object of extensive theoretical studies and experimental searches, which led to the particle’s detection in 2012 at the Large Hadron Collider (LHC) by ATLAS [4] and CMS [5]. This experimental success was not the end of the story: to date, several of the Higgs properties still have to be understood.

One of the areas still open to investigation concerns the interactions of the Higgs boson with the lighter generation fermions. Theoretically, the Higgs mechanism predicts that the couplings associated to such interactions, the Yukawa couplings y_f , are linearly proportional to the fermion masses. This has so far been confirmed [6–8] for the top quark, for the bottom quark and the tau lepton. For the top quark, the coupling is studied by measuring the rate with which the Higgs boson is produced in association with a top and anti-top pair, for the other two fermions, the decay rate of the the Higgs boson into $b\bar{b}$ and $\tau^+\tau^-$ pairs are respectively measured. Additional studies [9, 10] have also constrained the muon’s coupling to be in agreement with the Standard Model prediction, though these measurements currently have larger uncertainties than those of the third generation couplings. Figure 1.1 shows the associated Feynman diagrams for the processes previously mentioned.

Experimentally, the study of the lighter fermion couplings is complicated by the small size of their Yukawa couplings, thus suppressing their contributions to scattering processes involving the Higgs boson. Focusing on the deviations from the Standard Model predictions for the couplings, parameterised by the ratio $\kappa_f = y_f/y_f^{SM}$, it is of theoretical interest to find upper bounds for these deviations and of experimental interest to develop ways to probe them. For the missing charged lepton, the electron, there have been proposals for the study of its coupling at the Future Circular

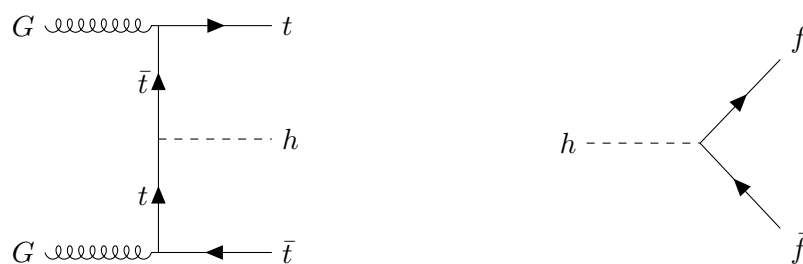


Figure 1.1: Feynman diagrams for the Higgs boson h production in association with a top and anti-top pair (left) and for the Higgs boson decays into fermions f (right). The gluons are denoted by the letter G . In both diagrams, the Higgs boson interacts with a fermion; the Yukawa coupling-dependence is picked up from those interaction vertices.

Second Generation		First Generation	
κ_c	< 1.2	κ_u	< 260
κ_s	< 13	κ_d	< 156
Source	[23]	Source	[25]

Table 1.1: Future projections for the values of the modifier κ_q for the first two quark generations for the High-Luminosity LHC (HL-LHC). These values will be used as comparison for the results found in this work; they will be referred to as "literature values".

electron-positron Collider (FCC-ee) [11]. For the strange and the first generation quarks, a further problem consists in the difficulty to tag them in the detectors.

There have been promising proposals for the charm quark's coupling: the associated production of the Higgs boson with a vector boson, with the Higgs then decaying into charm quark anti-quark pair, was studied by CMS [12] and ATLAS [13]. At a 95% Confidence Level, CMS found the charm quark coupling modifier to be bound by $1.1 < |\kappa_c| < 5.5$, while ATLAS reported $|\kappa_c| < 8.5$. Another proposal for the charm quark study is to consider the decays of the Higgs boson into vector mesons [14–16]. As for the other second generation quark, the strange, it has been suggested to perform strange tagging at the future electron-positron colliders [17].

As for the first generation quarks, many proposals have been made. Of these, three examples are Higgs pair production [18], Higgs plus jet production [19, 20] and Higgs plus photon associated production [21, 22]. The last one can also be applied to the second generation quarks; the CMS search [22] translated upper bounds, at a 95% Confidence Level, on the Higgs plus photon production cross-sections into constraints for the couplings modifiers, obtaining $|\kappa_u| \leq 16000$, $|\kappa_d| \leq 17000$, $|\kappa_s| \leq 1700$ and $|\kappa_c| \leq 190$.

Given that enhanced Yukawa couplings would lead to deviations of the Higgs boson decay branching ratios, global fits can be performed, finding the projections for the High Luminosity Large Hadron Collider (HL-LHC) $|\kappa_u| < 560$, $|\kappa_d| < 260$, $|\kappa_c| < 1.2$ and $|\kappa_s| < 13$ [23]. Furthermore, an enhancement of the first generation quark Yukawa couplings with respect to the Standard Model prediction would mean that Higgs boson production at hadron colliders receives a contribution directly from the parton constituents; this was taken into account, in the context of off-shell Higgs production, by [24, 25], with the latter obtaining projections for the HL-LHC of $|\kappa_u| < 260$ and $|\kappa_d| < 156$.

The aforementioned projected sensitivities (or for the charm quark bounds), are still quite loose. Therefore, it is of interest to consider how different New Physics models can give rise to enhanced Yukawa couplings. This thesis will hence address the question: *how large can the light quark Yukawa couplings be in concrete UV scenarios?*

In order to address this question, this thesis will focus on eight models involving pairs of heavy new particles called vector-like quarks. Even though such particles appear in several different extensions of the Standard Model, here they will be studied strictly within the context of modifications in the first and second-generation quark Yukawa couplings. Indeed, it will be shown that all these models generate, once the heavy quarks have been integrated out at the tree level, dimension-six effective operators that cause deviations in the light quark Yukawa couplings. The assumption that the vector-like quarks can only couple to one generation of Standard Model quarks at a time will be made.

The Standard Model Effective Field Theory will provide a model-independent framework to study deviations of experimental observables from the Standard Model predictions. For the models treated in this thesis, ElectroWeak and Higgs Physics observables will provide relevant constraints. Once the deviations have been studied in terms of the Effective Theory's coefficients, a matching condition between the specific New Physics model and the Effective Theory allows to recast the deviations in terms of the model's parameters, the vector-like quark masses and their Yukawa-like couplings to the Higgs boson. The resulting bounds on the parameter space can then be used to find the maximal value for the modifier κ_q compatible with the experimental results with a chosen confidence level. Finally, the results found will be compared to the reference values in Table 1.1.

The following Chapters are organised as follows:

- A brief review of the Standard Model of Particle Physics and of Effective Field Theories is presented in Chapters 2 and 3 respectively. These chapters will fix the notation used throughout the rest of the thesis;
- In Chapter 4 the Standard Model Effective Field Theory operators that cause deviations in the quark Yukawa couplings are first of all identified. Then, different New Physics models that can give rise to such operators are mentioned before selecting the eight models involving pairs of vector-like quarks;
- The matching between the Standard Model Effective Field Theory coefficients and the New Physics parameters is performed in Chapter 5. One model will be studied in detail in Section 5.1, while for the remaining seven only the main results will be presented;
- The comparison with experimental observables is performed in Chapter 6. Initially, the bounds from ElectroWeak Observables, Section 6.1, will be studied separately from those of Higgs Physics, Section 6.2. Then the two cases will be combined in Section 6.3;
- In Chapter 7 experimental searches for vector-like quarks at hadron colliders will be presented. In particular, the search performed by ATLAS [26] for pair-produced vector-like quarks with couplings only to the lighter quarks will be shown to provide a lower bound for the heavy mass scale;
- The conclusions are drawn and future outlooks are presented in Chapter 8.

Additionally, several Appendices are present. These serve the purpose of presenting material considered useful for the understanding of the topics being dealt with but that would disrupt the flow of the reading if inserted in the main text.

Chapter 2

The Standard Model of Particle Physics

The Standard Model of Particle Physics (abbreviated as SM) [27,28] currently provides the best description of particles and their strong and electroweak interactions.

The Standard Model is a quantum field theory; as such it is identified by:

1. a gauge group \mathcal{G} (Section 2.1);
2. the theory's particle content (Section 2.2);
3. a spontaneous symmetry breaking (SSB) pattern which leads to a new gauge group \mathcal{G}' (Section 2.4).

2.1 Gauge Group

The Standard Model is based on the (local) gauge symmetry \mathcal{G} , defined as

$$\mathcal{G} = \text{SU}(3)_c \times \text{SU}(2)_L \times \text{U}(1)_Y. \quad (2.1)$$

Each group is associated with one of the three fundamental forces described by the Standard Model. A summary of the Gauge Groups (containing the names of their couplings, the group generators, the name of the associated gauge bosons and the structure constants) is presented in Table 2.1. Relevant group theory information is reported in Appendix A.

Strong Interactions: associated with the $\text{SU}(3)$ gauge group. Such group has 8 generators $T^A = \frac{1}{2}\lambda^A$, where λ^A are the Gell-Mann matrices listed in Appendix A.1. The associated gauge boson is G_μ^A . The associated field strength tensor is defined as

$$G_{\mu\nu}^A = \partial_\mu G_\nu^A - \partial_\nu G_\mu^A + g_s f^{ABC} G_\mu^B G_\nu^C. \quad (2.2)$$

Strong interactions are described within Quantum Chromodynamics.

ElectroWeak Interactions: described by the $\text{SU}(2)_L \times \text{U}(1)_Y$ group. Treating the two subgroups individually,

Gauge group	Couplings	Group Generators	Gauge boson	multiplicity	Structure constant
$\text{SU}(3)_c$	g_S	$T^A = \frac{1}{2}\lambda^A$	G_μ^A	8	f^{ABC}
$\text{SU}(2)_L$	g_L	$\tau^J = \frac{1}{2}\sigma^J$	W_μ^J	3	ϵ^{JKL}
$\text{U}(1)_Y$	g_Y	$\mathbb{1}$	B_μ	1	0

Table 2.1: Gauge groups and corresponding bosons.

Field ψ	$q_{Lr} = \begin{pmatrix} u_{Lr} \\ d_{Lr} \end{pmatrix}$	$l_{Lr} = \begin{pmatrix} \nu_{Lr} \\ e_{Lr} \end{pmatrix}$	u_{Rr}	d_{Rr}	e_{Rr}
$SU(3)_c$	3	1	3	3	1
$SU(2)_L$	2	2	1	1	1
$U(1)_Y$	1/6	-1/2	2/3	-1/3	-1

Table 2.2: SM fermions with their charges under \mathcal{G} [29].

Gen.	u_r	d_r	e_r	ν_r
I ($r = 1$)	u	d	e	ν_e
II ($r = 2$)	c	s	μ	ν_μ
III ($r = 3$)	t	b	τ	ν_τ

Table 2.3: Fermion generations and compact notation.

- $SU(2)_L$ has as group generators $\tau^J = \frac{1}{2}\sigma^J$, where the Pauli matrices, σ^J , are defined in Appendix A.2. The gauge bosons associated with the group generators are W_μ^J , and the field strength tensor is

$$W_{\mu\nu}^J = \partial_\mu W_\nu^J - \partial_\nu W_\mu^J + g_L \epsilon^{JJK} W_\mu^J W_\nu^K; \quad (2.3)$$

- $U(1)_Y$ is an Abelian group. The associated gauge boson is B_μ , with field strength tensor

$$B_{\mu\nu} = \partial_\mu B_\nu - \partial_\nu B_\mu. \quad (2.4)$$

This sector is affected by the SSB mechanism $SU(2)_L \times U(1)_Y \rightarrow U(1)_{EM}$, though the details will be addressed in the corresponding section.

2.2 Particle Content

The particles described by the SM can be separated into two main categories based on their spin-statistics: fermions and bosons. Each category contains two subcategories: fermions are divided into quarks and leptons depending on whether they interact strongly or not, while bosons are separated into scalars and vectors depending on the value of their spin. In the following, each of these categories is described in more detail.

Fermions: these spin-1/2 particles are often called matter particles [30]. As mentioned, they can be either leptons or quarks. Their charges under the SM gauge group \mathcal{G} are presented in Table 2.2. Fermions are furthermore organised in three generations, which repetitively have the same charges under \mathcal{G} . This motivated the introduction of the compact notation in Table 2.3, the generations can be read horizontally and are labelled with the Roman numerals I, II, and III. Each generation consists of two quarks and two leptons; moving horizontally, the first-column particles all have an electric charge $+2/3$, the second-column particles have a charge $-1/3$, the third -1 , and finally the neutrinos are neutral. Except for the neutrinos (which are predicted to be massless by the SM), the fermions in the second generation are heavier than their first-generation counterparts and lighter than the third-generation.

Bosons: There are two types of bosons:

Scalars: only one SM particle falls into this category, the Higgs boson. In the unbroken phase, it is typically identified by the letter ϕ . It is a complex scalar doublet under $SU(2)_L$ with hypercharge $Y_\phi = \frac{1}{2}$. The Higgs field can be written in terms of four real scalar fields h_i as :

$$\phi(x) = \frac{1}{\sqrt{2}} \begin{pmatrix} ih_1(x) + h_2(x) \\ ih_3(x) + h_4(x) \end{pmatrix}. \quad (2.5)$$

However, as will be discussed in more detail later on, of these four degrees of freedom only one will appear as a physical particle. This is identified by the symbol h .

Vectors: particles which serve as force carriers. As seen in the previous section, each group which makes up \mathcal{G} has associated gauge bosons, in number equal to the number of generators of the group. Therefore, the vector content of the SM consists of the eight gluons G_μ^a , three W_μ^J , and B_μ . The situation is different in the broken phase: while the gluons remained untouched, the four mediators of the electroweak sector are "replaced" by the massive mediators of the weak force W^\pm and Z and the massless photon of electromagnetism A_μ .

A review, including also the masses of the particles, is given in [31].

2.3 The Lagrangian

The SM Lagrangian can be compactly written as shown in Equation (2.6). For convenience, the terms will be dealt with one by one.

$$\mathcal{L}_{SM} = \mathcal{L}_{kin}^{gauge} + \mathcal{L}_{kin}^{ferm} + \mathcal{L}_{Yuk}^{ferm} + \mathcal{L}_{Higgs}. \quad (2.6)$$

Gauge term: the explicit expression of $\mathcal{L}_{kin}^{gauge}$ is

$$\mathcal{L}_{kin}^{gauge} = -\frac{1}{4}(G_{\mu\nu}^A)^2 - \frac{1}{4}(W_{\mu\nu}^a)^2 - \frac{1}{4}(B_{\mu\nu})^2. \quad (2.7)$$

This term does not only contain the gauge bosons' kinetic term but also their triple and quartic self-interactions. Indeed, given the non-Abelian nature of $SU(3)_c$ and $SU(2)_L$, the field strength tensors take the form shown in Equations (2.2) and (2.3). By expanding the field strength contractions, three fields and one derivative or four field interactions can appear. Diagrammatically, these are respectively:

Fermion kinetic term: describes both the kinetic term of the fermion, but via the covariant derivative D_μ , also the interaction of the fermions with the gauge bosons,

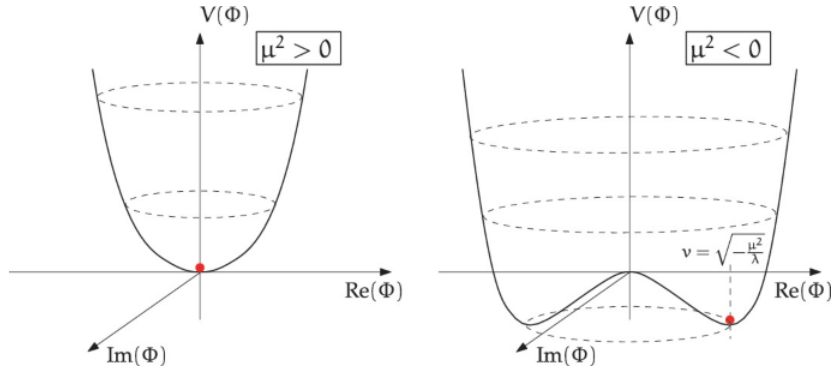
$$\mathcal{L}_{kin}^{ferm} = i\bar{\psi}\gamma^\mu D_\mu\psi, \quad \text{where } D_\mu\psi = (\partial_\mu + \underbrace{ig_s T^A G_\mu^A}_{\text{only for quarks}} + \underbrace{ig_L \tau^a W_\mu^a}_{\text{absent in case of } SU(2)_L \text{ singlets}} + ig_Y Y_\psi B_\mu)\psi. \quad (2.8)$$

Higgs sector The Higgs sector of the SM can be written as

$$\begin{aligned} \mathcal{L}_{Higgs} &= (D_\mu\phi)^\dagger D^\mu\phi - V(\phi^\dagger\phi), \\ V(\phi^\dagger\phi) &= \mu^2\phi^\dagger\phi + \lambda(\phi^\dagger\phi)^2. \end{aligned} \quad (2.9)$$

The first term in the Lagrangian is the Higgs kinetic term, which contains the interaction of the Higgs doublet with the W_μ^J and B_μ gauge bosons via the covariant derivative $D_\mu\phi = (\partial_\mu + ig_L \tau^a W_\mu^a + ig_Y Y_\psi B_\mu)\phi$. As for the second term, $V(\phi)$, denotes the Higgs potential. Two parameters appear, μ^2 a parameter with mass dimension two, and λ a dimensionless parameter. Of these, we must require $\lambda > 0$ to have a potential bounded from below. Instead, μ^2 can be both positive and negative. The shape of the potential depending on the sign of μ^2 is shown in Figure 2.1.

Yukawa sector: describes fermion interactions with the Higgs boson. In particular, a fermionic doublet and a fermionic

Figure 2.1: Higgs potential for two different sign choices for μ^2 .

singlet are coupled to the Higgs boson; the Lagrangian reads

$$\mathcal{L}_{Yuk}^{ferm} = -y_u \bar{q}_L \tilde{\phi} u_R - y_d \bar{q}_L \phi d_R - y_e \bar{l}_L \phi e_R + \text{h.c.}, \quad (2.10)$$

where $\tilde{\phi} = i\sigma_2 \phi^*$. It is important to notice that these terms are gauge invariant and lead to a mass term for the fermions upon electroweak symmetry breaking.

2.4 Symmetry Breaking

Up to this point, the SM particles are massless as a mass term would break gauge invariance. However, the particles that are experimentally observed are massive. The solution was found in the so called Higgs mechanism [1–3, 32]: the $SU(2)_L \times U(1)_Y$ symmetry is spontaneously broken to $U(1)_{EM}$, and particles acquire a mass. Hence the SSB pattern in the SM consists in

$$\mathcal{G} \xrightarrow{\text{SSB}} \mathcal{G}' = SU(3)_c \times U(1)_{EM}. \quad (2.11)$$

In the broken phase, the massless force mediators are the eight gluons (untouched by the Higgs mechanism since they do not interact with the Higgs field in the SM) and the photon.

To describe how the other particles in the SM are affected by the Higgs mechanism, one first of all needs to study how the Higgs boson can acquire a non-zero vacuum expectation value v . Then he can consider how the Higgs, the weak gauge bosons and the fermions acquire their mass terms.

Considering the Higgs potential in Equation (2.9), one finds that for $\mu^2 > 0$, the potential has a minimum for $\langle \phi \rangle = 0$ and the potential has the form on the left in Figure 2.1. In terms of the function h_i introduced in Equation (2.5), the vacuum expectation values satisfy $\langle h_i \rangle = 0, \forall i \in \{1, 4\}$.

When $\mu^2 < 0$, the potential takes the "Mexican hat" form and its minimum is no longer at the origin. The $h_4(x)$ component is chosen to acquire the vacuum expectation value $v/\sqrt{2}$, where $v = \sqrt{-\frac{\mu^2}{\lambda}} = 246 \text{ GeV}$. This spontaneously breaks the system's symmetry since a preferred direction has been chosen. The Higgs field can be written in the following manner around the minimum:

$$\phi(x) = \frac{1}{2} e^{i \frac{\vec{h} \cdot \vec{\sigma}}{v}} \begin{pmatrix} 0 \\ v + h(x) \end{pmatrix} \xrightarrow{\text{unitary gauge}} \phi(x) = \frac{1}{2} \begin{pmatrix} 0 \\ v + h(x) \end{pmatrix}. \quad (2.12)$$

The first three real scalars have null vacuum expectation values and make up the Goldstone bosons, denoted by $\vec{h}(x) = (h_1(x) \ h_2(x) \ h_3(x))^T$. From this point on, the x dependence is dropped.

Particle	Square mass	dofs	Particle	Square mass	dofs
W^+, W^-	$m_W^2 = \frac{g_L^2 v^2}{4}$	3+3	W^J	0	2+2+2
Z	$m_Z^2 = \frac{g_L^2 + g_Y^2}{4} v^2$	3	B	0	2
A	0	2	-	-	-
h	$2\lambda v^2$	1	ϕ	0	4
		12			12

Table 2.4: Bosonic degrees of freedom for the broken (left) and unbroken (right) phases. The total number of degrees of freedom is preserved, but their distribution varies. The massless gauge bosons carry two degrees of freedom each, while the massive ones have an extra degree of freedom. As for the Higgs, in the unbroken phase, it is a complex doublet (four degrees of freedom), while in the broken phase, it is a singlet (one degree of freedom).

2.4.1 Gauge and Higgs bosons masses

Starting from the Higgs kinetic term, equation (2.9), it is possible to derive the gauge boson masses simply by substituting the form of the Higgs in (2.12) and focusing on the terms that are quadratic in the gauge bosons.

The charged W_μ^\pm bosons are obtained via the mixing of W_μ^1 and W_μ^2 . Their mass and definition in terms of the original gauge bosons are:

$$m_W = \frac{g_L v}{2}, \quad \begin{pmatrix} W_\mu^+ \\ W_\mu^- \end{pmatrix} = \frac{1}{\sqrt{2}} \begin{pmatrix} +1 & -i \\ +1 & i \end{pmatrix} \begin{pmatrix} W_\mu^1 \\ W_\mu^2 \end{pmatrix}. \quad (2.13)$$

The mixing of W_μ^3 with B_μ results in a massless field, identified as the photon A_μ , and the massive neutral boson Z_μ . Defining the Weinberg angle to be $\tan \theta_W = \frac{g_Y}{g_L}$, the Z_μ mass and the definitions of Z_μ and A_μ are:

$$m_Z = \frac{\sqrt{g_L^2 + g_Y^2} v}{2}, \quad \begin{pmatrix} A_\mu \\ Z_\mu \end{pmatrix} = \begin{pmatrix} \sin \theta_W & \cos \theta_W \\ \cos \theta_W & -\sin \theta_W \end{pmatrix} \begin{pmatrix} W_\mu^3 \\ B_\mu \end{pmatrix}. \quad (2.14)$$

The interactions of the W^\pm and Z bosons with the Higgs can be recovered by performing the substitution $v \rightarrow h + v$; this means that the coupling between the massive gauge bosons W^\pm and Z with the Higgs boson is proportional to their mass squared.

The Higgs boson mass is picked up from the potential $V(\phi)$ defined in Equation (2.9). In Equation (2.15) the entire Higgs sector is written in the broken phase:

$$\mathcal{L}_{Higgs}^b = \frac{1}{2} \partial_\mu h \partial^\mu h - \mu^2 \left(\frac{v+h}{\sqrt{2}} \right)^2 - \lambda \left(\frac{v+h}{\sqrt{2}} \right)^4 = \frac{1}{2} \partial_\mu h \partial^\mu h - \underbrace{\lambda v^2}_{2m_h^2} h^2 - \lambda v h^3 - \frac{\lambda}{4} h^4. \quad (2.15)$$

From the above expression, one can appreciate that once the Higgs boson's mass has been measured all the parameters of the Higgs potential are determined. In particular, the Higgs boson self-coupling is proportional to the mass squared upon rewriting λ in terms of m_h :

$$m_h^2 = 2\lambda v^2 \quad \Rightarrow \quad \lambda = \frac{m_h^2}{2v^2}. \quad (2.16)$$

The number of bosonic degrees of freedom is the same in the broken (where the bosons are the gluons, the massive gauge bosons, the Higgs boson and the photon) and the unbroken phase (where the bosons are the Higgs doublet and the gauge bosons associated to the SM gauge groups), as shown in Table 2.4 for the electroweak sector. What changes between the two phases is how the degrees of freedom are distributed between the different particles.

Fields	u	d	e	ν
Charge	$\frac{2}{3}$	$-\frac{1}{3}$	-1	0

Table 2.5: Electromagnetic charges of the SM fermions.

2.4.2 Fermion masses

Considering the Yukawa component of \mathcal{L}_{SM} (Equation (2.10)) and using Equation (2.12) to rewrite the Higgs in the unitary gauge, one finds

$$-\mathcal{L}_{Yuk}^{ferm} = \frac{y_d v}{\sqrt{2}} \bar{d}_L d_R + \frac{y_u v}{\sqrt{2}} \bar{u}_L u_R + \frac{y_e v}{\sqrt{2}} \bar{e}_L e_R + \frac{y_d}{\sqrt{2}} h \bar{d}_L d_R + \frac{y_u}{\sqrt{2}} h \bar{u}_L u_R + \frac{y_e}{\sqrt{2}} h \bar{e}_L e_R + \text{h.c.} \quad (2.17)$$

The first three terms will allow the identification of the fermion masses $m_* = \frac{1}{\sqrt{2}} v y_*$ once the rotation into the mass basis has been performed (see Subsection 2.4.4), whereas the last three describe the interactions between the quarks and the Higgs boson. While the massive gauge bosons had coupling to the Higgs bosons proportional to the square of their mass, the fermion have a coupling with the Higgs boson that linearly depends on their mass.

2.4.3 Fermion interaction with the gauge bosons

Given the relevance in Chapter 7 of the quark interactions with the W_μ^\pm and Z_μ bosons, the description of such interactions is presented here. The steps will be shown explicitly only for the quarks but can be extended to the leptons. The starting point is in the quark kinetic terms, where the gauge bosons are contained in the covariant derivatives:

$$\mathcal{L}_{kin}^{quarks} = \bar{q}_L i \not{D} q_L + \bar{u}_R i \not{D} u_R + \bar{d}_R i \not{D} d_R \quad (2.18)$$

$$\supset -\bar{q}_L \left(\frac{gL}{2} \sigma^J \mathcal{W}^J + g_Y Y_q \mathcal{B} \right) q_L - g_Y Y_u \bar{u}_R \not{B} u_R - g_Y Y_d \bar{d}_R \not{B} d_R. \quad (2.19)$$

Then, using Equations (2.13) and (2.14), the Lagrangian description of the weak and electromagnetic interactions of the quarks is found:

$$-\mathcal{L}_{WI+EM} = \frac{gL}{\sqrt{2}} \left(\bar{u}_L \not{W}^+ d_L + \bar{d}_L \not{W}^- u_L \right) + \frac{gL}{\cos \theta_W} \left(\bar{q}_L \not{Z} g_L^{Zq} q_L + \bar{u}_R \not{Z} g_R^{Zu} u_R + \bar{d}_R \not{Z} g_R^{Zd} d_R \right) + e \bar{q}_L \not{A} Q_q q_L + e \bar{u}_R \not{A} Q_u u_R + \bar{d}_R \not{A} Q_d d_R. \quad (2.20)$$

The charges are defined as $Q_q = \tau_q^3 + Y_q \mathbb{1}$ and the Z couplings to left- and right-handed currents are defined, respectively, as

$$g_L^{Zq} = \tau_q^3 - Q_q \sin^2 \theta_W, \quad g_R^{Zq} = -Q_q \sin^2 \theta_W. \quad (2.21)$$

Using the values for the hypercharges reported in Table 2.2, the electromagnetic charge assignments are those in Table 2.5.

2.4.4 CKM matrix

So far the Lagrangian terms have been written in the so-called interaction basis, where the Yukawa matrices are 3×3 , non-diagonal matrices: Explicating the flavour indices of Equation (2.10), the Yukawa sector of the Lagrangian is:

$$-\mathcal{L}_{Yuk}^{ferm} = [y_u]_{rk} \bar{q}_{Lr} \tilde{\phi} u_{Rk} + [y_d]_{rk} \bar{q}_{Lr} \phi d_{Rk} + [y_e]_{rk} \bar{l}_{Lr} \phi e_{Rk} + \text{h.c.} \quad (2.22)$$

It is possible to diagonalise the Yukawa matrices (going into the mass basis) via a biunitary transformation. Let L_f and R_f be the unitary matrices, then:

$$\hat{y}_f = \text{diag}(y_{f1}, y_{f2}, y_{f3}) = L_f^\dagger y_f R_f. \quad (2.23)$$

The associated rotations for the quarks, with explicit family indices, are:

$$q_{Lr} \rightarrow [L_q]_{rk} q_{Lk}, \quad q_{Rr} \rightarrow [R_q]_{rk} q_{Rk}, \quad (2.24)$$

where $q = u, d$. Similarly for the leptons, the rotations read

$$\begin{aligned} e_{Lr} &\rightarrow [L_e]_{rk} e_{Lk}, & e_{Rr} &\rightarrow [R_e]_{rk} e_{Rk}, \\ \nu_{Lr} &\rightarrow [L_\nu]_{rk} \nu_{Lk}. \end{aligned} \quad (2.25)$$

These rotations into the mass basis have to be performed in all the sectors of the SM Lagrangian. By construction, the interactions with the neutral gauge bosons (the photon and the Z boson) in Equation (2.20) are left invariant since they do not mix the up and down type fermions. This is not true for the charged bosons, which couple fermions of different generations. Performing the rotations defined in Equations (2.24) and (2.25),

$$\mathcal{L}_W = -\frac{g_L}{\sqrt{2}} \left[\bar{u}_{Lr} \underbrace{[L_u^\dagger L_d]_{rk}}_{[V_{CKM}]_{rk}} W^+ d_{Lk} + \bar{\nu}_{Lr} \underbrace{[L_\nu^\dagger L_e]_{rk}}_{[U_{PMNS}]_{rk}} W^+ e_{Lk} + \text{h.c.} \right]. \quad (2.26)$$

The first matrix is the CKM matrix (from Cabibbo, Kobayashi and Maskawa), while the second is the PMNS matrix (from Pontecorvo, Maki, Nakagawa and Sakata).

The CKM matrix is a complex unitary 3×3 matrix. As such, it has nine real degrees of freedom, of which three correspond to rotation angles and six are associated to phases. However, it is possible to perform quark field rotations to remove all phases but one. Therefore, the CKM matrix bears four degrees of freedom: three rotation angles and one phase. The values for the angles and the phase have been measured and are reported in [31].

Since neutrinos are massless within the SM, one can pick an arbitrary L_ν to perform the rotation into the mass basis. If $L_\nu = L_e$, the $U_{PMNS} = \mathbb{1}_{3 \times 3}$.

Chapter 3

Effective Field Theories

Effective Theories often appear in Physics. Indeed, besides Particle Physics' well-known Fermi Theory [33, 34] (that provided the first description of Weak Interactions and is used for low-energy studies¹), they also appear in areas such as Cosmology (e.g., for the study of inflation [35, 36]) and Nuclear Physics [37]. Effective field theories provide a tool for the description of processes up to a given order in an expansion parameter without requiring knowledge of the underlying UV theory.

3.1 Effective Theories

One of the simplest examples of effective theories is how the gravitational force felt by an object of mass m on Earth can be approximated by the $F_g = mg$, instead of using Newton's force. For everyday use the difference between the two descriptions is negligible.

This simple example will be used to introduce the ingredients for an Effective Theory: let R be the Earth's radius and d the height of the object above the Earth's surface. Then, Newton's force can be expanded as

$$F_g^N = G \frac{m M_E}{(R + d)^2} = G \frac{m M_E}{R^2} \frac{1}{\left(1 + \frac{d}{R}\right)^2} \stackrel{d \ll R}{\approx} G \frac{m M_E}{R^2} \left(1 - 2 \frac{d}{R}\right). \quad (3.1)$$

Defining $g = G \frac{M_E}{R^2}$ and truncating at zero order, the usual weight force expression is obtained. The following ingredients can be identified:

- an expansion parameter, in this case d/R . The approximation made becomes increasingly worse as the distance d becomes comparable to the radius R . This is related to the existence of a separation of scales between the more complete theory and the particular case being studied;
- a symmetry, that in the effective theory consists of translational invariance at fixed height and invariance under rotation about the vertical axis (while the original system was invariant under rotations in the three-dimensional Euclidean space);
- a degree of freedom, here the presence of an object of mass m .

This example shows the "top-down" approach: the more complete theory is known, but via an appropriate series expansion a simplified version is found.

The other possible direction in which one can proceed is known as the "bottom-up": only the approximation is known and one would like to reconstruct the more fundamental description. In the case of the object feeling the gravitational

¹As will be better addressed later on, Effective Theories have a validity interval, below which the description provided is accurate and above which it breaks down. In the case of the Fermi theory, such energy scale is the W -boson mass $m_W \approx 80$ GeV.

force, the "bottom-up" approach would consist in starting from the weight force $F_g = mg$, setting it to be the zero-order term of a series expansion with expansion parameter d/R and adding higher order terms.

$$F_g = mg \left[\left(\frac{d}{R} \right)^0 + a_1 \left(\frac{d}{R} \right)^1 + a_2 \left(\frac{d}{R} \right)^2 + a_3 \left(\frac{d}{R} \right)^3 + \dots \right], \quad (3.2)$$

where the a_i coefficients are unknowns that have to be fitted to experimental data.

3.2 Effective Field Theories

When moving from an Effective Theory to an Effective *Field* Theory, symmetry preserves its relevance and the fields are the degrees of freedom. The effective theory's expansion is organised in terms of inverse powers of a heavy scale Λ . This organisation will be dealt with in the next section, considering the particular example of the Standard Model Effective Field Theory. In the following, some other general features are briefly addressed.

Consider a quantum field theory describing two interacting scalar particles, one called ϕ with mass m and a second Φ with mass Λ , such that $m \ll \Lambda$ [38]. They are described by a Lagrangian $\mathcal{L}_{UV} = \mathcal{L}_{UV}(\phi, \Phi, c)$, where c describes a set of couplings. If the experimental energy scale \mathcal{E} satisfies $m < \mathcal{E} \ll \Lambda$, then only the lighter ϕ can be produced and directly observed. The heavy Φ can still virtually contribute to scattering processes involving the lighter field as a propagator, which can be expanded as

$$\frac{1}{p^2 - \Lambda^2} = \frac{1}{\Lambda^2} \frac{-1}{1 - (p^2/\Lambda^2)} \stackrel{p^2 \ll \Lambda^2}{\approx} -\frac{1}{\Lambda^2} \left(1 - \frac{p^2}{\Lambda^2} + \dots \right). \quad (3.3)$$

Truncating the expansion to the zero-order term corresponds to shrinking the internal propagator to the point of having a contact interaction. Even if the full theory involving both fields is known, it is convenient to develop and work with an effective description $\mathcal{L}_{EFT} = \mathcal{L}_{EFT}(\phi, \tilde{c})$ which only depends on the lighter ϕ . The effects of Φ are encoded in the new coefficients \tilde{c} : the procedure of expressing \tilde{c} in terms of the original theory's parameters is referred to as matching. The matching can be performed in two ways:

1. Starting from the UV Lagrangian, the equations of motion for the heavy field Φ can be derived and substituted in \mathcal{L}_{UV} , losing the dependence on Φ . Rearranging the remaining terms, which only involve the field ϕ , the correspondence between c and \tilde{c} is found;
2. Using \mathcal{L}_{UV} and \mathcal{L}_{EFT} , the amplitude for a given process can be evaluated from both viewpoints. Requiring the two descriptions to be the same, the following matching condition is found:

$$\mathcal{M}_{UV}(\phi, \Phi, c) = \mathcal{M}_{EFT}(\phi, \tilde{c}). \quad (3.4)$$

This procedure will be explained in more detail in Chapter 5 for the concrete models and EFT considered in this thesis. Before moving on to the Effective Field Theory relevant to this thesis, a few words are spent on the Fermi Theory of Weak Interactions: Figure 3.1 puts side-by-side the two descriptions of the decay of the muon provided by the Standard Model and in Fermi Theory. In the Standard Model description, the decay involves two leptonic currents, connected by a W boson propagator. Given that the energy scale of the process, the muon mass, is much smaller than the W boson mass, the propagator shrinks to a point-like interaction as

$$\begin{aligned} D_{\mu\nu} &= \frac{i}{k^2 - m_W^2} \left(-g_{\mu\nu} + \frac{k_\mu k_\nu}{m_W^2} \right) = \frac{i}{m_W^2} \left(1 + \frac{k^2}{m_W^2} + \dots \right) \left(-g_{\mu\nu} + \frac{k_\mu k_\nu}{m_W^2} \right), \\ &\approx -\frac{i}{m_W^2} g_{\mu\nu} + O\left(\frac{k^2}{m_W^2}\right). \end{aligned} \quad (3.5)$$



Figure 3.1: UV versus EFT description of the muon decay.

The point-like interaction of the two leptonic currents in Fermi's description is given by

$$\mathcal{L}_{Fermi} = 4 \frac{G_F}{\sqrt{2}} [(\bar{\nu}_\mu L \gamma^\nu \mu_L) (\bar{e}_L \gamma_\nu \nu_{eL}) + \text{h.c.}] . \quad (3.6)$$

The G_F coefficient is known as Fermi's constant. It has mass dimension -2 and is defined in terms of the Standard Model g_L coupling and the mass of the heavy field that has been integrated out m_W ,

$$G_F = \sqrt{2} \frac{g_L^2}{8 m_W^2} = 1.166 \cdot 10^{-5} \text{ GeV}^{-2} . \quad (3.7)$$

Therefore, Fermi's theory acts like an effective field theory for the Standard Model, which includes the W^\pm bosons, if the energy scales being considered are much lower than the W^\pm mass.

At this point, the effective field theory relevant to the study performed in this thesis can be presented.

3.2.1 Standard Model Effective Field Theory

The success of the Standard Model in describing current experimental data suggests that there is a mass gap between its degrees of freedom and those of New Physics. Let Λ denote the energy scale at which New Physics appears: the Standard Model Effective Field Theory (SMEFT) was developed to parametrise deviations from the Standard Model at energy scales below Λ due to the presence of heavy new degrees of freedom in a model-independent manner. The SMEFT's region of validity is between the ElectroWeak scale and Λ , under the assumption that $v \ll \Lambda$.

Going below the ElectroWeak scale, another field theory known as LEFT (Low Energy Effective Field Theory) is commonly used. The particle content of LEFT consists in the massless gauge bosons (the photon and the gluons), all the SM leptons, the three down-type quarks and the two lighter up-type quarks [39].

The SMEFT Lagrangian is built starting from the SM Lagrangian density and adding a tower of higher-dimensional operators, organised as an expansion in inverse powers of Λ . These operators are required to be invariant under the SM gauge group \mathcal{G} and are built out of the SM fields. In general, the SMEFT Lagrangian can be written as

$$\mathcal{L}_{SMEFT} = \mathcal{L}_{SM} + \sum_{d>4} \sum_{i=1}^{n_d} \frac{\mathcal{C}_i^{(d)}(\mu)}{\Lambda^{d-4}} O_i^{(d)} , \quad (3.8)$$

in which $O_i^{(d)}$ are the new operators with dimension d and the dimensionless $\mathcal{C}_i^{(d)}(\mu)$ are Wilson coefficients. These coefficients are not constant: they depend on the energy scale μ being considered. The equations that describe the running of the Wilson Coefficients as a function of the energy scale are the Renormalisation Group Equations (RGEs) [40–42].

Figure 3.2 shows how the SMEFT can be used to study New Physics effects in three steps:

1. Matching at the high energy scale of the UV model with the SMEFT to express the corresponding Wilson coefficients in terms of the UV masses and couplings;

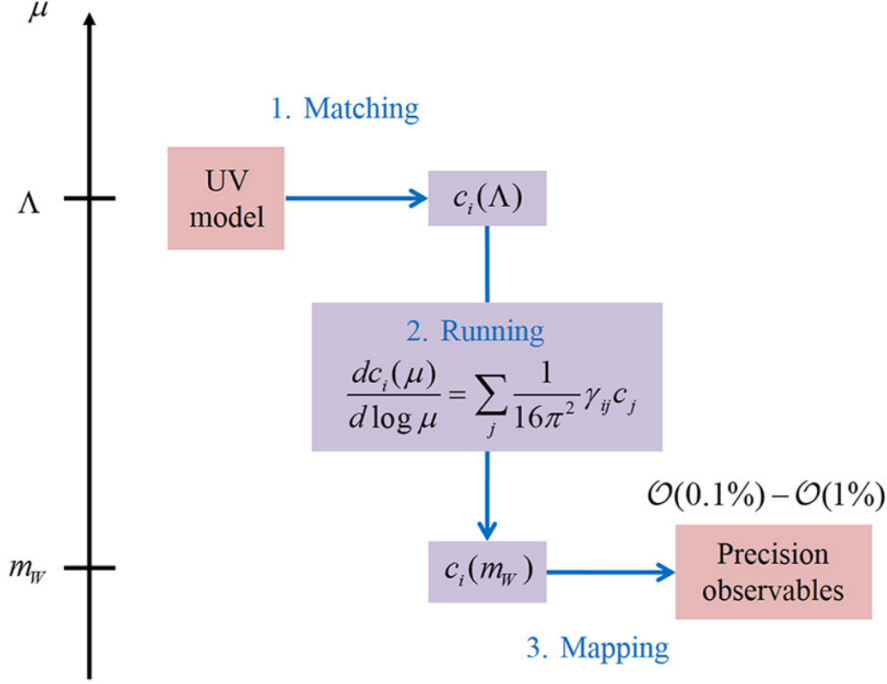


Figure 3.2: Schematic description of how SMEFT connects the UV parameters to the ElectroWeak Observables. Figure from [43].

2. Using the RGEs to run down the Wilson coefficients to the scale of the experiments of interest. In compact notation, they read

$$\dot{c}_i = \sum_j \gamma_{ij} c_j, \quad \dot{c}_i = 16\pi^2 \mu \frac{d}{d\mu} c_i, \quad (3.9)$$

where the matrix γ_{ij} is known as the anomalous dimension matrix. To integrate them, the leading log approximation is typically performed. This approximation consists in assuming that the left-hand side of Equation (3.9) is μ independent. Hence, the expression can be integrated and provides the following result:

$$c_i(\mu) = c_i(\Lambda) + \frac{1}{16\pi^2} \log\left(\frac{\mu}{\Lambda}\right) \sum_j \gamma_{ij} c_j(\Lambda). \quad (3.10)$$

For the specific example of Figure 3.2, the energy scale corresponds to the W boson mass, so $\mu = m_W$;

3. Mapping, in this particular case, into the ElectroWeak Precision Observables, getting bounds on the New Physics parameters. Only certain operators can generate deviations to a given observable: as will be shown in Chapter 6, once a dimension d has been fixed and an operator basis has been chosen, model-independent deviations in terms of Wilson coefficients can be written for each observable. Model-dependence is reintroduced once the explicit expressions of the Wilson coefficients are introduced.

At a given dimension d , several operators can be built. However, they are not all independent: one calls "redundant" all the interactions without physical effects. Typical examples of redundant operators are [44]:

- Those corresponding to total derivatives, except for those cases in which the asymptotic behaviour of fields cannot be neglected (for example in the presence of non-trivial topologies);
- Operators that are equivalent up to a field redefinition to an already present operator;
- Operators related to one another via relations such as the Fierz Identities. For example, at the dimension-six level, Fierz identities allow to reduce the number of independent four-fermion operators.

The operator with the smallest dimension introduced by SMEFT is the dimension-five Weinberg operator [45],

$$[\mathcal{O}_{\nu\nu}]_{pr} = \left(\tilde{\phi}^\dagger l_p \right)^T C \left(\tilde{\phi}^\dagger l_r \right). \quad (3.11)$$

This operator violates lepton number and generates neutrino masses in the broken phase. Since leptons will not be considered in this thesis and there are no other dimension-five operators, the first contribution is from the dimension-six operators.

Two operator bases often appear when dealing with the dimension-six SMEFT and will be used in this thesis: the Green's basis [46] and the Warsaw basis [47]. The elements of the former are independent under integration by parts, and those of the latter are independent under both integration by parts and use of equations of motion of the SM fields: the Warsaw basis is a non-redundant basis for SMEFT at the dimension-six level. Using the SM equations of motion it is possible to go from the Green's basis to the Warsaw basis [46].

So why should one not work directly with the non-redundant Warsaw basis? When the matching procedure is performed by imposing that the EFT and the UV amplitudes are the same, the equations of motion of the SM field are not involved. So the results of such matchings are in the Green's basis; the final step of a matching will be to go to Warsaw basis.

Finally, instead of working with dimensionless Wilson coefficients, the convention used here has the heavy scale of the expansion included in the coefficient. An operator \mathcal{O}_x will, therefore, contribute as

$$\mathcal{L}_{SMEFT} \supset \mathcal{C}_x \mathcal{O}_x, \quad \mathcal{C}_x \propto \frac{1}{M_1 M_2}. \quad (3.12)$$

Chapter 4

Identifying the New Physics Model

As seen in Chapter 2, in the Standard Model there is a unique correspondence between the fermion masses and the corresponding Yukawa couplings. Hence, a deviation from such relationship provides evidence of the presence of New Physics [48].

Figure 4.1, realised by the CMS collaboration [6], shows the search for such modifications performed using LHC data. The κ formalism¹ is introduced to parametrise deviations from the SM predictions of the couplings. If the general coupling is denoted by g , then the definition for the modifier is $\kappa = g^{NP}/g^{SM}$. In Sections 2.4.1 and 2.4.2, it was shown that in the Standard Model the couplings to the Higgs boson of the fermions and the massive gauge bosons are proportional to their mass and their mass squared, respectively. This, first of all, motivates why only the heavier particles are present in Figure 4.1: the larger the particle's mass, the bigger its coupling to the Higgs boson. Secondly, the aforementioned sections motivate why, to have a linear dependence on the particle mass in the plot, the modifier for the fermions κ_f appears linearly while for the gauge bosons, the modifier κ_V is under a square root.

Not the entire massive particle content of the Standard Model is present in Figure 4.1; while only the first generation charged lepton is missing (the electron²), both the first and the second generation quarks are absent. As mentioned in the Introduction, there have been several experimental proposals for the constraining of the second generation quarks (for example, the study of Vh production followed by the decay $h \rightarrow c\bar{c}$ for the charm quark [13, 50] and the use of strange tagging at lepton colliders for the strange quark [17]) and the modifier projections for the HL-LHC have been found to be $\kappa_c < 1.2$ and $\kappa_s < 13$ [23]. Meanwhile the currently loose constraints on the couplings of the first generation, with projections for the HL-LHC $\kappa_u < 260$ and $\kappa_d < 156$ from reference [25], allow it to be a playground for the development of new models. In particular, it is of interest to see whether it is possible to test interesting model parameter space when probing the light quark Yukawa couplings.

Before considering the New Physics models, the SMEFT operators which can lead to quark masses no longer being proportional to the Yukawa couplings have to be identified. In this context, the term "Yukawa coupling" denotes the coefficient that multiplies the interaction term between the Higgs field and two quarks. Identifying the relevant SMEFT operators serves as a tool for the identification of the New Physics models: a model which introduces new particles that do not generate, once they have been integrated out, the SMEFT operators of interest will not be considered as candidates.

¹The κ factors, also known as scale factors, are used to parametrise the deviations from the Standard Model predictions of the couplings, decay widths and cross-sections [49]. A list of the κ parameters can be found in Table 2 of reference [49].

²The Future e^+e^- Circular Collider (FCC-ee) might be able to investigate the electron Yukawa coupling [11].

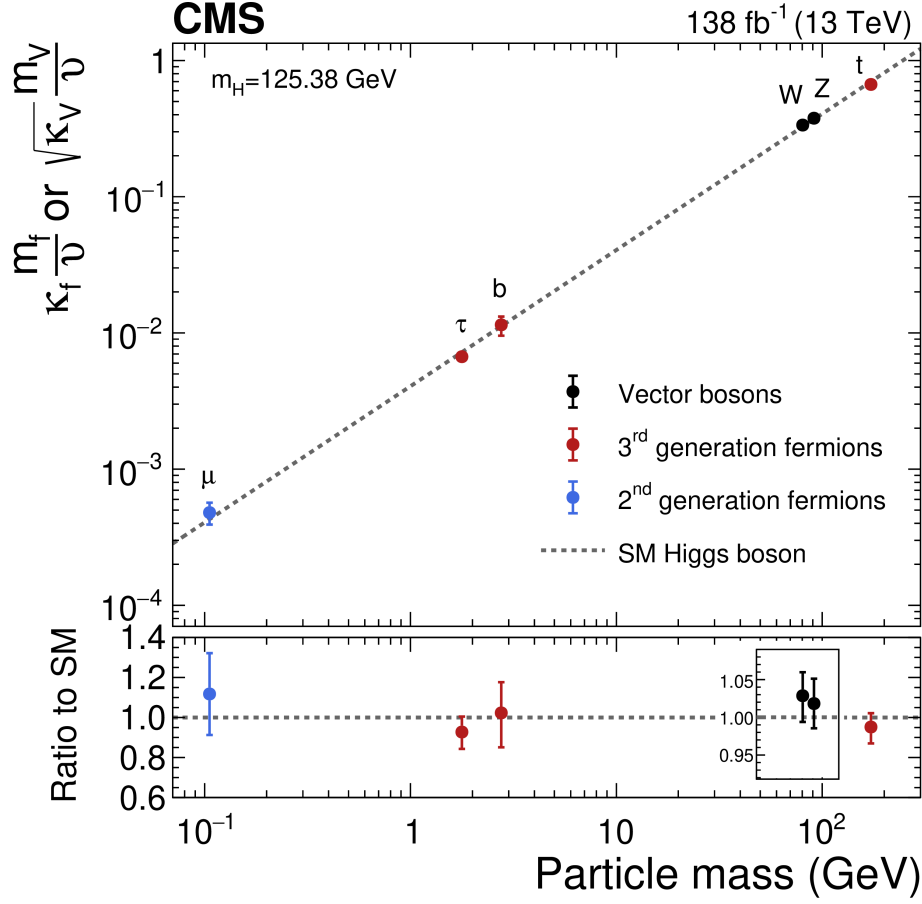


Figure 4.1: This plot taken from [6] shows the modifiers for the couplings of the Higgs boson with the heavier SM particles. These heavy particles consist in the third generation quarks, the second and third generation charged leptons, and the massive gauge bosons.

4.1 SMEFT Operators

Considering the Warsaw basis operators whose particle content consists in a Higgs boson doublet and quarks, the following two³ are found to affect the quark Yukawa couplings:

$$\mathcal{L}_{SMEFT} \supset \Delta\mathcal{L}_y \equiv \mathcal{C}_{u\phi}\mathcal{O}_{u\phi} + \mathcal{C}_{d\phi}\mathcal{O}_{d\phi} + \text{h.c.} = \phi^\dagger\phi \left([\mathcal{C}_{u\phi}]_{ij} \bar{q}_L^i \tilde{\phi} u_R^j + [\mathcal{C}_{d\phi}]_{ij} \bar{q}_L^i \phi d_R^j \right) + \text{h.c.} \quad (4.1)$$

They give rise to the tree-level Feynman diagrams shown in Figures 4.2 and 4.3. In the following, how the quark masses and couplings to the Higgs boson are affected is shown [25].

Mass terms: they are determined by substituting Equation (2.12) in $\mathcal{L}_{Yuk}^{ferm} + \Delta\mathcal{L}_y$ and end up to be

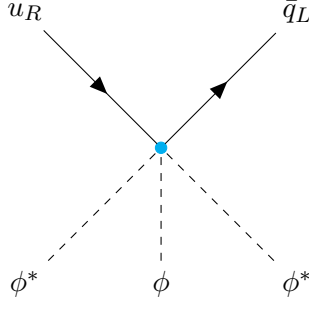
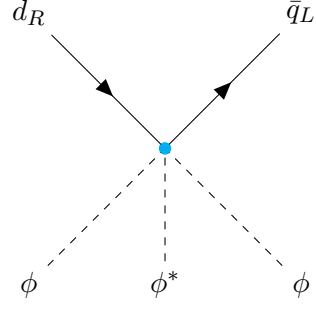
$$M_{ij}^u = \frac{v}{\sqrt{2}} \left(y_{ij}^u - \frac{1}{2} [\mathcal{C}_{u\phi}]_{ij} v^2 \right), \quad M_{ij}^d = \frac{v}{\sqrt{2}} \left(y_{ij}^d - \frac{1}{2} [\mathcal{C}_{d\phi}]_{ij} v^2 \right). \quad (4.2)$$

The rotation from the interaction into the mass basis takes place through a bi-unitary transformation V^q (with $q = u, d$):

$$m_{q_i} = \left[(V_L^q)^\dagger M^q V_R^q \right]_{ii}. \quad (4.3)$$

The CKM matrix is provided by $V_{CKM} = (V_L^u)^\dagger V_L^d$.

³Actually, there are two further operators ($\mathcal{O}_{\phi D}$ and $\mathcal{O}_{\phi\Box}$ studied in Section 5.1.1) that can affect the Higgs couplings. However, these affect all the Higgs couplings, not only those to the light quarks, and are therefore constrained to have a small contribution. Furthermore, in the models that will be considered here, they only appear at the one-loop level. Their contribution to the κ modifier is, therefore, neglected.

Figure 4.2: EFT tree level diagram for $\mathcal{O}_{u\phi}$.Figure 4.3: EFT tree level diagram for $\mathcal{O}_{d\phi}$.

Given (4.2), one can find the transformed Wilson coefficients $[\tilde{\mathcal{C}}_{q\phi}]_{ij} = [V_L^q]_{ni}^* [\mathcal{C}_{q\phi}]_{nm} [V_R^q]_{mj}$ in the mass basis.

$$\begin{cases} q_{L,i} \mapsto [V_L^q]_{ij} q_{L,j} \\ q_{R,i} \mapsto [V_R^q]_{ij} q_{R,j} \end{cases} \Rightarrow \bar{q}_{L,i} [\mathcal{C}_{q\phi}]_{ij} q_{R,j} \mapsto \bar{q}_{L,l} \underbrace{[V_L^q]_{il}^* [\mathcal{C}_{q\phi}]_{ij} [V_R^q]_{jk}}_{[\tilde{\mathcal{C}}_{q\phi}]_{lk}} q_{R,k}. \quad (4.4)$$

The tilde notation is dropped in the following to lighten the notation.

Quark interactions with the Higgs boson: These are obtained by matching terms in $\mathcal{L}_{Yuk}^{ferm} + \Delta\mathcal{L}^y$ with

$$\mathcal{L} \supset -g_{h\psi_i\bar{\psi}_j}\bar{\psi}_j\psi_i h - g_{hh\psi_i\bar{\psi}_j}\bar{\psi}_j\psi_i h^2 - g_{hhh\psi_i\bar{\psi}_j}\bar{\psi}_j\psi_i h^3. \quad (4.5)$$

The modified couplings $g_{h\psi_i\bar{\psi}_j}$, $g_{hh\psi_i\bar{\psi}_j}$ and $g_{hhh\psi_i\bar{\psi}_j}$ read

$$g_{hq_i\bar{q}_j} = \frac{m_q}{v} \delta_{ij} - \frac{v^2}{\sqrt{2}} [\mathcal{C}_{q\phi}]_{ij}; \quad (4.6)$$

$$g_{hhq_i\bar{q}_j} = -\frac{3}{2\sqrt{2}} v [\mathcal{C}_{q\phi}]_{ij}; \quad (4.7)$$

$$g_{hhhq_i\bar{q}_j} = -\frac{1}{2\sqrt{2}} [\mathcal{C}_{q\phi}]_{ij}. \quad (4.8)$$

In Equation (4.6) the modified Yukawa coupling between two quarks and the Higgs can be recognized. It is convenient to parameterise the deviation of the Yukawa coupling from the SM value via the κ parameter:

$$\kappa_{q_i} = \frac{g_{hq_i\bar{q}_i}}{m_{q_i}/v} = 1 - \frac{v^3}{\sqrt{2} m_{q_i}} [\mathcal{C}_{q\phi}]_{ii}, \quad q = u, d. \quad (4.9)$$

Notice that this definition is appropriate only for the diagonal couplings. Additionally, the presence of the quark masses in the denominator needs to be addressed: following [25] they are set to be $m_u = 2.2$ MeV and $m_d = 4.7$ MeV for the first generation; for the second generation $m_s = 95$ MeV and $m_c = 1.27$ GeV are used. This thesis will study, looking at concrete models, how large the κ_q factors can become.

4.2 NP Model Choice

At this point, one can consider NP particles contributing to the dimension-six SMEFT Lagrangian. A classification of all the NP particles that, once they have been integrated out, can contribute at tree level to the dimension-six operators in \mathcal{L}_{SMEFT} can be found in [51]; these particles can be scalars (S), vector-like fermions (F) or vector bosons (V). The complete Lagrangian, including the possibility of mixed terms (those that involve interactions of NP particles with

Name	U	D	Q_1	Q_5	Q_7	T_1	T_2
Irrep.	$(3, 1)_{\frac{2}{3}}$	$(3, 1)_{-\frac{1}{3}}$	$(3, 2)_{\frac{1}{6}}$	$(3, 2)_{-\frac{5}{6}}$	$(3, 2)_{\frac{7}{6}}$	$(3, 3)_{-\frac{1}{3}}$	$(3, 3)_{\frac{2}{3}}$

Table 4.1: Vector-like quarks presented in [51] which generate dimension-six contributions to the SMEFT at tree level.

Singlet + Doublet		Doublet + Triplet	
Model 1	$U + Q_1$	Model 5	$T_1 + Q_1$
Model 2	$D + Q_1$	Model 6	$T_1 + Q_5$
Model 3	$U + Q_7$	Model 7	$T_2 + Q_1$
Model 4	$D + Q_5$	Model 8	$T_2 + Q_7$

Table 4.2: New Physics models to be examined.

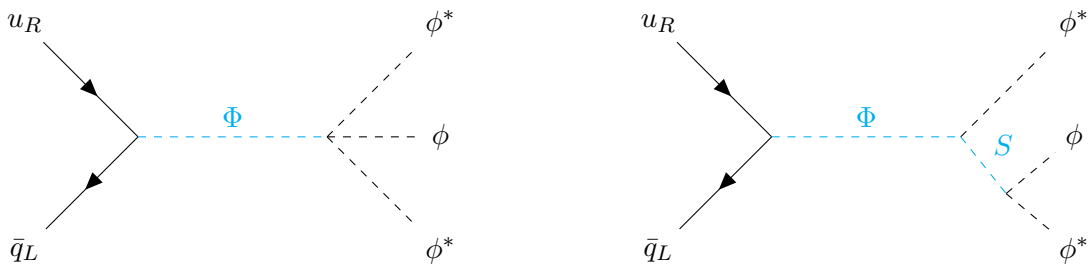
different spins), is written in the following manner:

$$\mathcal{L}_{NP}^c = \mathcal{L}_{SM} + \mathcal{L}_S + \mathcal{L}_F + \mathcal{L}_V + \underbrace{\mathcal{L}_{SF} + \mathcal{L}_{SV} + \mathcal{L}_{VF}}_{\text{mixed}}. \quad (4.10)$$

From Appendices C and D of [51], one can identify the NP particles that generate at tree level the operator $\mathcal{O}_{u\phi}$ and/or $\mathcal{O}_{d\phi}$: models can be constructed involving a scalar, a pair of scalars (both shown in Figure 4.4), a pair of vector-like quarks and a mixed case with one scalar and one vector-like quark. Tree level Feynman diagrams for the last two cases are found in Figure 4.5. Vector-like quarks will henceforth be referred to as VLQs.

In this thesis, models involving pairs of the VLQs in Table 4.1 will be considered: as an example, the operator of interest $\mathcal{O}_{u\phi}$ can be obtained by integrating out the cyan propagators of the diagram on the left in Figure 4.5. The number of models that can be constructed is finite and can be studied systematically: Table 4.2 shows the particle content of the models that will be studied, as well as the name with which they will be identified throughout the rest of the thesis. The presence of pairs implies that, besides the interactions of the heavy quarks with the SM ones, also interactions between VLQs can be studied. As will be explicitly shown in Section 5.1, the presence of a Yukawa-like coupling between VLQs is especially important as it appears in the unsuppressed term in the κ modifier's expression (Equation (4.9)) once the matching has been performed.

The characteristic of VLQs is that their right-handed and left-handed components transform in the same manner under the SM gauge group. This means that they can have a mass term without requiring the Higgs mechanism since it would not break gauge symmetry and that they could be very massive without introducing unnaturally big Yukawa-

Figure 4.4: Feynman diagrams for the contribution of models involving one new scalar (left) or two new scalars (right) to the operator $\mathcal{O}_{u\phi}$.

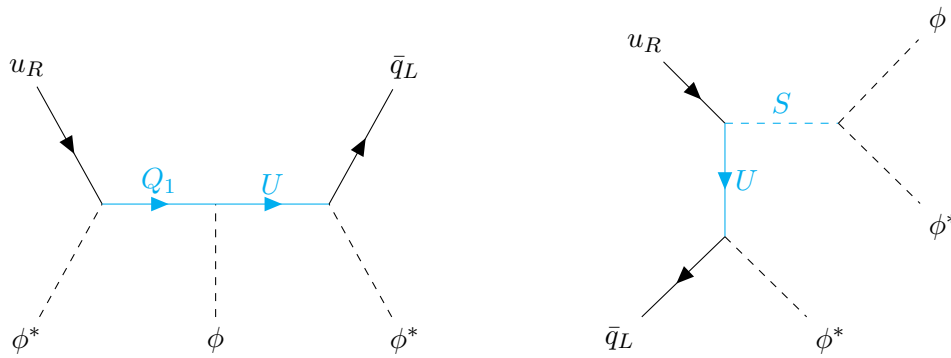


Figure 4.5: Tree level diagrams involving a pair of VLQs (left) and one VLQ and one scalar (right).

like couplings. This is a welcome attribute since the possibility of a further fourth generation of quarks, with Yukawa couplings bigger than those of the top quark, has already been excluded at LHC [52].

Another promising set of models, which should be the subject of future studies, involves one scalar and one vector-like quark. For example, a model containing the VLQ singlet $U \sim (3, 1)_{\frac{2}{3}}$ and the scalar $S \sim (1, 1)_0$ can generate the $\mathcal{O}_{u\phi}$ SMEFT operator by integrating out the cyan lines in the rightmost diagram of Figure 4.5. Such type of model, using a Vector-like lepton instead of a quark, was shown to result in up to $O(10)$ deviations of the electron Yukawa coupling [11]; these deviations are expected to be detectable at the FCC-ee.

4.2.1 Motivation for the use of vector-like quarks

Vector-like Quarks often appear in models aiming to address the open questions within the Standard Model [53,54]. For example, they appear in Composite Higgs models [55–57], Little Higgs models [58], the Left-Right Mirror Model [59], Top Colour [60, 61] and in solutions to the Strong CP problem without the use of axions [62, 63].

The focus of the thesis, thought of as a continuation of the work started in [64], will be on the VLQs themselves, without addressing the above models. In particular, the study of VLQs here is performed in the context of enhancing the light quark Yukawa couplings.

4.2.2 Lagrangian description

The entire New Physics Lagrangian introduced by [51] involving all seven VLQs reads

$$\mathcal{L}_{NP} = \mathcal{L}_{SM} + \mathcal{L}_{NP}^{quad} + \mathcal{L}_{NP}^{int}, \quad (4.11)$$

where the NP contributions have been split into two terms. The first, \mathcal{L}_{NP}^{quad} contains the kinetic and massive term for the VLQs. The interactions with the gauge bosons can be read here; since there are no triplets in the SM, the expression of the covariant derivative and the interactions with the W^\pm and Z bosons of the triplets T_1 and T_2 are reported in Appendix B. In general, this term is written as

$$\mathcal{L}_{NP}^{quad} = \sum_{\psi} (\bar{\psi} i \not{D} \psi - M_{\psi} \bar{\psi} \psi). \quad (4.12)$$

Field	Charges			
	$-\frac{4}{3}$	$-\frac{1}{3}$	$\frac{2}{3}$	$\frac{5}{3}$
U	-	-	U	-
D	-	D	-	-
Q_1	-	B	T	-
Q_5	Y	B	-	-
Q_7	-	-	T	X
T_1	$T_1^{-4/3}$	$T_1^{-1/3}$	$T_1^{2/3}$	-
T_2	-	$T_2^{-1/3}$	$T_2^{2/3}$	$T_2^{5/3}$

Table 4.3: Electric charge assignments for the components of the different VLQs being studied.

The last term in Equation (4.11) instead contains the Yukawa-like interactions of the VLQs with other terms.

$$\begin{aligned}
-\mathcal{L}_{NP}^{int} = & [\lambda_U]_r \bar{U}_R \tilde{\phi}^\dagger q_{Lr} + [\lambda_D]_r \bar{D}_R \phi^\dagger q_{Lr} + \\
& + [\lambda_{Q_1}^u]_r \bar{Q}_{1L} \tilde{\phi} u_{Rr} + [\lambda_{Q_1}^d]_r \bar{Q}_{1L} \phi d_{Rr} + [\lambda_{Q_5}]_r \bar{Q}_{5L} \tilde{\phi} d_{Rr} + [\lambda_{Q_7}]_r \bar{Q}_{7L} \phi u_{Rr} + \\
& + [\lambda_{T_1}]_r \bar{T}_{1R}^j \phi^\dagger \frac{\sigma^j}{2} q_{Lr} + [\lambda_{T_2}]_r \bar{T}_{2R}^j \tilde{\phi}^\dagger \frac{\sigma^j}{2} q_{Lr} + \\
& + \lambda_{UQ_1} \bar{U}_L \tilde{\phi}^\dagger Q_{1R} + \lambda_{DQ_1} \bar{D}_{1L} \phi^\dagger Q_{1R} + \lambda_{UQ_7} \bar{U}_L \phi^\dagger Q_{7R} + \lambda_{DQ_5} \bar{D}_L \tilde{\phi}^\dagger Q_{5R} + \\
& + \lambda_{T_1 Q_1} \bar{T}_{1L}^j \phi^\dagger \frac{\sigma^j}{2} Q_{1Rs} + \lambda_{T_1 Q_5} \bar{T}_{1L}^j \tilde{\phi}^\dagger \frac{\sigma^j}{2} Q_{5R} + \lambda_{T_2 Q_1} \bar{T}_{2L}^j \tilde{\phi}^\dagger \frac{\sigma^j}{2} Q_{1R} + \lambda_{T_2 Q_7} \bar{T}_{2L}^j \phi^\dagger \frac{\sigma^j}{2} Q_{7R} + \text{h.c.} .
\end{aligned} \tag{4.13}$$

The first three lines describe the interactions of the SM quarks with the VLQ singlets, doublets and triplets respectively; the last two lines contain the eight interactions that identify the models in Table 4.2.

We assume that only one generation of VLQs is present and that they couple to only one generation of SM quarks, either the first or the second ($r = 1, 2$).

The Feynman rules associated with such Yukawa-like interactions are written in Appendix C.1.

For future reference, the components of the VLQs and their charges under $U(1)_Y$ are reported in Table 4.3. Besides the usual quark electric charges $+2/3$ and $-1/3$, both the triplets and the Q_5 and Q_7 doublets introduce states with two new charges, $-4/3$ and $5/3$.

In the next two chapters, the eight models will be studied individually, performing first a matching onto the Warsaw SMEFT basis and then using these results to extract bounds on the VLQ couplings. Prompted by the recent ATLAS publication on the search for pair-produced VLQs at LHC [26], in Chapter 7 the branching ratios for the VLQ decay modes will be studied.

Chapter 5

Matching

At the beginning of the previous Chapter, it was shown how the introduction of the SMEFT operators $\mathcal{O}_{u\phi}$ and $\mathcal{O}_{d\phi}$ modifies the couplings of the quarks to the Higgs boson and a set of New Physics models that allow such operators to arise was identified. However, these two operators are not the only ones that can arise: already at the tree level several other SMEFT operators appear.

Recalling that the goal is to see how big the κ_q modifier can be made, it is important to first of all find its expression in terms of the NP parameters (masses of the VLQs and their couplings to the SM quarks and between themselves) and to have a way to associate a numerical value to such parameters. This is achieved via the following steps:

1. Identifying the relevant SMEFT operators that are obtained by integrating out the VLQs for each model;
2. Expressing the corresponding Wilson coefficients in terms of the NP parameters through a matching procedure;
3. Using ElectroWeak Precision Observables and Higgs Physics data to obtain bounds on the Wilson coefficients, that can then be translated in the NP parameters. The study of Flavour Changing Neutral Currents would allow to extract bounds from Flavour Physics; however, given that the VLQs in our models only couple to either the first or the second generation quarks but never both at the same time, only very weak bounds can be extracted from Flavour Physics for the VLQ models. More details are in Appendix D.

Starting from the first point, a SMEFT operator is relevant for this discussion if its presence can affect the Higgs or ElectroWeak observables used as bounds: the operators of interest are reported in Table 5.1. How SMEFT operators

		Tree Level		One-Loop			
		$\psi^2\phi^3$	$\psi^2\phi^2D$	$X^2\phi^2$		ϕ^4D^2	
$\mathcal{O}_{u\phi}$	$(\phi^\dagger\phi)(\bar{q}_L\tilde{\phi}u_R)$	$\mathcal{O}_{\phi q}^{(1)}$	$(\phi^\dagger i\overleftrightarrow{D}_\mu\phi)(\bar{q}_L\gamma^\mu q_L)$	$\mathcal{O}_{\phi G}$	$(\phi^\dagger\phi)(G_{\mu\nu}^A G^{A\mu\nu})$	$\mathcal{O}_{\phi\Box}$	$(\phi^\dagger\phi)\Box(\phi^\dagger\phi)$
$\mathcal{O}_{d\phi}$	$(\phi^\dagger\phi)(\bar{q}_L\phi d_R)$	$\mathcal{O}_{\phi q}^{(3)}$	$(\phi^\dagger iD_\mu^J\phi)(\bar{q}_L\sigma^J\gamma^\mu q_L)$	$\mathcal{O}_{\phi W}$	$(\phi^\dagger\phi)(W_{\mu\nu}^J W^{J\mu\nu})$	$\mathcal{O}_{\phi D}$	$ \phi^\dagger D^\mu\phi ^2$
-	-	$\mathcal{O}_{\phi u}$	$(\phi^\dagger i\overleftrightarrow{D}_\mu\phi)(\bar{u}_R\gamma^\mu u_R)$	$\mathcal{O}_{\phi B}$	$(\phi^\dagger\phi)(B_{\mu\nu}B^{\mu\nu})$	-	-
-	-	$\mathcal{O}_{\phi d}$	$(\phi^\dagger i\overleftrightarrow{D}_\mu\phi)(\bar{d}_R\gamma^\mu d_R)$	$\mathcal{O}_{\phi WB}$	$(\phi^\dagger\sigma^J\phi)(B_{\mu\nu}W^{J\mu\nu})$	-	-
-	-	$\mathcal{O}_{\phi ud}$	$(\tilde{\phi}^\dagger iD_\mu\phi)(\bar{u}_R\gamma^\mu d_R)$	-	-	-	-

Table 5.1: Operators in the Warsaw basis of interest for the experimental tests. The operator in grey only arises in the models involving the Q_1 doublet. By definition, $\phi^\dagger\overleftrightarrow{D}_\mu\phi = \phi^\dagger(D_\mu\phi) - (D_\mu\phi)^\dagger\phi$ and $\phi^\dagger\overleftrightarrow{D}_\mu^J\phi = \phi^\dagger\sigma^J(D_\mu\phi) - (D_\mu\phi)^\dagger\sigma^J\phi$.

Operator	Wilson Coefficient
$[\mathcal{O}_{u\phi}]_{rp}$	$\frac{1}{2M_U^2} [\lambda_U^*]_r [\lambda_U]_k [y_u]_{kp} + \frac{1}{2M_{Q_1}^2} [y_u]_{rk} [\lambda_{Q_1}^u]_k^* [\lambda_{Q_1}^u]_p - \frac{1}{M_{Q_1} M_U} [\lambda_U]_r^* [\lambda_{UQ_1}] (\lambda_{Q_1}^u)_p$
$[\mathcal{O}_{d\phi}]_{rp}$	$\frac{1}{2M_{Q_1}^2} [y_d]_{rk} [\lambda_{Q_1}^d]_k^* [\lambda_{Q_1}^d]_r$
$[\mathcal{O}_{\phi q}^{(1)}]_{rp}$	$\frac{1}{4M_U^2} [\lambda_U]_r^* [\lambda_U]_p$
$[\mathcal{O}_{\phi q}^{(3)}]_{rp}$	$-\frac{1}{4M_U^2} [\lambda_U]_r^* [\lambda_U]_p$
$[\mathcal{O}_{\phi u}]_{rp}$	$-\frac{1}{2M_{Q_1}^2} [\lambda_{Q_1}^u]_p [\lambda_{Q_1}^u]_r^*$
$[\mathcal{O}_{\phi d}]_{rp}$	$\frac{1}{2M_{Q_1}^2} [\lambda_{Q_1}^d]_p [\lambda_{Q_1}^d]_r^*$
$[\mathcal{O}_{\phi ud}]_{rp}$	$\frac{1}{M_{Q_1}^2} [\lambda_{Q_1}^u]_r^* [\lambda_{Q_1}^d]_p$

Table 5.2: Tree level matching results for Model 1.

can affect Higgs and Electroweak Observables will be seen in greater detail in Chapter 6, though some points will be mentioned in this Chapter to motivate the interest in the operators of Table 5.1.

The focus of this chapter is on the matching. It is performed in the following manner:

- For the tree level generated operators, the results by [51] are checked against the output of the MATHEMATICA [65] package Matchete¹ [66];
- For the one-loop operators, the Matchete results are cross-checked against the ones provided by SOLD² [67]. An exception is made for the operators $\mathcal{O}_{\phi D}$ and $\mathcal{O}_{\phi \square}$ which are not included in the current release of SOLD. These are computed explicitly for each of the eight models. Additionally, for Model 1 also the coefficients for the four $X^2\phi^2$ operators of interest will be computed.

Given the length of the coefficients' expressions after the matching, they will not all be explicitly written out. The results of the tree level matching are always reported, as well as the expressions and some details regarding their calculation for $\mathcal{C}_{\phi D}$ and $\mathcal{C}_{\phi \square}$. For Model 1, also the coefficients for the operators of the class $X^2\phi^2$ are presented. The generation indices are dropped.

5.1 Model 1: $Q_1 + U$

In the first model, the interactions of the VLQs with the Higgs boson and the SM quarks are described by the following Lagrangian density,

$$-\mathcal{L}_{NP, M.1}^{int} = [\lambda_U]_r \bar{U}_R \tilde{\phi}^\dagger q_{Lr} + [\lambda_{Q_1}^u]_r \bar{Q}_{1L} \tilde{\phi} u_{Rr} + [\lambda_{Q_1}^d]_r \bar{Q}_{1L} \phi d_{Rr} + \lambda_{UQ_1} \bar{U}_L \tilde{\phi}^\dagger Q_{1R} + \text{h.c.} \quad (5.1)$$

The results of the tree-level matching are reported in Table 5.2. Notice the dependence on the Yukawa couplings of the first two Wilson coefficients: given the interest in studying the light quark Yukawa couplings, they are set to zero.

¹Matchete (Matching Effective Theories Efficiently) allows to perform tree-level and one-loop matching to dimension six operators in the Warsaw basis. The user provides the gauge groups, the particle content, the masses and the couplings of the theory and the Lagrangian of the UV model.

²SOLD (SMEFT One Loop Dictionary) is another MATHEMATICA which only requires as an input the name of the fields and their charges under the SM gauge group and performs the one-loop matching to a specified Warsaw basis operator.

This means that the expressions for the κ_q modifiers for Model 1 are:

$$[\mathcal{C}_{u\phi}]_{ii} = -\frac{1}{M_{Q_1} M_U} [\lambda_U]_i^* [\lambda_{Q_1}^u]_i \lambda_{UQ_1} \Rightarrow \kappa_{u_i} = 1 + \frac{v^3}{\sqrt{2} m_{u_i} M_{Q_1} M_U} [\lambda_U]_i^* [\lambda_{Q_1}^u]_i \lambda_{UQ_1}, \quad (5.2)$$

$$[\mathcal{C}_{d\phi}]_{ii} = 0 \Rightarrow \kappa_{d_i} = 1. \quad (5.3)$$

From the expression for κ_{u_i} , it becomes clear why models involving pairs of VLQs are so interesting for the study of the Yukawa couplings enhancement: they provide an unsuppressed contribution to the coupling modifiers.

As for the remaining operators in Table 5.2, they are associated with deviations of the quark couplings to the gauge bosons and are therefore constrained by ElectroWeak Precision Observables (Section 6.1.1).

5.1.1 $\phi^4 D^2$ class operators

The first pair of one-loop-generated operators to be considered are $\mathcal{O}_{\phi D}$ and $\mathcal{O}_{\phi\Box}$. These operators are relevant for the Higgs and the Electroweak fit. Indeed, they modify the Higgs kinetic term and a field redefinition is necessary in order to reobtain the canonical normalisation for the Higgs kinetic term,

$$\phi = \frac{1}{\sqrt{2}} \begin{pmatrix} 0 \\ (1 + \mathcal{C}_{kin}^h) h + v \end{pmatrix}, \quad \mathcal{C}_{kin}^h = \frac{v^2}{\Lambda^2} \left(\mathcal{C}_{\phi\Box} - \frac{1}{4} \mathcal{C}_{\phi D} \right). \quad (5.4)$$

The consequence of the field redefinition is that the couplings of the Higgs h to all the other SM particles are modified. The result shown in Equation (4.9) gets corrected to

$$\kappa_{q_i} = 1 + \mathcal{C}_{kin}^h - \frac{v^3}{\sqrt{2} m_{q_i}} [\mathcal{C}_{q\phi}]_{ii}. \quad (5.5)$$

In all the models considered in this thesis, \mathcal{C}_{kin}^h gets generated at one-loop level only, hence this correction is expected to be negligible compared to the tree-level contribution, which in turn is enhanced by the factor v/m_{q_i} that is large for the first and second family quarks. Additionally, one should notice that it introduces a modification to all the couplings, including the heavy fermions and massive gauge bosons that are experimentally well-determined (Figure 4.1). The tree-level definition of the κ -modifier in Equation (4.9) is used in the rest of this thesis.

As for the ElectroWeak sector, an exemplary observable which is affected by the presence of the operator $\mathcal{O}_{\phi D}$, is the T parameter [68]. The formal expression and the experimental result [69] at the m_Z scale are expressed below read

$$T = -\frac{v^2}{2\alpha_{EM}} \mathcal{C}_{\phi D}, \quad T^{exp}(m_Z) = 0.06 \pm 0.06. \quad (5.6)$$

The matching for $\mathcal{O}_{\phi D}$ and $\mathcal{O}_{\phi\Box}$ is performed by computing the four-point Higgs scattering amplitudes in the New Physics (UV) models and in the SMEFT, and then requiring the two to provide the same description [70]:

$$\mathcal{M}_{UV}^{1L} = \mathcal{M}_{EFT}^{T.L.} + \mathcal{M}_{EFT}^{1L}. \quad (5.7)$$

In the NP model, such scattering process is loop-induced, whereas in the EFT both tree level and one-loop diagrams can contribute. In particular, the Wilson coefficients of interest both appear in $\mathcal{M}_{EFT}^{T.L.}$.

There are four operators in the Green's basis [46] that can contribute to the tree-level SMEFT process, which is described by the Feynman diagram in Figure 5.1; these operators are listed in Table 5.3. Their Wilson coefficients in the Green's basis are, respectively, $\mathcal{G}_{\phi\Box}$, $\mathcal{G}_{\phi D}$, $\mathcal{G}'_{\phi D}$, and $\mathcal{G}''_{\phi\Box}$, where the choice of using \mathcal{G} highlights the fact that the matching is performed in the Green's basis. To obtain the explicit expressions for these four coefficients, Equation (5.7) will be set up for four independent external momentum configurations for the Higgs bosons. Once the expressions are

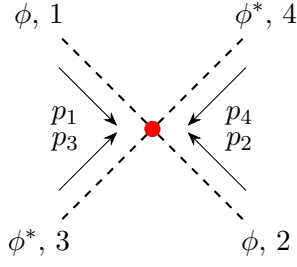
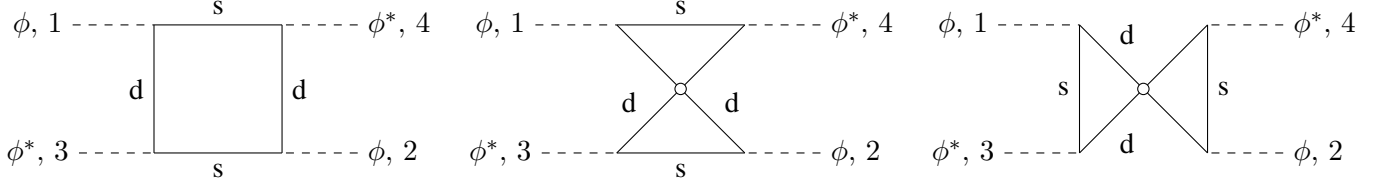


Figure 5.1: Tree level EFT diagrams.

Warsaw basis		only Green's Basis	
$\mathcal{Q}_{\phi\Box}$	$(\phi^\dagger\phi)\Box(\phi^\dagger\phi)$	$\mathcal{Q}'_{\phi D}$	$(\phi^\dagger\phi)(D_\mu\phi)^\dagger(D^\mu\phi)$
$\mathcal{Q}_{\phi D}$	$ \phi^\dagger D_\mu\phi ^2$	$\mathcal{Q}''_{\phi D}$	$(\phi^\dagger\phi)D_\mu(\phi^\dagger\overleftrightarrow{D}^\mu\phi)$

Table 5.3: Green's basis $\phi^4 D^2$ class SMEFT operators contributing at tree level to the four-point Higgs amplitude. In the first column, the two operators that also appear in the Warsaw basis are reported.Figure 5.2: The three types of UV diagrams that will be considered, by convention the external momenta are all pointing inwards. *Left*: "Box diagram", if the momentum flow is clockwise, the singlets s are of up-type (so either u_R or U), if instead the momentum flow is counter-clockwise then the singlet can only be d_R . *Center*: "Non-planar diagram type 1", if the upper line is oriented left to right, then the singlet is either u_R or U , otherwise it is d_R . *Right*: "Non-planar diagram type 2", if the rightmost vertical line is oriented upwards, the singlet is d_R , otherwise it can be either u_R or U .

found by solving the linear system with four unknowns, the transition into the Warsaw basis can be done by applying the results in Appendix B³ of [46]:

$$\mathcal{C}_{\phi\Box} = \mathcal{G}_{\phi\Box} + \frac{1}{2}\mathcal{G}'_{\phi D}, \quad (5.8)$$

$$\mathcal{C}_{\phi D} = \mathcal{G}_{\phi D}. \quad (5.9)$$

The labelling shown in Figure 5.1 is employed. The Higgs is charged under $SU(2)_L$, so the corresponding indices have to be accounted for. Two delta combinations can arise: $\delta^{13}\delta^{24}$ and $\delta^{14}\delta^{23}$, meaning that the amplitudes can be split into $\mathcal{M} = \mathcal{M}_1\delta^{13}\delta^{24} + \mathcal{M}_2\delta^{14}\delta^{23}$. To simplify the study, only the first combination is considered.

Step 1: Identifying and computing relevant UV diagrams.

The interest lies in diagrams that involve at least one vector-like quark since the ones involving only Standard Model particles would appear on both sides of (5.7) and hence cancel out.

The UV diagrams involve four fermionic propagators and are shown in Figure 5.2, going from left to right they are labelled as "box", "non-planar type 1" and "non-planar type 2" diagrams. The empty dot is used to indicate that the lines do not intersect. The doublets d available are Q_1 and q , whereas the singlets s are U , u and d . Since they have the same charges $(3, 1)_{\frac{2}{3}}$, U and u will be called up-type particles. One should notice that in the box diagram the singlets must either both be up-type or be the d quark, whereas the structure of the non-planar diagrams requires one singlet to be d and the other to be up-type. This also means that a diagram involving four VLQs can only be of box-type.

Given the interaction Lagrangian in Equation (5.1) and the SM Yukawa Lagrangian in Equation (2.10), the following particle combinations, extensively reported in Table 5.4, can be built:

1. four VLQs (two Q_1 and two U quarks is the only combination);
2. three VLQs and one SM quark. The SM quark can be the doublet q or one of the two singlets;

³Actually, the results in this thesis were found by further assuming that the other terms appearing in the expression for $\mathcal{C}_{\phi D}$ and $\mathcal{C}_{\phi\Box}$ in [46] give a subleading contribution due to the presence of the gauge couplings g_L and g_Y .

3. two VLQs and two SM quarks. Depending on whether the two VLQs are placed consecutively or not, the coupling combination associated with the diagram includes or does not include a SM Yukawa coupling;
4. one VLQ and three SM quarks. In this case there will always be a Standard Model Yukawa coupling dependence.

identifier	h. p.	l. p.	diagram	multiplicity	UV coefficient
4 heavy	$2U, 2Q_1$	0	box	1	$ \lambda_{UQ_1} ^4$
3 heavy	$2U, 1Q_1$	$1q$	box	2	$ \lambda_U ^2 \lambda_{UQ_1} ^2$
		$1u$	box	2	$ \lambda_{Q_1}^u ^2 \lambda_{UQ_1} ^2$
	$1U, 2Q_1$	$1d$	n.p. type 1	2	$ \lambda_{Q_1}^d ^2 \lambda_{UQ_1} ^2$
			n.p. type 2	2	$ \lambda_{Q_1}^d ^2 \lambda_{UQ_1} ^2$
2 heavy	$2U$	$2q$	box	1	$ \lambda_U ^4$
		$2u$	box	1	$ \lambda_{Q_1}^u ^4$
	$2Q_1$	$2d$	box	1	$ \lambda_{Q_1}^d ^4$
		$1u, 1d$	n.p. type 1	2	$ \lambda_{Q_1}^u ^2 \lambda_{Q_1}^d ^2$
			n.p. type 2	2	$ \lambda_{Q_1}^u ^2 \lambda_{Q_1}^d ^2$
		$1U, 1Q_1$	$1u, 1q$	box	4
	$1d, 1q$		n.p. type 1	4	$y_d^* \lambda_{Q_1}^d \lambda_{UQ_1}^* \lambda_U$ and $y_d^* \lambda_{Q_1}^d \lambda_{UQ_1}^* \lambda_U$
		n.p. type 2	4	$y_d^* \lambda_{Q_1}^d \lambda_{UQ_1}^* \lambda_U$ and $y_d^* \lambda_{Q_1}^d \lambda_{UQ_1}^* \lambda_U$	
1 heavy	$1Q_1$	$2u, 1q$	box	2	$ \lambda_{Q_1}^u ^2 y_u^2 $
		$2d, 1q$	box	2	$ \lambda_{Q_1}^d ^2 y_d^2 $
		$1u, 1d, 1q$	n.p. type 1	4	$y_u^* \lambda_{Q_1}^u \lambda_{Q_1}^{d*} y_d$ and $y_u \lambda_{Q_1}^{u*} \lambda_{Q_1}^d y_d^*$
	n.p. type 2		4	$y_u^* \lambda_{Q_1}^u \lambda_{Q_1}^{d*} y_d$ and $y_u \lambda_{Q_1}^{u*} \lambda_{Q_1}^d y_d^*$	
	$1U$	$2q, 1u$	box	2	$ \lambda_U ^2 y_u^2 $
		$2q, 1d$	n.p. type 1	2	$ \lambda_U ^2 y_d^2 $
n.p. type 2			2	$ \lambda_U ^2 y_d^2 $	

Table 5.4: Summary of the different contributions to the UV four-point amplitude. The heavy particle (h.p) and light particle (l.p.) content are specified, as well as the type of diagram they appear in and the total number of contributing diagrams. The various contributions to the same diagram type arise from the possibility to arrange the particles in the loops and to change the orientation of the loop momentum.

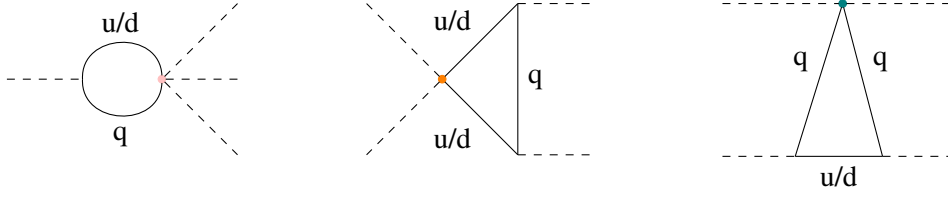


Figure 5.3: The three one-loop Feynman diagrams contributing to \mathcal{M}_{EFT}^{1L} , where one of the vertices involves a SMEFT operator from Table 5.5.

Number of particles	Type of particles	EFT operator involved	multiplicity
2	1u, 1q	$\mathcal{O}_{u\phi}$	4
	1d, 1q	$\mathcal{O}_{d\phi}$	4
3	2u, 1q	$\mathcal{O}_{\phi u}$	2
	2d, 1q	$\mathcal{O}_{\phi d}$	2
	1u, 2q	$\mathcal{O}_{\phi q}^{(1)}$	2
		$\mathcal{O}_{\phi q}^{(3)}$	4
	1d, 2q	$\mathcal{O}_{\phi q}^{(1)}$	2
		$\mathcal{O}_{\phi q}^{(3)}$	4
	1d, 1u, 1q	$\mathcal{O}_{\phi ud}$	4

Table 5.5: Summary of the one loop EFT contributions which must be accounted for, classified based on the number of particles in the loop.

Step 2: Identifying and computing relevant EFT operators.

In the Effective Field Theory calculation, the tree-level diagram in Figure 5.1 and the three different types of one-loop diagrams in Figure 5.3 are involved.

The tree level diagram receives contributions from the four operators in Table 5.3, whose Feynman rules for the $\delta^{13}\delta^{24}$ $SU(2)_L$ index contraction are summarised in Table 5.6.

As for the one-loop contributions, they can be seen as the counterparts of the UV diagrams with two and one heavy VLQs. Table 5.5 summarises the contributions to the calculation. Besides the particle content, also the type of Effective vertex and the number of independent contributions provided are listed. The Effective operators' Wilson coefficients in these cases are already known from the tree-level matching.

Step 3: Matching.

At this point four independent external momentum configurations $\mathcal{P} = (p_1, p_2, p_3, p_4)$ have to be chosen:

$$\mathcal{P}_1 = (q, -q, q, -q), \quad \mathcal{P}_2 = (q, q, -q, -q), \quad \mathcal{P}_3 = (0, 0, q, -q), \quad \mathcal{P}_4 = (q, -q, -q, q). \quad (5.10)$$

The linear system that has to be solved can be cast in the form $A_{\alpha\beta}\mathcal{G}_\beta = b_\alpha$, where the Greek indices label the different momentum configurations. $A_{\alpha\beta}$ is a 4×4 matrix, while \mathcal{G}_α and b_α are column vectors. The latter is defined as the difference between the UV and EFT one-loop amplitudes for the four momentum configurations, whereas the first two

Operator	Feynman Rule	Operator	Feynman Rule
$\mathcal{Q}_{\phi\Box}$	$-i\mathcal{G}_{\phi\Box}\left((p_1 + p_3)^2 + (p_2 + p_4)^2\right)$	$\mathcal{Q}'_{\phi D}$	$-i\mathcal{G}_{\phi D}\left(p_1 \cdot p_3 + p_2 \cdot p_4\right)$
$\mathcal{Q}_{\phi D}$	$-i\mathcal{G}'_{\phi D}\left(p_1 \cdot p_4 + p_2 \cdot p_3\right)$	$\mathcal{Q}''_{\phi D}$	$\mathcal{G}''_{\phi D}\left(p_1^2 + p_2^2 - p_3^2 - p_4^2\right)$

Table 5.6: Feynman Rules for the Green's basis operators contributing to the tree level EFT diagram.

are:

$$[A]_{\alpha\beta} = q^2 \begin{pmatrix} -8i & 2i & -2i & 0 \\ 0 & 2i & 2i & 0 \\ -2i & 0 & 0 & -2 \\ 0 & -2i & 2i & 0 \end{pmatrix}, \quad [\mathcal{G}]_{\alpha} = \begin{pmatrix} \mathcal{G}_{\phi\Box} \\ \mathcal{G}_{\phi D} \\ \mathcal{G}'_{\phi D} \\ \mathcal{G}''_{\phi D} \end{pmatrix}. \quad (5.11)$$

The final results, using Equations (5.8) and (5.9) to move from the Green's to the Warsaw basis and setting $y_u = y_d = 0$ and $M_U = M_{Q_1} = \Lambda$, are written below.

$$16\pi^2\Lambda^2\mathcal{C}_{\phi\Box} = -\frac{6}{5}|\lambda_{UQ_1}|^4 - \frac{5}{4}|\lambda_{UQ_1}|^2 \left(|\lambda_{Q_1}^d|^2 + 2|\lambda_{Q_1}^u|^2 + |\lambda_U|^2 \right) - \frac{3}{4} \left(|\lambda_{Q_1}^d|^4 + |\lambda_{Q_1}^u|^4 \right) + 2|\lambda_{Q_1}^d|^2|\lambda_{Q_1}^u|^2 - |\lambda_U|^4, \quad (5.12)$$

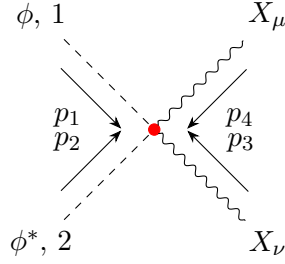
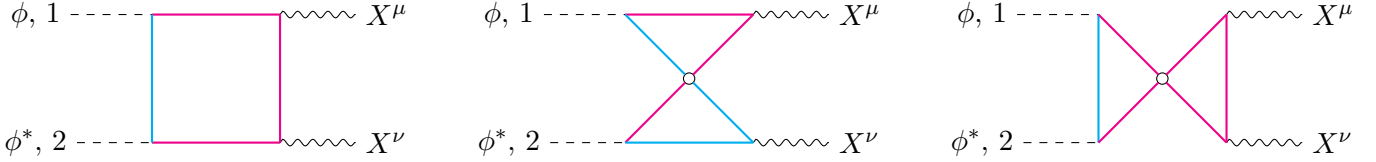
$$16\pi^2\Lambda^2\mathcal{C}_{\phi D} = -\frac{12}{5}|\lambda_{UQ_1}|^4 + \frac{5}{2}|\lambda_{UQ_1}|^2 \left(|\lambda_{Q_1}^d|^2 - |\lambda_{Q_1}^u|^2 - 2|\lambda_U|^2 \right) - 2 \left(|\lambda_{Q_1}^d|^4 + |\lambda_{Q_1}^u|^4 \right) + 4|\lambda_{Q_1}^d|^2|\lambda_{Q_1}^u|^2 - \frac{3}{2}|\lambda_U|^4. \quad (5.13)$$

The results were cross-checked with Matchete and found to be in agreement.

Before moving on to the second class of one-loop generated SMEFT operators, let us point out that the computation could have been simplified if from the start the SM Yukawa couplings had been set to zero. Indeed, only the tree-level Effective Field Theory diagram and a reduced number of UV diagrams do not carry a dependence on the SM Yukawa couplings. For the remaining seven models, this simplification will be performed right from the beginning. The masses, instead, will be kept separate, with the same mass limit taken only at the end of the matching.

Finally, it is interesting to point out that keeping the Yukawa couplings different from zero and the heavy masses to be possibly different, a consistency check can be made by requiring momentum independence to hold. Indeed, when the UV diagrams with one heavy particle and the EFT diagrams are evaluated, terms such as $\log(M_{\alpha}^2/q^2)$ and $\log(\mu^2/q^2)$ respectively appear (where $\alpha \in \{M_{Q_1}, M_U\}$). From the EFT side, the logarithm is multiplied by Wilson coefficients and SM couplings, whereas from the UV part a combination of UV and SM parameters appears. In the final expressions for the Wilson coefficients, one must be able to substitute the Wilson coefficients' expression in terms of the UV parameters and cancel out the dependence on q^2 . Indeed, q^2 serves the role of Infrared (IR) regulator and, given that the UV and Effective Theory have the same IR behaviour, it should cancel during the matching. The parameter μ which appears in the logarithm is called the renormalisation scale; it appears when loop calculations are performed within the dimensional regularisation scheme⁴. Consider for example the contributions to $\mathcal{G}_{\phi D}$ involving two down quarks d and one doublet q : from Table 5.4 there are two box diagram contributions from the UV side containing the heavy Q_1 , whereas from Table 5.5 there are two contributing EFT diagrams, both containing the operator $\mathcal{O}_{\phi d}$. The

⁴The integration over the internal virtual momentum in loop diagrams can lead to UV divergences. A renormalisation program allows to identify and remove the divergences. In dimensional regularisation, the dimension of the space being integrated over is reduced by a factor ϵ , which at the end of the calculations is sent to zero. If the dimension of the space is modified, then also the dimension of the Lagrangian density, and everything it contains, is affected (recall that, if the dimension of the space considered is d , then the Lagrangian density satisfies $[\mathcal{L}] = d$). $\mu^{\alpha\epsilon}$ terms, with α a number, are introduced in the Lagrangian to guarantee that observables, like the electric charge e , maintain their mass dimension.

Figure 5.4: Tree-level Feynman diagram generated by the operator $\mathcal{O}_{\phi X}$.Figure 5.5: The three colour-coded UV diagrams involved in the matching for the $\mathcal{O}_{\phi X}$ operators. The convention for the external momenta is that of Figure 5.4. *Left*: "Box diagram"; *Center*: "Non-planar diagram type 1"; *Right*: "Non-planar diagram type 2".

system's solution results in

$$\mathcal{G}_{\phi D} \supset \frac{N_c}{4\pi^2} \left(-\frac{1}{2M_{Q_1}^2} |y_d|^2 |\lambda_{Q_1}^d|^2 \log \left(\frac{M_{Q_1}^2}{q^2} \right) + \mathcal{C}_{\phi d} \log \left(\frac{\mu^2}{q^2} \right) \right) = \frac{N_c}{8\pi^2 M_{Q_1}^2} |y_d|^2 |\lambda_{Q_1}^d|^2 \log \left(\frac{\mu^2}{M_{Q_1}^2} \right). \quad (5.14)$$

The logarithmic dependence on the scale μ is typical of leading-log solution of the Renormalisation Group Equations, Equations (3.9) and (3.10). Indeed, what was just recovered is the $\mathcal{C}_{\phi d}$ contribution to the Renormalisation Group running of $\mathcal{C}_{\phi D}$, in agreement with the model-independent results found in reference [41]. The agreement between reference [41] and the one-loop matching serves as a further cross-check.

5.1.2 $X^2\phi^2$ class operators

Let X_μ^a be the generic gauge boson. The operator of interest can be written in the general form:

$$\mathcal{O}_{\phi X} = \left(\phi^\dagger \phi \right) \left(X^{a\mu\nu} X_{\mu\nu}^a \right), \quad (5.15)$$

where $X_{\mu\nu}^a$ is the field strength tensor associated with X_μ^a . The tree-level Feynman diagram generated by $\mathcal{O}_{\phi X}$ is shown in Figure 5.4. These operators are all relevant for Higgs physics: $\mathcal{O}_{\phi G}$ introduces a tree-level contribution to the gluon-gluon fusion production mechanism of the Higgs boson, the other three operators will appear in the modifications to the Higgs to photon-pair decay channel [71].

To perform the matching, Equation (5.7) requires the study of processes with two gauge bosons and two Higgs doublets as external states. Also, in this case, both the UV and EFT provide one-loop contributions, but only the EFT can contribute at the tree level.

From the UV point of view, the allowed diagrams involving at least one vector-like quark all contain four fermionic propagators; depending on the arrangement of the propagators, the diagrams of Figure 5.5 will be labelled as "box", "non-planar type 1" and "non-planar type 2" (from left to right). While in the previous study of $\mathcal{O}_{\phi D}$ and $\mathcal{O}_{\phi \square}$ there was a great number of possible particle arrangements in the loops, here the presence of the gauge bosons in two vertices sets a constraint: in such vertices the incoming and the outgoing quarks must be the same. This was colour-coded in Figure 5.5.

To see this, one should recall that the interaction between gauge bosons and quarks is picked up from the quark kinetic

Identifier	h.p.	l.p.	Diagram type	Multiplicity
4 heavy	$1 U, 3 Q_1$	0	box + non-planar 2	1+1
	$3 U, 1 Q_1$	0	box + non-planar 2	1+1
	$2 U, 2 Q_1$	0	non-planar 1	2
3 heavy	$3 U$	$1 q_L$	box + non-planar 2	1+1
	$3 Q_1$	$1 u_R$	box + non-planar 2	1+1
		$1 d_R$	box + non-planar 2	1+1
2 heavy	$2 U$	$2 q_L$	non-planar 1	2
	$2 Q_1$	$2 u_R$	non-planar 1	2
		$2 d_R$	non-planar 1	2
1 heavy	$1 U$	$3 q_L$	box + non-planar 2	1+1
	$1 Q_1$	$3 d_R$	box + non-planar 2	1+1
		$3 u_R$	box + non-planar 2	1+1

Table 5.7: UV diagram contributions. All of these contributions are relevant in the matching for the $\mathcal{C}_{\phi G}$ and $\mathcal{C}_{\phi B}$ coefficients, the diagrams in which a singlet would have to interact with a weak gauge boson X_μ^J must be removed when dealing with the SMEFT operators $\mathcal{O}_{\phi W}$ and $\mathcal{O}_{\phi WB}$.

term. If ψ denotes the generic quark, its kinetic term is:

$$\mathcal{L}_{kin}^\psi = \bar{\psi} i \gamma^\mu (\partial_\mu + i g_s T^A G_\mu^A + i g_L \tau^a W_\mu^a + i g_Y Y_\psi B_\mu) \psi.$$

The resulting Feynman rules are reported in Appendix C.2. The allowed combinations are then summarised in Table 5.7: considering that all the quarks couple to B_μ and G_μ^A while the singlets do not interact with the weak bosons W_μ^J , for $\mathcal{C}_{\phi G}$ and $\mathcal{C}_{\phi B}$ all the contributions in Table 5.7 contribute, while six less need to be computed for $\mathcal{C}_{\phi BW}$ and ten less for $\mathcal{C}_{\phi W}$. This will be addressed in more detail in the relevant sections.

As for the EFT contributions, the tree-level operators will be dealt with individually in the appropriate subsections; the one-loop contributions are shown explicitly for the first operator. For the other three cases, it is sufficient to replace the Gluon with the gauge boson of interest.

Considering that the gauge bosons are massless and the presence of the polarisation vectors, some simplifications can be made. Using the momentum labelling in Figure 5.4, these simplifications are defined as:

- kinematic simplification: $p_3^2 = 0$ and $p_4^2 = 0$;
- transversality simplification: $p_3 \cdot \epsilon_3 = \epsilon_4 \cdot p_4 = 0$.

Finally, the transformation from the Green's to the Warsaw basis is trivial for the coefficients in the $X^2 \phi^2$ class [46]:

$$\mathcal{C}_{\phi X} = \mathcal{G}_{\phi X}. \quad (5.16)$$

Even though there might be more than one operator contributing to the tree-level process, the solution of the linear system constructed by picking different external momentum configurations already supplies the Wilson coefficient in the Warsaw basis.

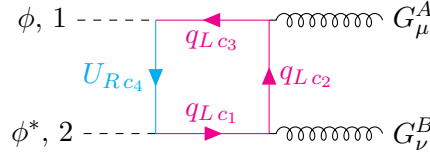
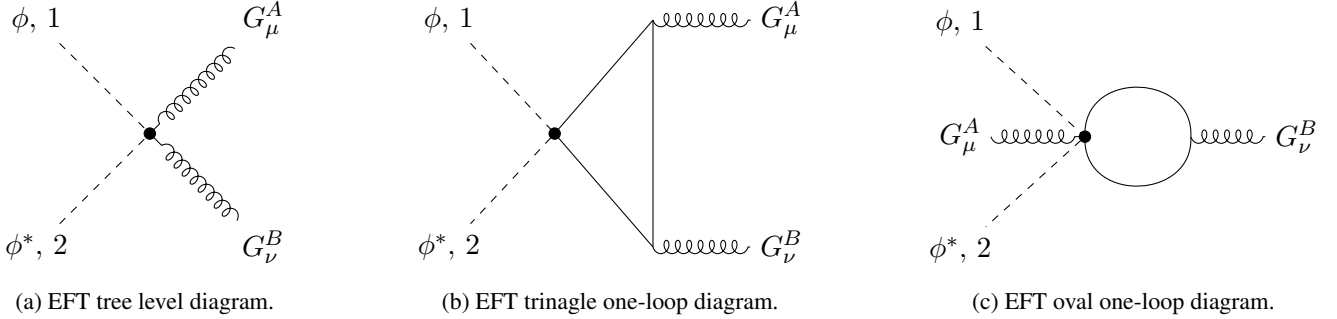


Figure 5.6: UV box diagram involving one VLQ where the colour indices have been explicitly written out.

Figure 5.7: Feynman diagrams with EFT vertices which could contribute to the matching of $\mathcal{C}_{\phi G}$. A fourth diagram can be obtained from the third by exchanging the two gluons. In the one-loop diagrams, the internal momenta can oriented clockwise or counter-clockwise.

5.1.2.1 Operator $\mathcal{O}_{\phi G}$

The first case to be studied is the operator $\mathcal{O}_{\phi G}$, which appears in the Lagrangian density as:

$$\mathcal{L}_{SMEFT} \supset \mathcal{C}_{\phi G} \mathcal{O}_{\phi G} = \mathcal{C}_{\phi G} (\phi^\dagger \phi) (G_{\mu\nu}^A G^{A\mu\nu}). \quad (5.17)$$

UV diagrams.

The UV diagrams in Table 5.7 are all involved since every quark can interact with the Gluons.

Gellmann matrices are present in the Gluon vertices, so it is of interest to study the colour index contractions⁵. In all three types of UV diagrams, the contraction results in a factor $\frac{1}{2}\delta^{AB}$. For example, the Feynman diagram in Figure 5.6 was obtained by specifying the colour indices of the quarks in the loop; the index contraction is performed as follows:

$$\delta_{c_1 c_4} \delta_{c_4 c_3} \frac{\lambda_{c_3 c_2}^A}{2} \frac{\lambda_{c_2 c_1}^B}{2} = \text{Tr} \left[\frac{\lambda^A}{2} \frac{\lambda^B}{2} \right] = \frac{1}{2} \delta^{AB}. \quad (5.18)$$

EFT diagrams

The EFT diagrams that can contribute to the matching of $\mathcal{C}_{\phi G}$ are shown in Figure 5.7, they are:

- The tree level diagram in Figure 5.7a, which is associated with the UV diagrams with four heavy VLQs whose propagators have been shrunk to a point. There is only one SMEFT operator in the Green's basis that can generate such diagram, which is the operator of interest $\mathcal{O}_{\phi G}$;
- The one-loop diagram in Figure 5.7b, that involves three SM quark propagators and an EFT vertex containing two quarks and two Higgs doublets. Its UV counterpart are the diagrams with one heavy VLQ;
- Finally, the UV diagrams involving two heavy particles have as EFT counterpart the diagram in Figure 5.7c. In this case the Effective vertex involves two Higgs doublets, a gluon and two SM quarks.

Considering both one-loop diagrams, all the operators in Table 5.8 can contribute. The colour cyan is used to highlight the operators that, once the SM equations of motion are used to go to the Warsaw basis, are no longer present. It turns out that the knowledge of the expressions for the Wilson coefficients associated to the operators in Table 5.8 is

Operator	Definition	Operator	Definition
$O_{\phi q}^{(1)}$	$\left(\phi^\dagger i \overleftrightarrow{D}_\mu \phi \right) (\bar{q}_L \gamma^\mu q_L)$	$O_{\phi u}$	$\left(\phi^\dagger i \overleftrightarrow{D}_\mu \phi \right) (\bar{u}_R \gamma^\mu u_R)$
$O'_{\phi q}{}^{(1)}$	$(\phi^\dagger \phi) \left(\bar{q}_L i \overleftrightarrow{\not{D}} q_L \right)$	$O'_{\phi u}$	$(\phi^\dagger \phi) \left(\bar{u}_R i \overleftrightarrow{\not{D}} u_R \right)$
$O_{\phi q}^{(3)}$	$\left(\phi^\dagger i D_\mu^j \phi \right) (\bar{q}_L \sigma^j \gamma^\mu q_L)$	$O_{\phi d}$	$\left(\phi^\dagger i \overleftrightarrow{D}_\mu \phi \right) (\bar{d}_R \gamma^\mu d_R)$
$O'_{\phi q}{}^{(3)}$	$(\phi^\dagger \sigma^j \phi) \left(\bar{q}_L i \overleftrightarrow{\not{D}}^j q_L \right)$	$O'_{\phi d}$	$(\phi^\dagger \phi) \left(\bar{d}_R i \overleftrightarrow{\not{D}} d_R \right)$

Table 5.8: Dimension six operators involved in the EFT computation for the $\mathcal{C}_{\phi G}$ matching in the Green's basis. The cyan ones appear only in the Greens' basis.

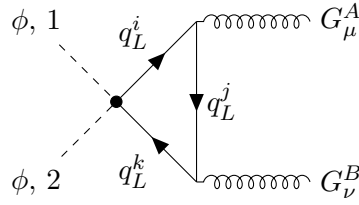


Figure 5.8: EFT triangle diagram involving the operator $\mathcal{O}_{\phi q}^{(3)}$ with explicit weak structure.

not required: the combination of the kinematic and transversality simplifications, of the weak index contraction and of the fact that the diagrams appear in pairs with different internal momenta leads to having an overall null one-loop contribution from the Effective theory side.

The Wilson coefficient, setting the Yukawa matrices to be zero and the masses of the VLQs to be the same Λ , is

$$16\pi^2 \Lambda^2 \mathcal{C}_{\phi G} = \frac{g_s^2}{6} \left(|\lambda_{Q_1}^d|^2 + |\lambda_{Q_1}^u|^2 + |\lambda_U|^2 - 2|\lambda_{UQ_1}|^2 \right). \quad (5.19)$$

Before moving on to the next operator, an example of how also index contractions can reduce the number of involved diagrams is shown. Weak index contraction shows that $\mathcal{O}_{\phi q}^{(3)}$ gives a null contribution: using as reference the diagram in Figure 5.8 and the Feynman Rules reported in Appendix C.3, weak index contraction leads to

$$\sigma_{21}^j \sigma_{ik}^j \delta_{ij} \delta_{jk} = (2\delta_{2k} \delta_{1i} - \delta_{12} \delta_{ik}) \delta_{ij} \delta_{jk} = 2\delta_{2j} \delta_{1j} - \delta_{12} \delta_{jj} = 2\delta_{12} - 2\delta_{12} = 0. \quad (5.20)$$

Operator	Category	Definition	Feynman Rule after Transversality and Kinematics
$\mathcal{O}_{\phi B}$	$X^2 \phi^2$	$(\phi^\dagger \phi) B_{\mu\nu} B^{\mu\nu}$	$4i\mathcal{C}_{\phi G} (p_4^\nu p_3^\mu - p_3 \cdot p_4 g^{\mu\nu})$
$\mathcal{O}_{BD\phi}$	$\phi^2 X D^2$	$\partial_\nu B^{\mu\nu} \left(i\phi^\dagger \overleftrightarrow{D}_\mu \phi \right)$	0
$\mathcal{O}_{D\phi}$	$\phi^2 D^4$	$(D_\mu D^\mu \phi)^\dagger (D_\nu D^\nu \phi)$	$iY_\phi^2 g_Y^2 \mathcal{G}_{D\phi} (g^{\mu\nu} (p_1^2 + p_2^2) - 4(p_2^\nu p_1^\mu + p_2^\mu p_1^\nu))$

Table 5.9: Green's basis operators contributing to the tree level EFT diagram for the matching of $\mathcal{O}_{\phi B}$. The first one is also present in the Warsaw basis.

5.1.2.2 Operator $\mathcal{O}_{\phi B}$

From the UV point of view, all the contributions in Table 5.7 appear. The only difference with respect to the previous case is that instead of a Gell-Mann matrix, the hypercharge of the quarks entering and exiting is picked up at the interaction vertex (for the Feynman rule of quark interactions with the B_μ boson, see Appendix C.2).

Moving to the EFT side, the tree level diagram in Figure 5.4 with $X_\mu = B_\mu$ can be generated by the three operators in Table 5.9. The first one belongs to the Warsaw basis, the other two appear in the Green's basis⁶. Besides the name and definition of the operators, also the Feynman rules are listed.

Transversality and kinematic simplifications allow us to recognize that the contribution of the $\mathcal{O}_{BD\phi}$ operator is null. Let us show this: first of all, pick up the two B_μ contributions,

$$\mathcal{O}_{BD\phi} = \partial_\nu B^{\mu\nu} \left(i\phi^\dagger \overleftrightarrow{D}_\mu \phi \right) \supset \partial_\nu (\partial^\mu B^\nu - \partial^\nu B^\mu) i \left(2i\phi^\dagger B_\mu \phi \right).$$

At this point, notice that the two derivatives act on the same gauge boson field, therefore only the following combinations are generated when moving to momentum space:

$$\underbrace{p_3^\mu p_3^\nu, p_4^\mu p_4^\nu}_{\text{contribution vanishes due to transversality}}, \quad \underbrace{p_4^2 g^{\mu\nu} \ \& \ p_3^2 g^{\mu\nu}}_{\text{contribution vanishes due to kinematics}}. \quad (5.21)$$

So a two-equation system has to be set up and solved.

The EFT one-loop diagrams can be recovered by Figure 5.7 by substituting the gluons with B_μ bosons, the involved operators are still those listed in Table 5.8.

The final expression for the Wilson coefficient associated with $\mathcal{O}_{\phi B}$ is

$$16\pi^2 \Lambda^2 \mathcal{C}_{\phi B} = g_Y^2 \left(\frac{1}{36} |\lambda_{Q_1}^d|^2 + \frac{5}{18} |\lambda_{Q_1}^u|^2 + \frac{5}{72} |\lambda_U|^2 - \frac{143}{360} |\lambda_{UQ_1}|^2 \right). \quad (5.22)$$

The masses of the VLQ were set to be the same and the Yukawa matrices were set to zero from the beginning.

⁶The first B_μ boson is picked up from the field strength term, the second comes from the Higgs doublet's covariant derivative

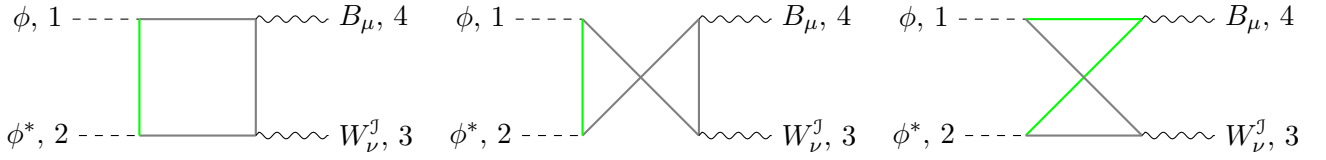


Figure 5.9: Allowed singlet (green) and doublet (grey) arrangements in the UV one-loop diagrams involving two Higgs doublets, one B and one W^J gauge bosons.

Identifier	h.p.	l.p.	Diagram type	Multiplicity	
4 heavy	$1U, 3Q_1$	0	box + non planar 1	1+1	
	$2U, 2Q_1$	0	non planar 2	1	
3 heavy	$3Q_1$	$1u_R$	box + non planar 1	1+1	
		$1d_R$	box + non planar 1	1+1	
2 heavy	$2Q_1$	$2U$	$2q_L$	non planar 2	1
		$2u_R$	non planar 2	1	
			non planar 2	1	
		$2d_R$	non planar 2	1	
non planar 2	1				
1 heavy	$1U$	$3q_L$	box + non planar 1	1+1	

Table 5.10: UV diagram contributions to the matching of the $\mathcal{O}_{\phi WB}$ operator.

5.1.2.3 Operator $\mathcal{O}_{\phi WB}$.

The matching of the NP model to the operator $\mathcal{O}_{\phi WB}$ is the only case in which two different gauge bosons are involved. As shown in Figure 5.9, in the UV one-loop diagrams the presence of one vertex involving W^J_μ , which only couples to the doublets, constrains the particles' placement in the loops. The final counting of the UV contributions is summarised in Table 5.10.

As for the EFT side, there are a total number of four Green's operators which can provide the fields of interest. The different contributions are listed in Table 5.11, along with their Feynman rules after accounting for kinematic and transversality constraints.

The final expression for the Wilson coefficient in the same mass limit is:

$$16\pi^2\Lambda^2\mathcal{C}_{\phi WB} = -g_L g_Y \left(\frac{1}{12} |\lambda_{Q_1}^d|^2 + \frac{1}{6} |\lambda_{Q_1}^u|^2 + \frac{1}{4} |\lambda_U|^2 - \frac{19}{60} |\lambda_{UQ_1}|^2 \right). \quad (5.23)$$

Operator	Category	Definition	Feynman Rule after kinematics and transversality
$\mathcal{O}_{\phi WB}$	$X^2\phi^2$	$(\phi^\dagger \sigma^J \phi) (W^J_{\mu\nu} B^{\mu\nu})$	$2i\mathcal{C}_{\phi WB}(p_3^\mu p_4^\nu - p_3 \cdot p_4 g^{\mu\nu})\sigma^J$
$\mathcal{O}_{WD\phi}$	$\phi^2 X D^2$	$D_\nu W^J{}^{\mu\nu} (\phi^\dagger \overset{\leftrightarrow}{D}{}^J{}_\mu \phi)$	0
$\mathcal{O}_{BD\phi}$	$\phi^2 X D^2$	$\partial_\nu B^{\mu\nu} (\phi^\dagger \overset{\leftrightarrow}{D}{}_\mu \phi)$	0
$\mathcal{O}_{D\phi}$	$\phi^2 D^4$	$(D_\mu D^\mu \phi)^\dagger (D_\nu D^\nu \phi)$	$i g_L g_Y Y_\phi \mathcal{S}_{D\phi} ((p_1^2 + p_2^2) g^{\mu\nu} - 2(p_1^\mu p_2^\nu + p_1^\nu p_2^\mu)) \sigma^J$

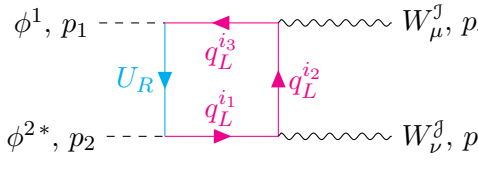
Table 5.11: EFT operators contributing to the tree-level diagram of interest for the matching of $\mathcal{O}_{\phi WB}$. All four can be found in the Green's basis, but only the first remains in the Warsaw basis after the equations of motion have been applied.

Identifier	h.p.	l.p.	Diagram type	Multiplicity
4 heavy	$1 U, 3 Q_1$	0	box + non planar 1	1+1
3 heavy	$3 Q_1$	$1 u_R$ $1 d_R$	box + non planar 1 box + non planar 1	1+1 1+1
1 heavy	$1 U$	$3 q_L$	box + non planar 1	1+1

Table 5.12: UV diagram contributions to the matching to the $\mathcal{C}_{\phi W}$ coefficient.

5.1.2.4 Operator $\mathcal{O}_{\phi W}$

Out of the four matching computations performed in this section, this one involves the least number of diagrams. Indeed, compared to the previous case the number of vertices containing W_μ^J has been increased to two. The counting is summarised in Table 5.12, from which one can appreciate how the non-planar type 2 diagrams no longer provide any contribution. Indeed, while in the other two types of UV diagrams the vertices involving the gauge bosons are connected by only one propagator, in type 2 two propagators are used to go from one gauge boson vertex to the other, passing through a Yukawa interaction vertex. Yukawa interactions in this model involve a Higgs doublet, a quark doublet and a singlet: a non-planar type 2 diagram would lead to having a singlet entering in the W^J vertex. At the interaction vertices with the W bosons, the Pauli matrices are picked up. The study of the weak index construction is more subtle in this case as two contributions, one proportional to $\delta^{J\mathcal{J}}$, the other to $\epsilon^{J\mathcal{J}\mathcal{K}}\sigma^{\mathcal{K}}$, arise.



$$\begin{aligned} \epsilon_{1i_3} \frac{\sigma_{i_3 i_2}^J}{2} \frac{\sigma_{i_2 i_1}^J}{2} \epsilon_{i_1 2} &= \epsilon_{1i_3} \left(\frac{\delta^{J\mathcal{J}}}{4} \delta_{i_1 i_3} + i \frac{\epsilon^{J\mathcal{J}\mathcal{K}}}{4} \sigma_{i_3 i_1}^{\mathcal{K}} \right) \epsilon_{i_1 2} = \\ &= -\frac{1}{4} \delta^{J\mathcal{J}} \delta_{12} + \frac{i}{4} \epsilon^{J\mathcal{J}\mathcal{K}} \sigma_{21}^{\mathcal{K}}. \end{aligned} \quad (5.24)$$

However, the Feynman rule obtained for the operator $\mathcal{O}_{\phi W}$, Table 5.13, only contains a term proportional to $\delta^{J\mathcal{J}}$. This motivates the further simplification⁷ of keeping only terms proportional to $\delta^{J\mathcal{J}}$.

From the EFT side, three operators in the Green's basis can contribute to the tree-level diagram.

Once the presence of the transversality and kinematic constraints are accounted for, the expression for the Wilson coefficient is found to be.

$$16\pi^2 \Lambda^2 \mathcal{C}_{\phi W} = g_L^2 \left(\frac{1}{8} |\lambda_U|^2 - \frac{7}{40} |\lambda_{U Q_1}|^2 \right). \quad (5.25)$$

Operator	Category	Definition	Feynman Rules after transversality and kinematics
$\mathcal{O}_{\phi W}$	$X^2 \phi^2$	$(\phi^\dagger \phi)(W_{\mu\nu}^J W^{\mu\nu J})$	$4i \mathcal{C}_{\phi W} (p_3^\mu p_4^\nu - p_3 \cdot p_4 g^{\mu\nu}) \delta^{J\mathcal{J}}$
$\mathcal{O}_{WD\phi}$	$\phi^2 X D^2$	$D_\nu W^{\mu\nu J} (\phi^\dagger i \overleftrightarrow{D}_\mu^J \phi)$	0
$\mathcal{O}_{D\phi}$	$\phi^2 D^4$	$(D_\mu D^\mu \phi)^\dagger (D_\nu D^\nu \phi)$	$ig_L^2 \mathcal{G}_{D\phi} (g^{\mu\nu} (p_1^2 + p_2^2) - 4(p_2^\nu p_1^\mu + p_2^\mu p_1^\nu)) \delta^{J\mathcal{J}}$

Table 5.13: SMEFT operators contributing to the tree level EFT diagram containing two Higgs doublets and two W^J gauge bosons. All three belong to the Green's basis, but only the first remains also in the Warsaw basis. The Feynman rules being shown have already taken into account the transversality and kinematic constraints.

⁷The goal of this part of the thesis was to reproduce the results provided by the MATHEMATICA packages SOLD and Matchete, however another verification of the calculations performed here is to identify all the other contributions proportional to $\epsilon^{J\mathcal{J}\mathcal{K}}$ and verify that they cancel out in the final result.

Operator	Wilson Coefficient
$[\mathcal{O}_{u\phi}]_{rp}$	$\frac{1}{2M_{Q_1}^2} [y_u]_{rt} [\lambda_{Q_1}^u]_t^* [\lambda_{Q_1}^u]_p$
$[\mathcal{O}_{d\phi}]_{rp}$	$\frac{1}{2M_D^2} [y_d]_{kp} [\lambda_D]_k [\lambda_D]_r^* + \frac{1}{2M_{Q_1}^2} [y_d]_{rk} [\lambda_{Q_1}^d]_k^* [\lambda_{Q_1}^d]_p - \frac{1}{M_{Q_1} M_D} [\lambda_D]_r^* [\lambda_{Q_1}^d]_p \lambda_{DQ_1}$
$[\mathcal{O}_{\phi q}^{(1)}]_{rp}$	$-\frac{1}{4M_D^2} [\lambda_D]_p [\lambda_D]_r^*$
$[\mathcal{O}_{\phi q}^{(3)}]_{rp}$	$-\frac{1}{4M_D^2} [\lambda_D]_r^* [\lambda_D]_p$
$[\mathcal{O}_{\phi u}]_{rp}$	$-\frac{1}{2M_{Q_1}^2} [\lambda_{Q_1}^u]_p [\lambda_{Q_1}^u]_r^*$
$[\mathcal{O}_{\phi d}]_{rp}$	$\frac{1}{2M_{Q_1}^2} [\lambda_{Q_1}^d]_p [\lambda_{Q_1}^d]_r^*$
$[\mathcal{O}_{\phi ud}]_{rp}$	$\frac{1}{M_{Q_1}^2} [\lambda_{Q_1}^u]_r^* [\lambda_{Q_1}^d]_p$

Table 5.14: Tree level matching for Model 2.

5.2 Model 2: $Q_1 + D$

The NP interaction Lagrangian for Model 2 is given by

$$-\mathcal{L}_{NP, M.2}^{int} = [\lambda_D]_r \bar{q}_L r \phi D_R + [\lambda_{Q_1}^u]_r \bar{Q}_{1L} \tilde{\phi} u_{Rr} + [\lambda_{Q_1}^d]_r \bar{Q}_{1L} \phi d_{Rr} + \lambda_{DQ_1} \bar{Q}_{1L} \phi D_R + \text{h.c.} \quad (5.26)$$

The results of the tree-level matching are given in Table 5.14. Setting the light quark Yukawa couplings to zero, the up-type quark modifier is $\kappa_{u_i} = 1$, while for the down-sector the modifier reads

$$\kappa_{d_i} = 1 + \frac{v^3}{\sqrt{2} m_{d_i} M_D M_{Q_1}} [\lambda_D]_i^* [\lambda_{Q_1}^d]_i \lambda_{DQ_1}. \quad (5.27)$$

For the $\mathcal{C}_{\phi D}$ and $\mathcal{C}_{\phi \square}$ coefficients, accounting for the contributions in Table 5.15 where the Yukawa couplings are set to zero, one finds in the same mass limit:

$$16\pi^2 \Lambda^2 \mathcal{C}_{\phi \square} = -\frac{6}{5} |\lambda_{DQ_1}|^4 - \frac{5}{4} |\lambda_{DQ_1}|^2 \left(|\lambda_{Q_1}^u|^2 + 2|\lambda_{Q_1}^d|^2 + |\lambda_D|^2 \right) - \frac{3}{4} \left(|\lambda_{Q_1}^d|^4 + |\lambda_{Q_1}^u|^4 \right) - 2|\lambda_{Q_1}^u|^2 |\lambda_{Q_1}^d|^2 - |\lambda_D|^4, \quad (5.28)$$

$$16\pi^2 \Lambda^2 \mathcal{C}_{\phi D} = -\frac{12}{5} |\lambda_{DQ_1}|^4 + \frac{5}{2} |\lambda_{DQ_1}|^2 \left(|\lambda_{Q_1}^u|^2 - |\lambda_{Q_1}^d|^2 - 2|\lambda_D|^2 \right) - 2 \left(|\lambda_{Q_1}^d|^4 + |\lambda_{Q_1}^u|^4 \right) + 4|\lambda_{Q_1}^u|^2 |\lambda_{Q_1}^d|^2 - \frac{3}{2} |\lambda_D|^4. \quad (5.29)$$

Identifier	h. p.	l. p.	diagram	multiplicity	Identifier	h. p.	l. p.	diagram	multiplicity
4 heavy	$2D, 2Q_1$	0	box	1	2 heavy	$2D$	$2q$	box	1
	$2D, 1Q_1$	$1q$	box	2		$2u$	box	1	
3 heavy	$1D, 2Q_1$	$1d$	box	2		$2Q_1$	$2d$	box	1
		$1u$	n.p. type 1	2		$1u, 1d$	n.p. type 1	2	
			n.p. type 2	2		n.p. type 2	2		

Table 5.15: Summary of the different contributions accounted for in the UV diagrams for the matching of $\mathcal{O}_{\phi D}$ and $\mathcal{O}_{\phi \square}$ of Model 2, organised based on the number and type of heavy particles (h.p.) present and the type of light particles (l.p.). As for Model 1, the UV diagrams can be a box or the two types of non-planar (n.p.) diagrams.

Operator	Wilson Coefficient
$[\mathcal{O}_{u\phi}]_{rp}$	$\frac{1}{2M_{Q_7}^2} [y_u]_{rs} [\lambda_{Q_7}]_s^* [\lambda_{Q_7}]_p + \frac{1}{2M_U^2} [y_u]_{sp} [\lambda_U]_s [\lambda_U]_r^* - \frac{1}{M_U M_{Q_7}} [\lambda_U]_r^* [\lambda_{Q_7}]_p \lambda_{UQ_7}$
$[\mathcal{O}_{\phi q}^{(1)}]_{rp}$	$\frac{1}{4M_U^2} [\lambda_U]_p [\lambda_U]_r^*$
$[\mathcal{O}_{\phi q}^{(3)}]_{rp}$	$-\frac{1}{4M_U^2} [\lambda_U]_p [\lambda_U]_r^*$
$[\mathcal{O}_{\phi u}]_{rp}$	$\frac{1}{2M_{Q_7}^2} [\lambda_{Q_7}]_r^* [\lambda_{Q_7}]_p$

Table 5.16: Tree level matching for Model 3.

5.3 Model 3: $Q_7 + U$

The Yukawa-like interactions of the Model 3's VLQ content, where $Q_7 \sim (3, 2)_{\frac{7}{6}}$, is described by

$$-\mathcal{L}_{NP, M.3}^{int} = [\lambda_U]_r \bar{U}_R \tilde{\phi}^\dagger q_{Lr} + [\lambda_{Q_7}]_r \bar{Q}_{7L} \phi u_{Rr} + \lambda_{UQ_7} \bar{U}_R \phi Q_{7L} + \text{h.c.} \quad (5.30)$$

From this expression, the absence of d quarks in the tree-level generated operators (Table 5.16) and in the UV one-loop diagrams contributing to the $\mathcal{C}_{\phi D}$ and $\mathcal{C}_{\phi\Box}$ matching (Table 5.17) is expected. This means that for this model, $\kappa_{d_i} = 1$ exactly, while in the previous two models one of the modifiers was equal to 1 up to corrections proportional to the Yukawa couplings.

The up-type quark modifier in this case is

$$\kappa_{u_i} = 1 + \frac{v^3}{\sqrt{2} m_{u_i} M_U M_{Q_7}} [\lambda_U]_i^* [\lambda_{Q_7}]_i \lambda_{UQ_7}. \quad (5.31)$$

Finally, the Wilson coefficients for the two $\phi^4 D^2$ operators are found by following the same steps used in Model 1.

Their final expression, having set $M_U = M_{Q_7} = \Lambda$, is

$$16\pi^2 \Lambda^2 \mathcal{C}_{\phi\Box} = -\frac{6}{5} |\lambda_{UQ_7}|^4 + \frac{5}{4} |\lambda_{UQ_7}|^2 (|\lambda_U|^2 - 2|\lambda_{Q_7}|^2) - |\lambda_U|^4 - \frac{3}{4} |\lambda_{Q_7}|^4, \quad (5.32)$$

$$16\pi^2 \Lambda^2 \mathcal{C}_{\phi D} = -\frac{12}{5} |\lambda_{UQ_7}|^4 + \frac{5}{2} |\lambda_{UQ_7}|^2 (2|\lambda_U|^2 - |\lambda_{Q_7}|^2) - \frac{3}{2} |\lambda_U|^4 - 2|\lambda_{Q_7}|^4. \quad (5.33)$$

Identifier	h.p.	l.p.	Diagram	Multiplicity
4 heavy	$2 Q_7, 2 U$	0	Box	1
3 heavy	$2 Q_7, 1 U$	$1 u_R$	Box	2
	$1 Q_7, 2 U$	$1 q_L$	Non-planar type 1	2
2 heavy	$2 Q_7$	$2 u_R$	Box	2
	$2 U$	$2 q_L$	Box	2

Table 5.17: One-loop diagrams contributing to the UV four point Higgs function for Model 3. In this model there are no down-type particle contributions.

Operator	Wilson Coefficient
$[\mathcal{O}_{d\phi}]_{rp}$	$\frac{1}{2M_D^2} [yd]_{sp} [\lambda_D]_s [\lambda_D]_r^* + \frac{1}{2M_{Q_5}^2} [\lambda_{Q_5}]_p [\lambda_{Q_5}]_s^* [yd]_{rs} - \frac{1}{M_D M_{Q_5}} [\lambda_D]_r^* [\lambda_{Q_5}]_p \lambda_{DQ_5}$
$[\mathcal{O}_{\phi q}^{(1)}]_{rp}$	$-\frac{1}{4M_D^2} [\lambda_D]_p [\lambda_D]_r^*$
$[\mathcal{O}_{\phi q}^{(3)}]_{rp}$	$-\frac{1}{4M_D^2} [\lambda_D]_p [\lambda_D]_r^*$
$[\mathcal{O}_{\phi d}]_{rp}$	$-\frac{1}{2M_{Q_5}^2} [\lambda_{Q_5}]_r^* [\lambda_{Q_5}]_p$

Table 5.18: Operators generated at the tree level in Model 4 along with their Wilson coefficients in terms of the VLQ masses and couplings.

5.4 Model 4: $Q_5 + D$

Model 4 introduces, besides D which has the same quantum numbers of the SM down singlet, the doublet $Q_5 \sim (3, 2)_{-\frac{5}{6}}$, with interactions described by

$$-\mathcal{L}_{NP, M.4}^{int} = [\lambda_D]_r \bar{q}_L r \phi D_R + [\lambda_{Q_5}]_r \bar{Q}_{5L} \tilde{\phi} d_{Rr} + \lambda_{DQ_5} \bar{Q}_{5L} \tilde{\phi} D_R + \text{h.c.} \quad (5.34)$$

This model is complementary to the previous one as it does not involve the u singlets. From Table 5.18 we can read $\kappa_{u_i} = 1$, while the down-type coupling modifier is

$$\kappa_{d_i} = 1 + \frac{v^3}{\sqrt{2} m_{d_i} M_D M_{Q_5}} [\lambda_D]_i^* [\lambda_{Q_5}]_i \lambda_{DQ_5}. \quad (5.35)$$

The Wilson coefficients for the $\mathcal{O}_{\phi\Box}$ and $\mathcal{O}_{\phi D}$ operators, evaluating the diagrams presented in Table 5.19 in the same mass limit, are

$$16\pi^2 \Lambda^2 \mathcal{C}_{\phi\Box} = -\frac{6}{5} |\lambda_{DQ_5}|^4 + \frac{5}{4} |\lambda_{DQ_5}|^2 (|\lambda_D|^2 - 2|\lambda_{Q_5}|^2) - |\lambda_D|^4 - \frac{3}{4} |\lambda_{Q_5}|^4, \quad (5.36)$$

$$16\pi^2 \Lambda^2 \mathcal{C}_{\phi D} = -\frac{12}{5} |\lambda_{DQ_5}|^4 + \frac{5}{2} |\lambda_{DQ_5}|^2 (2|\lambda_D|^2 - |\lambda_{Q_5}|^2) - \frac{3}{2} |\lambda_{Q_5}|^4 - 2|\lambda_D|^4. \quad (5.37)$$

These are tied to the results for Model 3 by performing the replacements

$$\lambda_U \mapsto \lambda_D, \quad \lambda_{Q_7} \mapsto \lambda_{Q_5}, \quad \lambda_{UQ_7} \mapsto \lambda_{DQ_5}. \quad (5.38)$$

Identifier	h.p.	l.p.	Diagram type	Multiplicity
4 heavy	$2 Q_5, 2 D$	0	Box	1
3 heavy	$2 Q_5, 1 D$	$1 d_R$	Box	2
	$1 Q_5, 2 D$	$1 q_L$	Non Planar type 1	2
2 heavy	$2 Q_5$	$2 d_R$	Box	1
	$2 D$	$2 q_L$	Box	1

Table 5.19: One-loop diagrams involving Model 4's VLQ content contributing to the UV four point Higgs function.

Operator	Wilson Coefficient
$[\mathcal{O}_{u\phi}]_{rp}$	$\frac{1}{2M_{Q_1}^2} [y_u]_{rk} \left[\lambda_{Q_1}^u \right]_p \left[\lambda_{Q_1}^u \right]_k^* + \frac{1}{4M_{T_1}^2} [y_u]_{kp} [\lambda_{T_1}]_k [\lambda_{T_1}]_r^* - \frac{1}{2M_{T_1} M_{Q_1}} \lambda_{T_1 Q_1} [\lambda_{T_1}]_r^* \left[\lambda_{Q_1}^u \right]_p$
$[\mathcal{O}_{d\phi}]_{rp}$	$\frac{1}{2M_{Q_1}^2} [y_d]_{rk} \left[\lambda_{Q_1}^d \right]_p \left[\lambda_{Q_1}^d \right]_k^* + \frac{1}{8M_{T_1}^2} [y_d]_{kp} [\lambda_{T_1}]_k [\lambda_{T_1}]_r^* - \frac{1}{4M_{T_1} M_{Q_1}} \lambda_{T_1 Q_1} [\lambda_{T_1}]_r^* \left[\lambda_{Q_1}^d \right]_p$
$[\mathcal{O}_{\phi q}^{(1)}]_{rp}$	$-\frac{3}{16M_{T_1}^2} [\lambda_{T_1}]_r^* [\lambda_{T_1}]_p$
$[\mathcal{O}_{\phi q}^{(3)}]_{rp}$	$\frac{1}{16M_{T_1}^2} [\lambda_{T_1}]_r^* [\lambda_{T_1}]_p$
$[\mathcal{O}_{\phi u}]_{rp}$	$-\frac{1}{2M_{Q_1}^2} \left[\lambda_{Q_1}^u \right]_r \left[\lambda_{Q_1}^u \right]_p$
$[\mathcal{O}_{\phi d}]_{rp}$	$\frac{1}{2M_{Q_1}^2} \left[\lambda_{Q_1}^d \right]_r \left[\lambda_{Q_1}^d \right]_p$
$[\mathcal{O}_{\phi ud}]_{rp}$	$\frac{1}{M_{Q_1}^2} \left[\lambda_{Q_1}^u \right]_r \left[\lambda_{Q_1}^d \right]_p$

Table 5.20: Tree-level matching results for Model 5.

5.5 Model 5: $Q_1 + T_1$

Model 5 is the first model which introduces an SU(2) triplet, $T_1 \sim (3, 3)_{-\frac{1}{3}}$. Its Yukawa-like interactions with the SM and with the Q_1 doublet read

$$-\mathcal{L}_{NP, M.5}^{int} = [\lambda_{Q_1}^u]_r \bar{Q}_{1L} \tilde{\phi} u_{Rr} + [\lambda_{Q_1}^d]_r \bar{Q}_{1L} \phi d_{Rr} + \frac{[\lambda_{T_1}]_r}{2} \bar{T}_{1R}^j \phi^\dagger \sigma^j q_{Lr} + \frac{\lambda_{T_1 Q_1}}{2} \bar{T}_{1L}^j \phi^\dagger \sigma^j Q_{1Rs} + \text{h.c.} \quad (5.39)$$

The tree level matching results are reported in Table 5.20; in this model, both coupling modifiers deviate from 1. Their expressions are:

$$\kappa_{u_i} = 1 + \frac{v^3}{2\sqrt{2}m_{u_i} M_{T_1} M_{Q_1}} [\lambda_{Q_1}^u]_i [\lambda_{T_1}]_i^* \lambda_{T_1 Q_1}, \quad \kappa_{d_i} = 1 + \frac{v^3}{4\sqrt{2}m_{d_i} M_{T_1} M_{Q_1}} [\lambda_{Q_1}^d]_i [\lambda_{T_1}]_i^* \lambda_{T_1 Q_1}. \quad (5.40)$$

Finally, the matching for $\mathcal{C}_{\phi\Box}$ and $\mathcal{C}_{\phi D}$ receives the contributions in Table 5.21; the coefficients in the same mass limit are:

$$16\pi^2 \Lambda^2 \mathcal{C}_{\phi\Box} = -\frac{3}{8} |\lambda_{T_1 Q_1}|^4 + \frac{15}{64} |\lambda_{T_1 Q_1}|^2 (4|\lambda_{Q_1}^u|^2 - 3|\lambda_{T_1}|^2) - \frac{3}{4} (|\lambda_{Q_1}^u|^4 + |\lambda_{Q_1}^d|^4) - 2|\lambda_{Q_1}^u|^2 |\lambda_{Q_1}^d|^2 - \frac{1}{4} |\lambda_{T_1}|^4, \quad (5.41)$$

$$16\pi^2 \Lambda^2 \mathcal{C}_{\phi D} = -\frac{3}{4} |\lambda_{T_1 Q_1}|^4 - \frac{15}{16} |\lambda_{T_1 Q_1}|^2 (2|\lambda_{Q_1}^d|^2 - 2|\lambda_{Q_1}^u|^2 + |\lambda_{T_1}|^2) - 2 (|\lambda_{Q_1}^u|^4 + |\lambda_{Q_1}^d|^4) + 4|\lambda_{Q_1}^u|^2 |\lambda_{Q_1}^d|^2 - \frac{19}{32} |\lambda_{T_1}|^4. \quad (5.42)$$

Identifier	h.p.	l.p.	Diagram	Mult.	Identifier	h.p.	l.p.	Diagram	Mult.
4 heavy	$2 T_1, 2 Q_1$	0	Box	2	2 heavy	$2 T_1$	$2 q_L$	Box	2
	$2 T_1, 1 Q_1$	$1 q_L$	Box	4		$2 u_R$	Box	1	
3 heavy	$1 T_1, 2 Q_1$	$1 u_R$	n.p. type 1	2	$2 Q_1$	$2 d_R$	Box	1	
			n.p. type 2	2		$1 d_R, 1 u_R$	n.p. type 1	2	
	$1 T_1, 2 Q_1$	$1 d_R$	Box	4			n.p. type 2	2	

Table 5.21: Summary of the different contributions accounted for in the UV diagrams with Model 5's particle content.

Operator	Wilson Coefficient
$[\mathcal{O}_{u\phi}]_{rp}$	$\frac{1}{4M_{T_1}^2} [yu]_{sp} [\lambda_{T_1}]_s [\lambda_{T_1}]_r^*$
$[\mathcal{O}_{d\phi}]_{rp}$	$\frac{1}{2M_{Q_5}^2} [yd]_{rk} [\lambda_{Q_5}]_p [\lambda_{Q_5}]_k^* + \frac{1}{8M_{T_1}^2} [yd]_{kp} [\lambda_{T_1}]_k [\lambda_{T_1}]_r^* + \frac{1}{4M_{T_1}M_{Q_5}} \lambda_{T_1 Q_5} [\lambda_{T_1}]_r^* [\lambda_{Q_5}]_p$
$[\mathcal{O}_{\phi q}^{(1)}]_{rp}$	$-\frac{3}{16M_{T_1}^2} [\lambda_{T_1}]_r^* [\lambda_{T_1}]_p$
$[\mathcal{O}_{\phi q}^{(3)}]_{rp}$	$\frac{1}{16M_{T_1}^2} [\lambda_{T_1}]_r^* [\lambda_{T_1}]_p$
$[\mathcal{O}_{\phi d}]_{rp}$	$-\frac{1}{2M_{Q_5}^2} [\lambda_{Q_5}]_r^* [\lambda_{Q_5}]_p$

Table 5.22: Tree-level matching for Model 6.

5.6 Model 6: $Q_5 + T_1$

The interaction NP Lagrangian density for Model 6 reads

$$-\mathcal{L}_{int, M.6}^{NP} = [\lambda_{Q_5}]_r \bar{Q}_{5L} \tilde{\phi} d_{Rr} + [\lambda_{T_1}]_r \bar{T}_{1R}^A \phi^\dagger \frac{\sigma^A}{2} q_{Lr} + \lambda_{T_1 Q_5} \bar{T}_{1L}^A \tilde{\phi}^\dagger \frac{\sigma^A}{2} Q_{5R} + \text{h.c.} \quad (5.43)$$

The tree-level generated Warsaw operators are set in Table 5.22, together with the expressions for the Wilson coefficients after the matching. The expression for the down-type modifier is

$$\kappa_{d_i} = 1 - \frac{v^3}{4\sqrt{2}m_{d_i}M_{T_1}M_{Q_5}} [\lambda_{T_1}]_i^* [\lambda_{Q_5}]_i \lambda_{T_1 Q_5}. \quad (5.44)$$

The up-type quark coupling modifier is instead $\kappa_{u_i} = 1$ once the SM Yukawa couplings have been set to zero.

Table 5.23 summarises the UV contributions to the matching for $\mathcal{C}_{\phi\Box}$ and $\mathcal{C}_{\phi D}$, whose expressions in the same mass limit are, respectively,

$$16\pi^2\Lambda^2\mathcal{C}_{\phi\Box} = -\frac{3}{8}|\lambda_{T_1 Q_5}|^4 - \frac{15}{64}|\lambda_{T_1 Q_5}|^2|\lambda_{T_1}|^2 - \frac{1}{4}|\lambda_{T_1}|^4 - \frac{3}{4}|\lambda_{Q_5}|^4, \quad (5.45)$$

$$16\pi^2\Lambda^2\mathcal{C}_{\phi D} = -\frac{3}{4}|\lambda_{T_1 Q_5}|^4 - \frac{15}{16}|\lambda_{T_1 Q_5}|^2(2|\lambda_{Q_5}|^2 - |\lambda_{T_1}|^2) - \frac{19}{32}|\lambda_{T_1}|^4 - 2|\lambda_{Q_5}|^4. \quad (5.46)$$

Identifier	h.p.	l.p.	Diagram	Multiplicity
4 heavy	$2 T_1, 2 Q_5$	0	Box	2
3 heavy	$2 T_1, 1 Q_5$	1 q_L	n.p. type 1	2
			n.p. type 2	2
	$1 T_1, 2 Q_5$	1 d_R	Box	4
2 heavy	$2 T_1$	2 q_L	Box	2
	$2 Q_5$	2 d_R	Box	2

Table 5.23: Summary of the different contributions accounted for in the UV diagrams with Model 6's particle content.

Coefficient	Matching result
$[\mathcal{O}_{u\phi}]^{rp}$	$\frac{1}{2M_{Q_1}^2} [yu]_{rk} \left[\lambda_{Q_1}^u \right]_p \left[\lambda_{Q_1}^u \right]_k^* + \frac{1}{8M_{T_2}^2} [yu]_{kp} [\lambda_{T_2}]_k [\lambda_{T_2}]_r^* - \frac{1}{4M_{Q_1}M_{T_2}} \lambda_{T_2 Q_1} [\lambda_{T_2}]_r^* \left[\lambda_{Q_1}^u \right]_p$
$[\mathcal{O}_{d\phi}]_{rp}$	$\frac{1}{2M_{Q_1}^2} [yd]_{rk} \left[\lambda_{Q_1}^d \right]_p \left[\lambda_{Q_1}^d \right]_k^* + \frac{1}{4M_{T_2}^2} [yd]_{kp} [\lambda_{T_2}]_k [\lambda_{T_2}]_r^* - \frac{1}{2M_{Q_1}M_{T_2}} \lambda_{T_2 Q_1} [\lambda_{T_2}]_r^* \left[\lambda_{Q_1}^d \right]_p$
$\left[\mathcal{O}_{\phi q}^{(1)} \right]_{rp}$	$\frac{3}{16M_{T_2}^2} [\lambda_{T_2}]_p [\lambda_{T_2}]_r^*$
$\left[\mathcal{O}_{\phi q}^{(3)} \right]_{rp}$	$\frac{1}{16M_{T_2}^2} [\lambda_{T_2}]_p [\lambda_{T_2}]_r^*$
$[\mathcal{O}_{\phi u}]_{rp}$	$-\frac{1}{2M_{Q_1}^2} \left[\lambda_{Q_1}^u \right]_r \left[\lambda_{Q_1}^u \right]_p$
$[\mathcal{O}_{\phi d}]_{rp}$	$\frac{1}{2M_{Q_1}^2} \left[\lambda_{Q_1}^d \right]_r \left[\lambda_{Q_1}^d \right]_p$
$[\mathcal{O}_{\phi ud}]_{rp}$	$\frac{1}{M_{Q_1}^2} \left[\lambda_{Q_1}^u \right]_r \left[\lambda_{Q_1}^d \right]_p$

Table 5.24: Tree-level matching for Model 7.

5.7 Model 7: $Q_1 + T_2$

The last VLQ introduced in [51] is another triplet, $T_2 \sim (3, 2)_{\frac{2}{3}}$. It interacts with the SM doublets and the Q_1 doublet as described by the following Lagrangian density

$$-\mathcal{L}_{NP}^{int, M.7} = [\lambda_{Q_1}^u]_r \bar{Q}_{1L} \tilde{\phi} u_{Rr} + [\lambda_{Q_1}^d]_r \bar{Q}_{1L} \phi d_{Rr} + \frac{[\lambda_{T_2}]_r}{2} \bar{T}_{2R}^A \tilde{\phi}^\dagger \sigma^A q_{Lr} + \frac{\lambda_{T_2 Q_1}}{2} \bar{T}_{2L}^A \tilde{\phi}^\dagger \sigma^A Q_{1R} + \text{h.c.} \quad (5.47)$$

In Tables 5.24 and 5.25 the tree-level matching results and the UV diagrams required for the calculation of $\mathcal{C}_{\phi\Box}$ and $\mathcal{C}_{\phi D}$ are respectively shown. The coupling modifiers for Model 7 are:

$$\kappa_{u_i} = 1 + \frac{v^3}{4\sqrt{2}m_{u_i}M_{Q_1}M_{T_2}} [\lambda_{T_2}]_i^* [\lambda_{Q_1}^u]_i \lambda_{T_2 Q_1}, \quad \kappa_{d_i} = 1 + \frac{v^3}{2\sqrt{2}m_{d_i}M_{Q_1}M_{T_2}} [\lambda_{T_2}]_i^* [\lambda_{Q_1}^d]_i \lambda_{T_2 Q_1}. \quad (5.48)$$

The $\mathcal{C}_{\phi D}$ and $\mathcal{C}_{\phi\Box}$ coefficients read

$$16\pi^2 \Lambda^2 \mathcal{C}_{\phi\Box} = -\frac{3}{8} |\lambda_{T_2 Q_1}|^4 + \frac{15}{64} |\lambda_{T_2 Q_1}|^2 \left(4|\lambda_{Q_1}^d|^2 - 3|\lambda_{T_2}|^2 \right) - \frac{3}{4} \left(|\lambda_{Q_1}^u|^4 + |\lambda_{Q_1}^d|^4 \right) - 2|\lambda_{Q_1}^u|^2 |\lambda_{Q_1}^d|^2 - \frac{1}{4} |\lambda_{T_2}|^4, \quad (5.49)$$

$$16\pi^2 \Lambda^2 \mathcal{C}_{\phi D} = -\frac{3}{4} |\lambda_{T_2 Q_1}|^4 + \frac{15}{16} \left(2|\lambda_{Q_1}^d|^2 - 2|\lambda_{Q_1}^u|^2 - |\lambda_{T_2}|^2 \right) - 2 \left(|\lambda_{Q_1}^u|^4 + |\lambda_{Q_1}^d|^4 \right) + 4|\lambda_{Q_1}^u|^2 |\lambda_{Q_1}^d|^2 - \frac{19}{32} |\lambda_{T_2}|^4. \quad (5.50)$$

Identifier	h.p.	l.p	Diagram	Mult.	Identifier	h.p.	l.p	Diagram	Mult.
4 heavy	$2T_2, 2Q_1$	0	Box	2	2 heavy	$2T_2$	$2q_L$	Box	2
	$1T_1, 2Q_1$	$1q_L$	Box	4		$2u_R$	Box	1	
3 heavy	$2T_2, 1Q_1$	$1u_R$	Box	4	$2Q_1$	$2d_R$	Box	1	
		$1d_R$	n.p. type 1	2	$1d_R, 1u_R$	n.p. type 1	2		
			n.p. type 2	2		n.p. type 2	2		

Table 5.25: Contributing UV diagrams for Model 7 to the matching for $\mathcal{C}_{\phi\Box}$ and $\mathcal{C}_{\phi D}$ coefficients.

Coefficient	Wilson Coefficient
$[\mathcal{O}_{u\phi}]_{rp}$	$\frac{1}{2M_{Q_7}^2} [y_u]_{rk} [\lambda_{Q_7}]_p [\lambda_{Q_7}]_k^* + \frac{1}{8M_{T_2}^2} [y_u]_{kp} [\lambda_{T_2}]_k [\lambda_{T_2}]_r^* + \frac{1}{4M_{Q_7}M_{T_2}} \lambda_{T_2 Q_7} [\lambda_{T_2}]_r^* [\lambda_{Q_7}]_p$
$[\mathcal{O}_{d\phi}]_{rp}$	$\frac{1}{4M_{T_2}^2} [y_d]_{kp} [\lambda_{T_2}]_k [\lambda_{T_2}]_r^*$
$[\mathcal{O}_{\phi q}^{(1)}]_{rp}$	$\frac{3}{16M_{T_2}^2} [\lambda_{T_2}]_p [\lambda_{T_2}]_r^*$
$[\mathcal{O}_{\phi q}^{(3)}]_{rp}$	$\frac{1}{16M_{T_2}^2} [\lambda_{T_2}]_p [\lambda_{T_2}]_r^*$
$[\mathcal{O}_{\phi u}]_{rp}$	$\frac{1}{2M_{Q_7}^2} [\lambda_{Q_7}]_r^* [\lambda_{Q_7}]_p$

Table 5.26: Tree-level matching for Model 8.

5.8 Model 8: $Q_7 + T_2$

The interaction NP Lagrangian density for this model reads

$$-\mathcal{L}_{NP, M.8}^{int} = (\lambda_{Q_7})_s \bar{Q}_{7L} \phi u_{Rs} + \frac{(\lambda_{T_2})_s}{2} \bar{T}_{2R}^A \tilde{\phi}^\dagger \sigma^A q_{Ls} + \frac{(\lambda_{T_2 Q_7})}{2} \bar{T}_{2L}^A \phi^\dagger \sigma^A Q_{7R} + \text{h.c.} \quad (5.51)$$

The non-trivial coupling modifier in this case regards the up-sector. Using the tree-level matching results in Table 5.26, the κ -parameter reads

$$\kappa_{u_i} = 1 - \frac{v^3}{4\sqrt{2}m_{u_i}M_{T_2}M_{Q_7}} [\lambda_{Q_7}]_i [\lambda_{T_2}]_i^* \lambda_{T_2 Q_7}. \quad (5.52)$$

To conclude, the final expressions for the coefficients $\mathcal{C}_{\phi\Box}$ and $\mathcal{C}_{\phi D}$ after the matching in the same mass limit are:

$$16\pi^2 \Lambda^2 \mathcal{C}_{\phi\Box} = -\frac{3}{8} |\lambda_{T_2 Q_7}|^4 - \frac{15}{64} |\lambda_{T_2 Q_7}|^2 |\lambda_{Q_7}|^2 - \frac{1}{4} |\lambda_{T_2}|^4 - \frac{3}{4} |\lambda_{Q_7}|^4, \quad (5.53)$$

$$16\pi^2 \Lambda^2 \mathcal{C}_{\phi D} = -\frac{3}{4} |\lambda_{T_2 Q_7}|^4 - \frac{15}{16} |\lambda_{T_2 Q_7}|^2 (2|\lambda_{Q_7}|^2 - |\lambda_{T_2}|^2) - \frac{19}{32} |\lambda_{T_2}|^4 - 2|\lambda_{Q_7}|^4. \quad (5.54)$$

The UV contributions in this case are found in Table 5.27.

At this point, having concluded the matching, it is possible to move on to the next Chapter, in which the bounds on the parameters arising from Higgs Physics and ElectroWeak Precision Observables will be discussed.

Identifier	h.p.	l.p.	Diagram	Multiplicity
4 heavy	$2T_2, 2Q_7$	0	Box	2
	$1T_2, 2Q_7$	$1 u_R$	Box	4
3 heavy	$2T_2, 1Q_7$	$1q_L$	n.p. type 1	2
			n.p. type 2	2
2 heavy	$2Q_7$	$2u_r$	Box	2
	$2T_2$	$2q_L$	Box	2

Table 5.27: UV diagrams involved in the calculation of $\mathcal{C}_{\phi\Box}$ and $\mathcal{C}_{\phi D}$ for Model 8.

Chapter 6

Experimental Tests

With the matching results from the previous chapter, the parameter space of the VLQ Yukawa-like couplings can be constrained for each of the models. Once the bounds on the couplings have been found, the deviations of the SM quarks' Yukawa couplings can be quantified within the κ -parametrisation and compared with the results available in the literature (Table 1.1). The mass of the VLQs is set to be $\Lambda = 2 \text{ TeV}$ for the rest of this chapter.

Given the assumption that the VLQs only couple to one generation of SM quarks and the consequent exclusion of strong bounds from flavour physics, the effects of introducing SMEFT operators on ElectroWeak Precision Observables (EWPO) and on Higgs Physics (HP) were considered. Let $\{O_\alpha\}_\alpha$ be the set of observables pertaining to either HP or EWPO; for each observable, there is an associated theoretical value denoted by O_α^{th} and an experimental value O_α^{exp} . Regarding the theoretical values, if O_α^{SM} denotes the SM prediction for a given observable, the presence of SMEFT operators introduces a deviation δO_α^{SMEFT} which can be expressed in terms of the Wilson coefficients and therefore scales as Λ^{-2} . Considering, for example, the calculation of cross-sections, one finds

$$\sigma \propto |\mathcal{M}_{SM} + \frac{1}{\Lambda^2} \mathcal{M}_{d=6}|^2 \approx |\mathcal{M}_{SM}|^2 + \frac{1}{\Lambda^2} (\mathcal{M}_{SM}^* \mathcal{M}_{d=6} + \mathcal{M}_{SM} \mathcal{M}_{d=6}^*) + O(\Lambda^{-4}). \quad (6.1)$$

The squared dimension-six contribution is dropped since it is more suppressed than the other terms. The theoretical SMEFT predictions read

$$O_\alpha^{th} = O_\alpha^{SM} + \delta O_\alpha^{SMEFT}. \quad (6.2)$$

The experimental and theoretical values for the observables are used to construct the χ^2 function as

$$\chi_{EWPO/HP}^2 = \sum_{\alpha\beta} (O_\alpha^{exp} - O_\alpha^{th})(\sigma^{-2})_{\alpha\beta} (O_\beta^{exp} - O_\beta^{th}), \quad (6.3)$$

where $(\sigma^{-2})_{\alpha\beta}$ is the inverse of the covariance matrix, which describes the correlation between the different observables. The χ^2 has a known statistical distribution and is used to test statistical hypotheses [72]: provided a number of degrees of freedom N and a fixed Confidence Level (CL), a threshold value $\bar{\chi}^2 = \chi^2(N, \text{CL})$ is associated. Let $\chi_{EWPO/HP}^{2\min}$ be the minimum of the function just built: two sets of bounds are found by imposing CL= 68% and CL= 95% and graphically studying

$$\chi_{EWPO/HP}^2 \leq \chi_{EWPO/HP}^{2\min} + \chi^2(N, 0.68), \quad \chi_{EWPO/HP}^2 \leq \chi_{EWPO/HP}^{2\min} + \chi^2(N, 0.95). \quad (6.4)$$

At this point, the model independence guaranteed by the use of SMEFT becomes clear: the χ^2 function is entirely constructed within the SMEFT, with no knowledge concerning the original NP model. Model dependence is intro-

duced by substituting the matching results found in the previous chapter. The number of degrees of freedom is given by the number of couplings in the NP model. The regions of the parameter space that do not satisfy Equation (6.4) are excluded with a CL equal to 68% and 95%.

The HP and EWPO cases are studied independently only for Model 1 coupled to the first generation of quarks; for the remaining models and for the second generation a combined fit is performed, obtained by considering the total χ^2 -function defined as $\chi_t^2 = \chi_{HP}^2 + \chi_{EWPO}^2$.

6.1 ElectroWeak Physics

The presence of the $\psi^2\phi^2 D$ -class operators, of $\mathcal{O}_{\phi D}$ and of $\mathcal{O}_{\phi WB}$ modifies the couplings of the massive gauge bosons to the quarks, thus affecting the EWPOs. In this section the form of the modifications is first of all investigated, then the ElectroWeak χ^2 function is constructed following [70, 73].

6.1.1 W^\pm and Z boson coupling to quarks

First of all, the effects of the operators in the $\psi^2\phi^2 D$ -class of Table 5.1 are presented. Such operators are always generated at the tree level by the models considered in this thesis. All these operators involve a product of two terms: one is a quark current while the other contains a pair of Higgs doublets and the covariant derivative, from which the gauge bosons are picked up. Based on how the latter term is constructed, the study of these operators can be divided into three cases:

- $\mathcal{O}_{\phi u}$, $\mathcal{O}_{\phi d}$ and $\mathcal{O}_{\phi q}^{(1)}$ can be generalised to $(\phi^\dagger i \overleftrightarrow{D}_\mu \phi) (\bar{\psi} \gamma^\mu \psi)$, where $\psi = u_R, d_R, q_L$ respectively. Considering only the contents of the first parenthesis, picking up the W_μ^J and B_μ from the covariant derivatives, substituting $Y_\phi = \frac{1}{2}$ and performing SSB, the quark currents will be multiplied by

$$\phi^\dagger i \overleftrightarrow{D}_\mu \phi \supset -\phi^\dagger \left(g_L \sigma^J W_\mu^J + g_Y B_\mu \right) \phi \stackrel{\text{Eqs.(2.12)(2.14)}}{\supset} + \frac{g_L v^2}{2 \cos \theta_W} Z_\mu. \quad (6.5)$$

All three operators cause a modification to the Z boson couplings to the SM quarks;

- $\mathcal{O}_{\phi q}^{(3)} = (\phi^\dagger i D_\mu^J \phi) (\bar{q}_L \sigma^J \gamma^\mu q_L)$: this will generate deviations in the couplings of both the Z and the W^\pm bosons. Again considering only the Higgs structure, the quark current will be multiplied by

$$\begin{aligned} \phi^\dagger i D_\mu^J \phi &\supset -\phi^\dagger \left(\frac{g_L}{2} W_\mu^{\mathcal{K}} \underbrace{(\sigma^J \sigma^{\mathcal{K}} + \sigma^{\mathcal{K}} \sigma^J)}_{\{\sigma^J, \sigma^{\mathcal{K}}\} = 2\delta^{\mathcal{K}J} \mathbb{1}} + g_Y B_\mu \sigma^J \right) \phi, \\ &\stackrel{\text{Eq.(2.12)}}{\supset} -\frac{v^2}{2} \left(g_L W_\mu^1 \delta^{1J} + g_L W_\mu^2 \delta^{2J} + (g_L W_\mu^3 - g_Y B_\mu) \delta^{3J} \right), \\ &\stackrel{\text{Eqs.(2.13)(2.14)}}{\supset} -\frac{v^2}{2} \left[\frac{g_L}{\sqrt{2}} W_\mu^+ (\delta^{1J} + i\delta^{2J}) + \frac{g_L}{\sqrt{2}} W_\mu^- (\delta^{1J} - i\delta^{2J}) + \frac{g_L}{\cos \theta_W} Z_\mu \delta^{3J} \right]; \end{aligned} \quad (6.6)$$

- $\mathcal{O}_{\phi ud} = (\tilde{\phi}^\dagger i D_\mu \phi) (\bar{u}_R \gamma^\mu d_R)$: this gives rise to the interaction of the charged gauge bosons W^\pm with right-handed SM quarks,

$$(\tilde{\phi}^\dagger i D_\mu \phi) \supset \tilde{\phi}^\dagger \left(\frac{g_L}{2} \sigma^J W_\mu^J + g_Y Y_\phi B_\mu \right) \phi \stackrel{\text{Eqs.(2.12)(2.13)}}{\supset} + \frac{g v^2}{2\sqrt{2}} W_\mu^+. \quad (6.7)$$

The operator $\mathcal{O}_{\phi ud}$ is non-hermitian, so it appears in the SMEFT Lagrangian along with its hermitian conjugate that introduces an interaction term of the W^- to the right-handed quarks. The coupling of the W^\pm bosons



Figure 6.1: Feynman diagrams for the Z boson two-point function at the SM tree level (left) and the correction due to the SMEFT operators $\mathcal{O}_{\phi WB}$ and $\mathcal{O}_{\phi D}$ once the Higgs boson has assumed its vacuum expectation value (right).

to right-handed quarks induced by the $\mathcal{O}_{\phi ud} + \text{h.c.}$ is absent in the SM; Equation (6.1) then states that these deviations only enter the W -pole observables quadratically since there is no interference term between SM and dimension-six contributions. The contributions due to $\mathcal{O}_{\phi ud} + \text{h.c.}$ are neglected given that they are suppressed by Λ^{-4} , while for all the other operators an interference term with the SM prediction is present and leads to contribution suppressed only by Λ^{-2} .

While the previous effects are quark-family dependent (there are family indices in the quark currents), the effects of the loop generate operators $\mathcal{O}_{\phi WB}$ and $\mathcal{O}_{\phi D}$ turn out to be family-universal.

In the broken phase the $\mathcal{O}_{\phi D}$ and $\mathcal{O}_{\phi WB}$ operators cause a deviation in the Z -boson mass (as a correction to the Z two-point function, as shown in Figure 6.1) and the Weinberg angle θ_W associated to the rotation from the interaction to the mass basis. Substituting $\phi = \begin{pmatrix} 0 & v/\sqrt{2} \end{pmatrix}^T$ into the expressions for the two operators, one finds:

$$\mathcal{C}_{\phi WB} \left(\phi^\dagger \sigma^J \phi \right) \left(W_{\mu\nu}^J B^{\mu\nu} \right) \rightarrow -\frac{v^2}{2} \mathcal{C}_{\phi WB} W_{\mu\nu}^3 B^{\mu\nu}, \quad (6.8)$$

$$\mathcal{C}_{\phi D} |\phi^\dagger D_\mu \phi|^2 \rightarrow \frac{v^4}{16} \mathcal{C}_{\phi D} \left(-g_L W_\mu^3 + g_Y B_\mu \right)^2. \quad (6.9)$$

The ElectroWeak Lagrangian, accounting for some of the SM terms and these two SMEFT operators reads

$$\mathcal{L}_{SMEFT} \supset -\frac{1}{4} W_{\mu\nu}^J W^{J\mu\nu} - \frac{1}{4} B_{\mu\nu} B^{\mu\nu} - \frac{v^2}{2} \mathcal{C}_{\phi WB} W_{\mu\nu}^3 B^{\mu\nu} + \frac{v^2}{8} \left(1 + \frac{v^2}{2} \mathcal{C}_{\phi D} \right) \left(-g_L W_\mu^3 + g_Y B_\mu \right)^2. \quad (6.10)$$

It is therefore possible to identify the modifications to the rotation into the mass basis, the tangent of the Weinberg angle and the Z boson mass scale, in agreement with the results of [42]. In particular, the last two are written as their SM definitions multiplied by a correction term between parentheses, so that

$$\begin{pmatrix} W_\mu^3 \\ B_\mu \end{pmatrix} = \begin{pmatrix} 1 & -\frac{v^2}{2} \mathcal{C}_{\phi WB} \\ -\frac{v^2}{2} \mathcal{C}_{\phi WB} & 1 \end{pmatrix} \begin{pmatrix} \cos \theta & \sin \theta \\ -\sin \theta & \cos \theta \end{pmatrix} \begin{pmatrix} Z_\mu \\ A_\mu \end{pmatrix}, \quad (6.11)$$

$$\tan \theta_W = \frac{g_Y}{g_L} \left(1 + \frac{v^2}{2} \mathcal{C}_{\phi WB} \left(\frac{g_L}{g_Y} - \frac{g_Y}{g_L} \right) \right), \quad (6.12)$$

$$M_Z^2 = v^2 \frac{g_L^2 + g_Y^2}{4} \left(1 + \frac{v^2}{2} \mathcal{C}_{\phi D} + 2v^2 \frac{g_Y g_L}{g_L^2 + g_Y^2} \mathcal{C}_{\phi WB} \right). \quad (6.13)$$

The modification to the electric charge e and the sine and cosine of the Weinberg angle can also be found. However, this is not the end of the calculation. In order to employ the construction of the χ^2 performed by the authors of [70, 73], the (α_e, G_F, m_Z) input scheme has to be adopted.

The SM is an overconstrained system: it depends on 27 parameters, in terms of which a large number of experimental observables can be constructed [29]. It is therefore possible to express one observable in terms of others¹ to test the SM predictions. Given that α_e , G_F and m_Z are among the best-known experimental observables, the input scheme in which these fiducial quantities are fixed to their experimental values is the most used in the ElectroWeak precision studies [74]. To move to the (α_e, G_F, m_Z) input scheme, the deviations caused by the SMEFT coefficients have to be translated onto other ElectroWeak Observables. This is achieved by following the steps detailed in reference [29]: the fiducial quantities are written in terms of the SM and SMEFT parameters, and then these expressions are inverted. The

¹A simple example is provided by the gauge boson masses. Indeed, one can write $m_W = g_L v/2$ and $m_Z = \sqrt{g_L^2 + g_Y^2} v/2$, or, recalling that in the SM $\cos \theta_W = g_L / \sqrt{g_L^2 + g_Y^2}$, one has the W boson mass expressed as $m_W = \cos \theta_W m_Z$.

newfound SM and SMEFT parameters written in terms of the fiducial quantities are then substituted in the definitions of other observables. These steps were explicitly performed and led to the following W boson mass modification:

$$\delta m_W = -\frac{v^2}{4} \frac{g_L^2}{g_L^2 - g_Y^2} \mathcal{C}_{\phi D} - v^2 \frac{g_L g_Y}{g_L^2 - g_Y^2} \mathcal{C}_{\phi WB}. \quad (6.14)$$

As for the modifications to the W and Z boson couplings to the quarks, the results found by [70] are reported in the following. Defining the universal factor $\delta^U(T^3, Q)$ to be

$$\delta^U(T^3, Q) = -\frac{v^2}{4} \left(T^3 + Q \frac{g_Y^2}{g_L^2 - g_Y^2} \right) \mathcal{C}_{\phi D} - v^2 Q \frac{g_L g_Y}{g_L^2 - g_Y^2} \mathcal{C}_{\phi WB}, \quad (6.15)$$

the modified Z sector in the (α_e, G_F, m_Z) input scheme can be written as

$$\begin{aligned} \mathcal{L}_Z = & -\frac{g_L}{\cos \theta_W} Z_\mu \sum_{\psi=u,d} \left(\left(g_L^{Z\psi} \delta_{ij} + [\delta g_L^{Z\psi}]_{ij} \right) \bar{\psi}_L^i \gamma^\mu \psi_L^j + \left(g_R^{Z\psi} \delta_{ij} + [\delta g_R^{Z\psi}]_{ij} \right) \bar{\psi}_R^i \gamma^\mu \psi_R^j \right) \\ & + \frac{1}{2} \frac{g_L^2 + g_Y^2}{4} v^2 Z_\mu Z^\mu. \end{aligned} \quad (6.16)$$

The modified expressions of the couplings, including the CKM matrix, are:

$$\begin{aligned} [\delta g_L^{Zu}]_{ij} &= -\frac{v^2}{2} V_{il} \left([\mathcal{C}_{\phi q}^{(1)}]_{lm} - [\mathcal{C}_{\phi q}^{(3)}]_{lm} \right) V_{mj}^\dagger + \delta^U \left(\frac{1}{2}, \frac{2}{3} \right) \delta_{ij}, \\ [\delta g_R^{Zu}]_{ij} &= -\frac{v^2}{2} [\mathcal{C}_{\phi u}]_{ij} + \delta^U \left(0, \frac{2}{3} \right) \delta_{ij}, \\ [\delta g_L^{Zd}]_{ij} &= -\frac{v^2}{2} \left([\mathcal{C}_{\phi q}^{(1)}]_{ij} + [\mathcal{C}_{\phi q}^{(3)}]_{ij} \right) + \delta^U \left(-\frac{1}{2}, -\frac{1}{3} \right) \delta_{ij}, \\ [\delta g_R^{Zd}]_{ij} &= -\frac{v^2}{2} [\mathcal{C}_{\phi d}]_{ij} + \delta^U \left(0, -\frac{1}{3} \right) \delta_{ij}. \end{aligned} \quad (6.17)$$

As for the quark interactions with the W^\pm bosons, the Lagrangian density and the coupling modifier read

$$\mathcal{L}_W = -\frac{g_L}{\sqrt{2}} W_\mu^+ \left(V_{ij} + [\delta g_W]_{ij} \right) \bar{u}_L^i \gamma^\mu d_L^j + \text{h.c.} + \frac{g_L^2 v^2}{4} (1 + \delta m_W)^2 W^{+\mu} W_\mu^-, \quad (6.18)$$

$$[\delta g_W]_{ij} = v^2 V_{ik} [\mathcal{C}_{\phi q}^{(3)}]_{kj} + V_{ij} \delta^U(1, 1). \quad (6.19)$$

Alternatively, the W -coupling modifier can be written as $[\delta g_W]_{ij} = [g_L^{Zu}]_{ik} V_{kj} - V_{ik} [g_L^{Zd}]_{kj}$, showing that the coupling modifiers are not all independent [73].

6.1.2 Application to Model 1

Following [70], the Z -pole and W -pole observables listed in Tables 1 and 2 respectively in [73] are used to construct the χ^2 function in terms of the Wilson coefficients for the $\psi^2 \phi^2 D$ operators (except for $\mathcal{O}_{\phi ud}$) with first family indices, $\mathcal{C}_{\phi D}$ and $\mathcal{C}_{\phi WB}$.

The goal of the procedure that is about to be described, and that will also be followed in the rest of the Chapter, is twofold: graphically solving the inequalities in Equation (6.4) and finding the largest allowed value for the coupling modifier at a 95% CL. The model parameter space and the curves associated to the κ_q modifiers will be shown in the same plot. To perform two-dimensional plots, the χ^2 has to be reduced to depend on only two couplings. Depending on the model, the starting χ^2 function can depend on either three or four couplings. In Model 1's case, there is a dependence on the four VLQ couplings λ_U , $\lambda_{Q_1}^u$, $\lambda_{Q_1}^d$ and λ_{UQ_1} . The couplings are assumed to be real and the

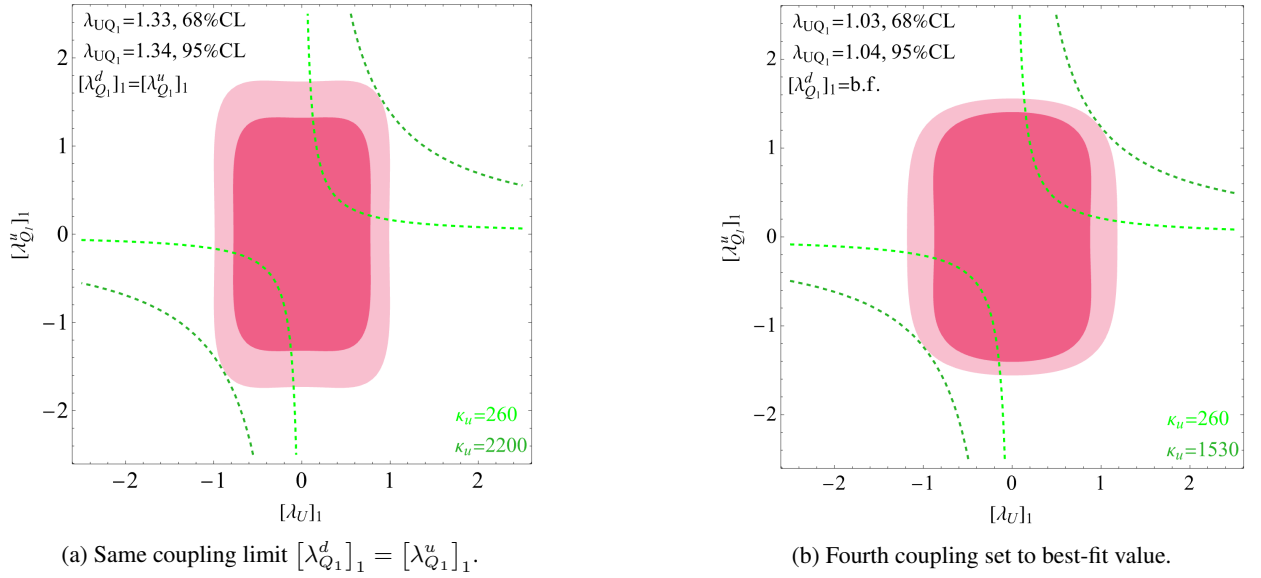


Figure 6.2: Results for the fit involving only EWPO for Model 1. The darker region corresponds to a 68% Confidence Level (CL), the lighter one to 95% CL. The associated values for the VLQ-VLQ coupling are reported in the plots, the 95% CL value is used to draw the κ_u curve.

expression of the modifier is

$$\kappa_u = 1 + \frac{v^3}{\sqrt{2}m_u\Lambda^2} [\lambda_U]_1 [\lambda_{Q_1}^u]_1 \lambda_{UQ_1}, \quad (6.20)$$

with no dependence on the fourth coupling $[\lambda_{Q_1}^d]_1$. To have both the χ^2 function and κ_u depend on two couplings, $[\lambda_{Q_1}^d]_1$ and one of the other three couplings are fixed. Two different procedures are identified:

1. In the first scenario the Q_1 couplings to the SM quarks are set to be the same $[\lambda_{Q_1}^d]_1 = [\lambda_{Q_1}^u]_1$. The χ^2 is now a function of the remaining three couplings and is minimised to find χ_{EWPO}^{2min} required by Equation (6.4). The other fixed coupling is λ_{UQ_1} . For the 68% CL case, λ_{UQ_1} is set to the value that maximises the coupling product in Equation (6.20), remaining below $\chi_{EWPO}^{2min} + \chi^2(3, 0.68)$; similarly is done for the 95% CL region. The latter value is also used in the κ_u modifier. This scenario results in Figure 6.2a;
2. In the second scenario the minimum value, χ_{EWPO}^{2min} , of the χ^2 function is found as a function of all four VLQ couplings. The χ^2 is then evaluated at the minimising $[\lambda_{Q_1}^d]_1$ value (that will be called henceforth best-fit, or b.f., value), obtaining once again a function of three couplings. λ_{UQ_1} is instead treated in the same manner as the previous scenario. The allowed values for the remaining two couplings, satisfying the inequalities in Equation (6.4) are shown in Figure 6.2b.

In both plots of Figure 6.2, two κ_u lines are shown: the value in green, $\kappa_u = 260$, is the projected sensitivity limit for the HL-LHC found in [25] while the teal curve is required to be tangent to the 95%CL region and is associated to the largest value of the coupling modifier. In the first scenario, the up quark Yukawa coupling can be up to 2200 times the SM prediction; in the second case the enhancement is more constrained, with $\kappa_u < 1530$. While the allowed interval for $[\lambda_U]_1$ does not differ significantly between the two treatments, a reduction of $[\lambda_{Q_1}^u]_1$'s space when the best-fit value is used can be noticed.

6.2 Higgs Fit

The presence of SMEFT operators affects Higgs Physics by modifying both the Higgs production modes and the decay observables. Both these effects are encoded in the signal strength μ : chosen a Higgs decay channel labelled by α , the

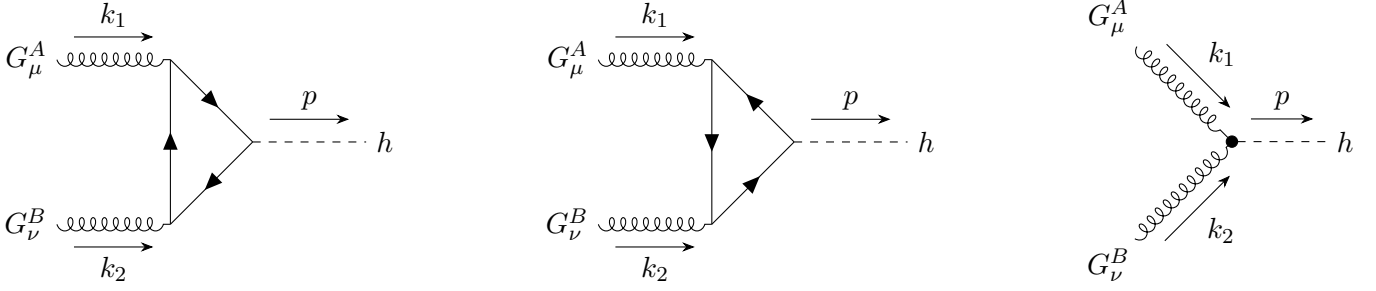


Figure 6.3: Gluon-gluon fusion production of the Higgs boson. The left and middle diagrams are the SM contributions, while the diagram on the right is generated by the SMEFT operator $\mathcal{O}_{\phi G}$.

theoretical prediction for the signal strengths accounting for SMEFT modification reads

$$\mu_\alpha^{th} = \frac{\sigma_{SMEFT} \text{BR}_{SMEFT, \alpha}}{\sigma_{SM} \text{BR}_{SM, \alpha}}, \quad (6.21)$$

where σ is the Higgs boson production cross-section and the BR_α is the branching ratio for the chosen decay mode. The associated experimental values are found by replacing the SMEFT predictions with the experimental results at the numerator. CMS reported in [6] the signal strength measurements for the Higgs boson decays into pairs of gauge bosons ($\gamma\gamma$, W^+W^- and ZZ) and fermion-antifermion pairs ($\bar{b}b$, $\bar{\tau}\tau$ and $\bar{\mu}\mu$).

The final piece for the construction of χ_{HP}^2 is the covariance matrix, supplied in the auxiliary files of [6].

6.2.1 Modified Higgs production cross-section

The following two Higgs boson production channels are considered: gluon-gluon fusion and quark anti-quark annihilation.

Gluon-gluon fusion is the leading production channel for the Higgs boson at the Large Hadron Collider [75]. Given the absence of a coupling in the SM between gluons and the Higgs boson, the production is mediated by a fermionic loop as shown in the one-loop diagrams of Figure 6.3. The Standard Model amplitude, considering only the top quark contribution, reads

$$\mathcal{M}_{SM} = i \frac{\alpha_s}{2\pi v} \epsilon_\mu^A \epsilon_\nu^B \delta_{AB} (k_1^\nu k_2^\mu - k_1 \cdot k_2 g^{\mu\nu}) \tau_t (1 + (1 - \tau_t) f(\tau_t)), \quad (6.22)$$

where $\tau_t = 4m_t^2/m_h^2$ and the function $f(\tau_t)$ is defined as

$$f(\tau_t) = \begin{cases} \arcsin^2 \frac{1}{\sqrt{\tau_t}} & \tau_t \geq 1 \\ -\frac{1}{4} \left[\log \frac{1+\sqrt{1-\tau_t}}{1-\sqrt{1-\tau_t}} - i\pi \right]^2 & \tau_t < 1 \end{cases}. \quad (6.23)$$

Moving to the SMEFT Lagrangian, one can recognise that the operator $\mathcal{O}_{\phi G}$ introduces a tree level contribution to gluon-gluon to Higgs boson fusion, with Feynman diagram also shown in Figure 6.3, as

$$\mathcal{O}_{\phi G} = (G^{A\mu\nu} G_{\mu\nu}^A) (\phi^\dagger \phi) \xrightarrow{\text{SSB}} (G^{A\mu\nu} G_{\mu\nu}^A) \frac{v^2}{2} \left(1 + 2\frac{h}{v} + \frac{h^2}{v^2} \right). \quad (6.24)$$

The amplitude, accounting for the presence of this new operator, becomes

$$\mathcal{M}_{SMEFT} = i \frac{\alpha_s}{2\pi v} \epsilon_\mu^A \epsilon_\nu^B \delta_{AB} (k_1^\nu k_2^\mu - (k_1 \cdot k_2) g^{\mu\nu}) \left(\tau_t (1 + (1 - \tau_t) f(\tau_t)) + \frac{8\pi}{\alpha_s} v^2 \mathcal{C}_{\phi G} \right). \quad (6.25)$$

According to the SM prediction, the production channel associated with the annihilation of first generation quark-

antiquark pairs is negligible, given the small predicted value for the Yukawa couplings. The quark-antiquark annihilation channels (corresponding to $u\bar{u} \rightarrow h$ and $d\bar{d} \rightarrow h$) become increasingly relevant as the Yukawa couplings of the two quarks are enhanced, as considered in references [18, 25], becoming comparable to the gluon fusion cross-section for $O(1000)$ enhancements.

Overall, the production cross-section has the general form

$$\sigma_{SMEFT} = \sigma_{SM} + \sigma_{\phi G} v^2 \mathcal{C}_{\phi G} + \sigma_{uuh} \kappa_u^2 + \sigma_{ddh} \kappa_d^2. \quad (6.26)$$

For the numerical values for the cross-sections, the results found by references [18, 25] were used.

6.2.2 Modified Higgs total width and branching ratios

The leading order effects of the SMEFT operators on the Higgs decay width and branching ratios were studied in [71]. Taking also into account that the decay widths for $h \rightarrow \gamma\gamma$ and $h \rightarrow GG$ are affected by the Higgs field redefinition² and that an enhancement of the first family quark couplings leads to a modification of the decay widths for $h \rightarrow u\bar{u}$ and $h \rightarrow d\bar{d}$, the total decay width reads

$$\begin{aligned} \Gamma_h^{SMEFT} = & \Gamma_h^{SM} \left(1 - 1.50v^2 \mathcal{C}_{\phi W} + 1.21v^2 \mathcal{C}_{\phi WB} + 50.6v^2 \mathcal{C}_{\phi G} + 1.83v^2 \mathcal{C}_{\phi \square} - 0.43v^2 \mathcal{C}_{\phi D} + \right. \\ & + 0.002v^2 \mathcal{C}_{\phi q}^{(1)} + 0.06v^2 \mathcal{C}_{\phi q}^{(3)} + 0.001v^2 \mathcal{C}_{\phi u} - 0.0007v^2 \mathcal{C}_{\phi d} + \\ & \left. + 2v^2 (\text{BR}(h \rightarrow \gamma\gamma) + \text{BR}(h \rightarrow GG)) \mathcal{C}_{kin}^h \right) + \\ & + \hat{\Gamma} \left((1 - \kappa_d)^2 m_d^2 + (1 - \kappa_u)^2 m_u^2 \right). \end{aligned} \quad (6.27)$$

$\hat{\Gamma}$ is obtained by rescaling the decay width for $h \rightarrow b\bar{b}$; once multiplied by $(1 - \kappa_q)^2 m_q^2$ it provides the SMEFT decay width for $h \rightarrow q\bar{q}$, with $q = u, d$.

The SMEFT branching ratios for the decays considered by [6] are taken from [71], corrected by the Higgs field redefinition effects.

It is important to point out that the Higgs Physics construction carries a direct dependence on the coupling modifier: κ_q is directly probed. This was not the case in the ElectroWeak case, therefore it is reasonable to expect that the parameter spaces for the two cases will differ.

Finally, the modifiers enter the χ^2 construction quadratically, introducing a dependence on $O(1/\Lambda^4)$ terms.

6.2.3 Application to Model 1

Considering the specific case of Model 1, the χ^2 function depends on four couplings while the coupling modifier depends on three, as was shown in Equation (6.20). Both the χ^2 and κ_u are brought to depend on only two couplings in the following manner:

- the treatment of $\left[\lambda_{Q_1}^d \right]_1$ is divided in two cases, in the first it is set to be the same as $\left[\lambda_{Q_1}^u \right]_1$ while in the second the HP χ^2 function is minimised as a function of the four couplings and then evaluated at the best-fit value for $\left[\lambda_{Q_1}^d \right]_1$. Both treatments provide a χ^2 function that only depends on three couplings;
- the coupling $\left[\lambda_{Q_1}^u \right]_1$ was set to the value that maximises the contribution to the modifier κ_u . For the 68% CL region, the maximisation is performed requiring that the χ^2 function stays below $\chi_{HP}^{2min} + \chi^2(3, 0.68)$; for the 95% CL case the constraint is to stay below $\chi_{HP}^{2min} + \chi^2(3, 0.95)$. The latter coupling value is substituted in κ_u ;

²Described in Section 5.1, a field redefinition is required to guarantee the canonical normalisation of the Higgs kinetic term. The field redefinition was presented in Equation (5.4)

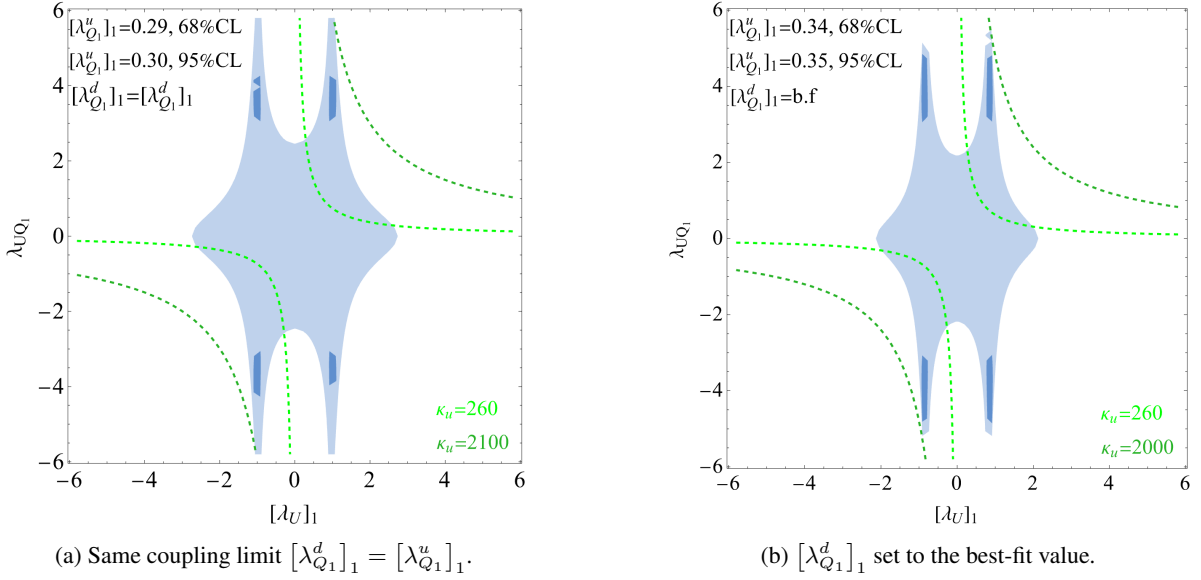


Figure 6.4: 68% and 95% CL regions as a function of the $[\lambda_U]_1$ and λ_{UQ_1} couplings. The value of $[\lambda_{Q_1}^u]_1$ is set to the value that maximises the contribution to κ_u . The two different choices for the fourth coupling $[\lambda_{Q_1}^d]_1$.

- the couplings λ_{UQ_1} and $[\lambda_U]_1$ were left free to vary.

The graphical results are shown in Figure 6.4. Some things should be kept in mind to avoid being misled; first of all, the fact that the origin is excluded in the 68% CL parameter space but included in the 95% CL case does not have implications on the validity of the SM. Indeed, the plots were realised by making assumptions on two of the four couplings, if they were all simultaneously set to zero then the SM would be recovered. Secondly, the two variables left free to vary in the HP study differ from those employed in the ElectroWeak case, as trying to perform graphical studies in terms of $\lambda_{UQ_1}^u$ and λ_U does not result in a parameter space. This is likely due to the fact that the minimum value of the HP χ^2 in both treatments of the $[\lambda_{Q_1}^d]_1$ coupling is ≈ 1.3 , while the SM value is ≈ 5.9 . Having a small minimum value for the χ^2 has an impact on the solution of the inequalities of Equation (6.4).

An alternative treatment that should be investigated in future studies is the removal of degrees of freedom via marginalisation instead of substituting the best-fit value, or the value that maximises the contribution to the coupling modifier. The solution adopted in this thesis is to study the total χ_t^2 accounting for both EWPO and HP at the same time.

6.3 Combined Fit

Having determined χ_{EWPO}^2 and χ_{HP}^2 , they are summed to obtain the total χ_t^2 . For all models, the 68% and 95% CL regions are shown along with the κ -modifiers: two κ -curves are shown in each plot, one corresponding to the projected sensitivity limits of [25] for comparison purposes and the other that is tangent to the region found with the 95% CL constraints. The following convention for the colours and line style is adopted:

- the curves associated with κ_d are shown in solid lines, the literature's value $\kappa_d = 156$ is plotted in cyan, the tangent is in blue;
- for the up-sector, dashed lines are employed, in green for the value from the literature ($\kappa_u = 260$) and in teal the value found in this thesis.

The models involving Q_1 are separated from those that do not: given that Q_1 is the only VLQ that can couple to two different SM quarks, the models that contain it introduce four VLQ couplings, those that do not introduce three couplings.

The κ_q modifiers depend on the product of three couplings, of which one is always associated to the Yukawa-like

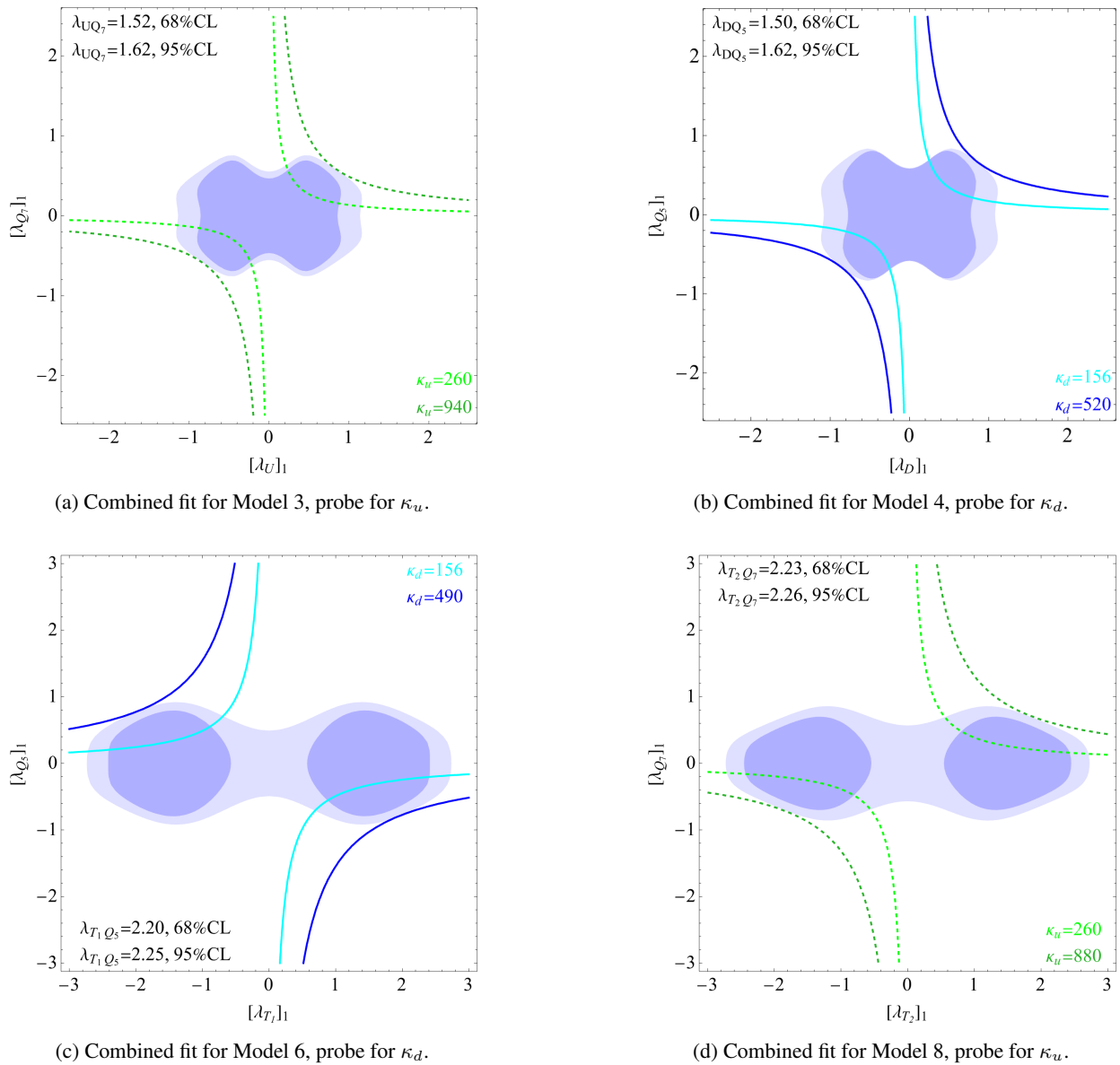


Figure 6.5: 68% and 95% CL regions for Models 3, 4, 6 and 8.

interaction between two VLQs. Therefore, this is the VLQ coupling that will be fixed to the value that maximises the contribution to the coupling modifier κ_q within the 68% and 95% CL constraints; the corresponding values are written in the plot legends. The value associated to the 95% CL maximisation is also used to draw the κ_q curves. An alternative choice would be to set such coupling to 1 and is mentioned in Appendix E.

6.3.1 Models without Q_1

Four models do not contain Q_1 ; they involve either the Q_5 , which can lead to large κ_d , or the Q_7 doublet, which results in a non trivial κ_u . Given the presence of only three couplings, the two scenarios considered for Model 1 are not necessary: it is sufficient to fix the VLQ-VLQ coupling to the value that maximises the contribution to the modifier and to graphically solve the inequalities in Equation (6.4) in terms of the VLQ singlet/triplet and the VLQ doublet couplings to the SM quarks.

The results for the various models are shown in Figure 6.5. The κ -curves associated to the literature values always intersect the allowed parameter space. For these models, κ_u can reach $O(1000)$ values, while κ_d can only go up to $O(500)$, which is expected given that $m_d/m_u \approx 2$ and that the coupling modifiers are mass-dependent. The largest

allowed enhancements are:

$$\kappa_u < 940, \quad \kappa_d < 520. \quad (6.28)$$

The singlet and doublet couplings lie in the approximate interval $[-1, 1]$, instead the two triplet couplings are bound in $[-3, 3]$. This results in the more elongated forms of plots 6.5c and 6.5d. The plots also exhibit cuts that mimic the κ_q curves, hinting at the importance of the Higgs physics contribution (recall that it is in the HP construction that one explicitly introduces the κ -modifiers in the χ^2 -function, see Equations (6.26) and (6.27)).

6.3.2 Models involving Q_1

Moving on to the models containing the Q_1 doublet, the two different scenarios that involve either fixing its two couplings to the SM quarks to be the same or setting one of them to its best-fit value are considered.

The first choice is to set Q_1 's two couplings to be the same before χ^2 is minimised. The third coupling (for the VLQ-VLQ interaction with the Higgs boson) is set to the value that maximises the contribution to the coupling modifier. The resulting plots are shown in Figure 6.6. Notice that while Model 1 (Figure 6.6a) can only generate deviations from 1 of κ_u and Model 2 (Figure 6.6b) deviations of κ_d , Models 5 (Figure 6.6c) and 7 (Figure 6.6d) allow modifications of both. In Model 7 the sets of lines for κ_u and κ_d are very close together: the $m_d/m_u \approx 2$ factor is compensated by the different numerical factors in $\mathcal{C}_{u\phi}$ and $\mathcal{C}_{d\phi}$ from Table 5.24.

Overall, κ_u can achieve up to $O(1000)$ enhancements except for Model 7 in which $\kappa_u < 480$; as for κ_d $O(500)$ values can be reached, except for Model 5 where κ_d 's maximal allowed value is just slightly above the sensitivity limit found by [25]. These enhanced are smaller than the ones obtained in by the models without the Q_1 doublet.

In the second scenario, one of the two Q_1 couplings is set to the best-fit value. For the first two models, the coupling that is fixed is the one that does not appear in the non-trivial modifier, so $\lambda_{Q_1}^d$ for Model 1 (Figure 6.7a) and $\lambda_{Q_1}^u$ for Model 2 (Figure 6.7b). For Models 5 (Figure 6.7c) and 7 (Figure 6.7d), noticing that the electric charge content is skewed towards negative values for Model 5 and positive values for Model 7 justified fixing the values of $\lambda_{Q_1}^u$ and $\lambda_{Q_1}^d$ respectively. In this case Models 5 and 7 no longer allow to study both κ_u and κ_d as functions of two couplings, as can be seen by considering their explicit expressions

$$\begin{aligned} \kappa_u^{M5} &= 1 + \frac{v^3}{2\sqrt{2}m_u M_{T_1} M_{Q_1}} [\lambda_{Q_1}^u]_1 [\lambda_{T_1}]_1 \lambda_{T_1 Q_1}, & \kappa_d^{M5} &= 1 + \frac{v^3}{4\sqrt{2}m_d M_{T_1} M_{Q_1}} [\lambda_{Q_1}^d]_1 [\lambda_{T_1}]_1 \lambda_{T_1 Q_1}, \\ \kappa_u^{M7} &= 1 + \frac{v^3}{4\sqrt{2}m_u M_{Q_1} M_{T_2}} [\lambda_{T_2}]_1 [\lambda_{Q_1}^u]_1 \lambda_{T_2 Q_1}, & \kappa_d^{M7} &= 1 + \frac{v^3}{2\sqrt{2}m_d M_{Q_1} M_{T_2}} [\lambda_{T_2}]_1 [\lambda_{Q_1}^d]_1 \lambda_{T_2 Q_1}. \end{aligned} \quad (6.29)$$

For each model the two modifier expressions differ only for the Q_1 coupling: fixing it and the VLQ-VLQ coupling leaves one of the two modifiers to depend on only one coupling. For Model 5, κ_u^{M5} is left to depend only on $[\lambda_{T_1}]_1$; reading the left-most allowed value for this coupling from Figure 6.7c, one finds $\kappa_u^{M5} < 880$. For Model 7, κ_d^{M7} only depends on $[\lambda_{T_2}]_1$, from Figure 6.7d the modifier $\kappa_d^{M7} < 300$ is found. Overall, there are no significant differences with respect to the previous scenario.

Summing up, Models involving pairs of VLQs coupled only to the first generation quarks can generate enhancements of the up quark coupling to the Higgs boson, making the coupling up to $O(1000)$ times its Standard Model value; the down quark can have a Yukawa coupling $O(500)$ times the Standard Model prediction, while maintaining a good agreement with experimental constraints. The largest enhancements are provided by Model 3 for the up quark coupling and by Model 4 for the down coupling; the corresponding values were reported in Equation (6.28).

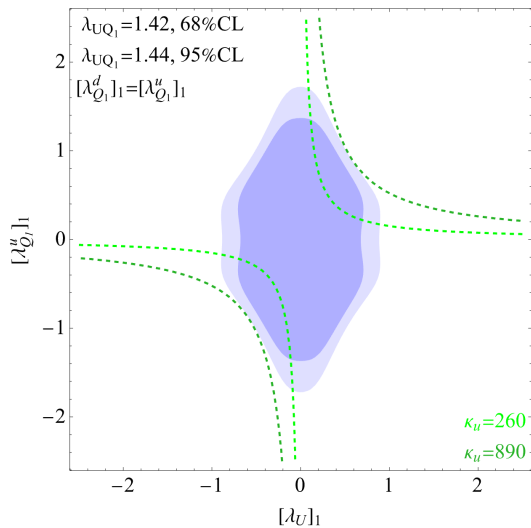
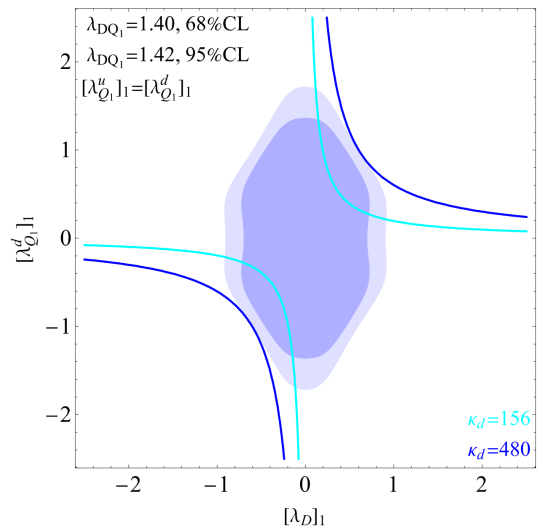
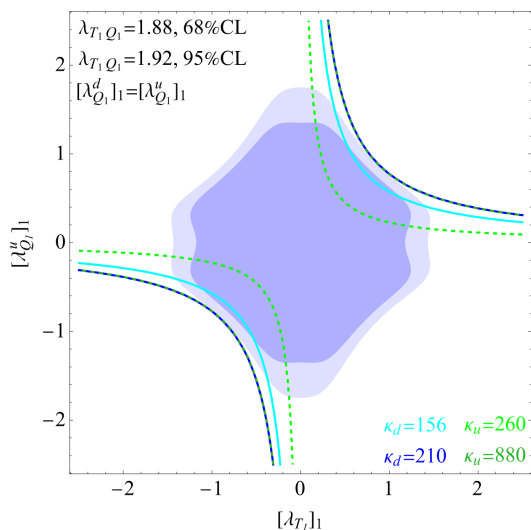
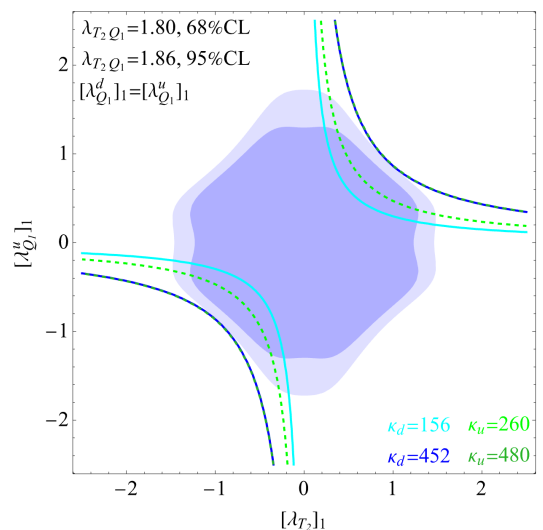
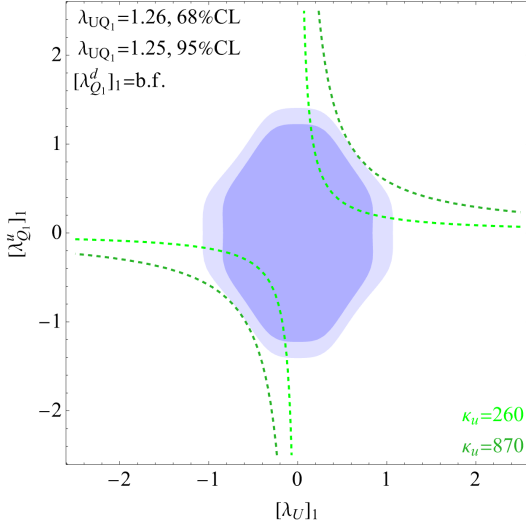
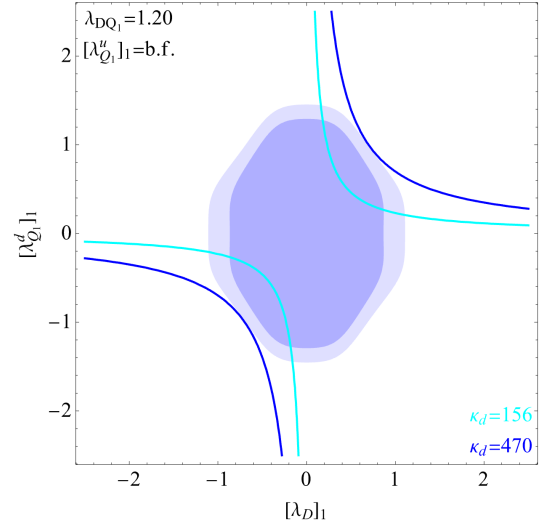
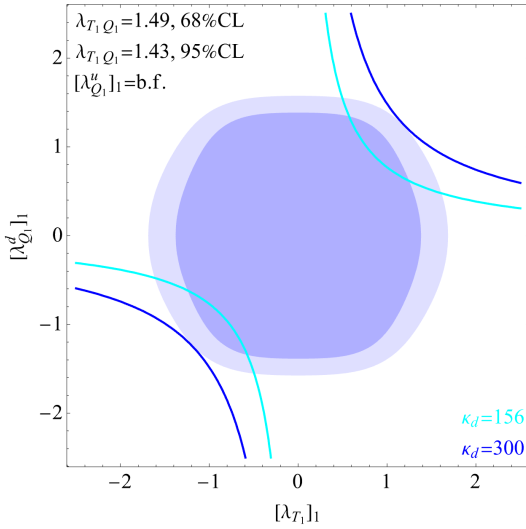
(a) Combined fit for Model 1, probe for κ_u .(b) Combined fit for Model 2, probe for κ_d .(c) Combined fit for Model 5, which introduces deviations both in κ_u and in κ_d .(d) Combined fit for Model 7 along with the different curves for κ_u and κ_d .

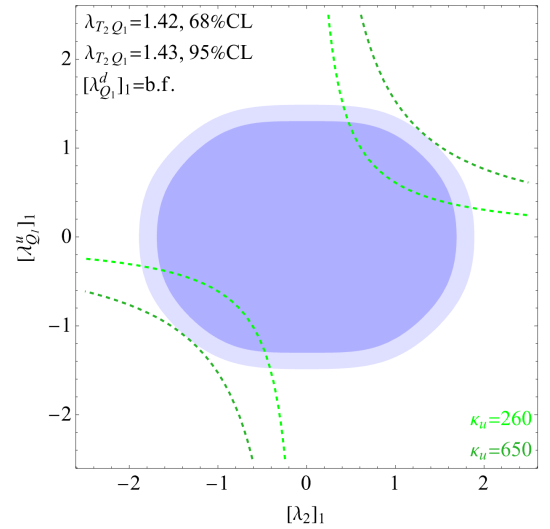
Figure 6.6: 68% and 95% CL regions for models 1, 2, 5 and 7 with $[\lambda_{Q_1}^d]_1 = [\lambda_{Q_1}^u]_1$. Models 5 and 7 allow to probe both κ_u (dashed lines) and κ_d (continuous lines).

As far as the coupling parameter space is concerned, all the couplings of VLQs to SM quarks are found to live in an interval centred on the origin that is at most bounded by $[-3, 3]$.

Considering that for Model 1 both the Higgs and the ElectroWeak fit were performed individually, Figure 6.6a can be compared to the ElectroWeak result in Figure 6.2a, and Figure 6.7a compared to Figure 6.2b, to observe the effects on the ElectroWeak result of including the Higgs Physics contribution. Starting from the original oval shape of the ElectroWeak study, the removal of four portions, approximately following the κ -curves, allows to obtain the combined study's result. The same form is exhibited by the other three models involving the Q_1 doublet: they can all be traced back to ovals from which four portions along the diagonals of the plot frame have been cut out. An exception occurs when considering Model 5 and Model 7 in which the best-fit value for one of the Q_1 couplings has been chosen (Figures 6.7c and 6.7d). However, the same models in the same coupling limit (Figures 6.6c and 6.6d) exhibit the behaviour detailed above; this is another reminder that the choices adopted in this thesis for the removal of coupling-dependences, though reasonable and motivated, are not the unique available solution.

(a) Combined fit for Model 1, probe for κ_u .(b) Combined fit for Model 2, probe for κ_d .

(c) Combined fit for Model 5.



(d) Combined fit for Model 7.

Figure 6.7: 68% and 95% CL regions for models 1, 2, 5 and 7 with one of the two Q_1 couplings $[\lambda_{Q_1}^u]_1$ or $[\lambda_{Q_1}^d]_1$ set to their best-fit value after the minimisation of the χ^2_t . In the case of Model 2, the maximal value of the VLQ-VLQ coupling is the same in for both the 68% and 95% CL cases.

6.4 Application to the Second Generation

For the application to the second generation quarks, the ElectroWeak χ^2 function is constructed considering the presence of the Wilson coefficients $\mathcal{C}_{\phi D}$, $\mathcal{C}_{\phi WB}$ and the second-family coefficients associated with the $\psi^2 \phi^2 D$ -class operators, except for the operator $\mathcal{O}_{\phi ud}$.

For the study of the effects on Higgs Physics, the χ^2 is built accounting for the modifications to Higgs boson decay branching ratios for the final states considered by CMS [6] and for the modification to the Higgs production cross-section due to the presence of the $\mathcal{O}_{\phi G}$ operator and of enhanced charm and strange Yukawa couplings in the quark and anti-quark annihilation channel. Even though there have been dedicated searches for charm quark Yukawa couplings, such as [12, 13, 50], they will not be used in the construction of χ^2_{HP} .

The study is divided into two cases, depending on the presence or not of Q_1 in the model. As was done for the first generation quarks, two-dimensional plots are performed, in which both the κ_q curves and the total χ^2 function depend on two couplings. The VLQ-VLQ couplings always appear in the expressions for the κ modifiers and are fixed in order

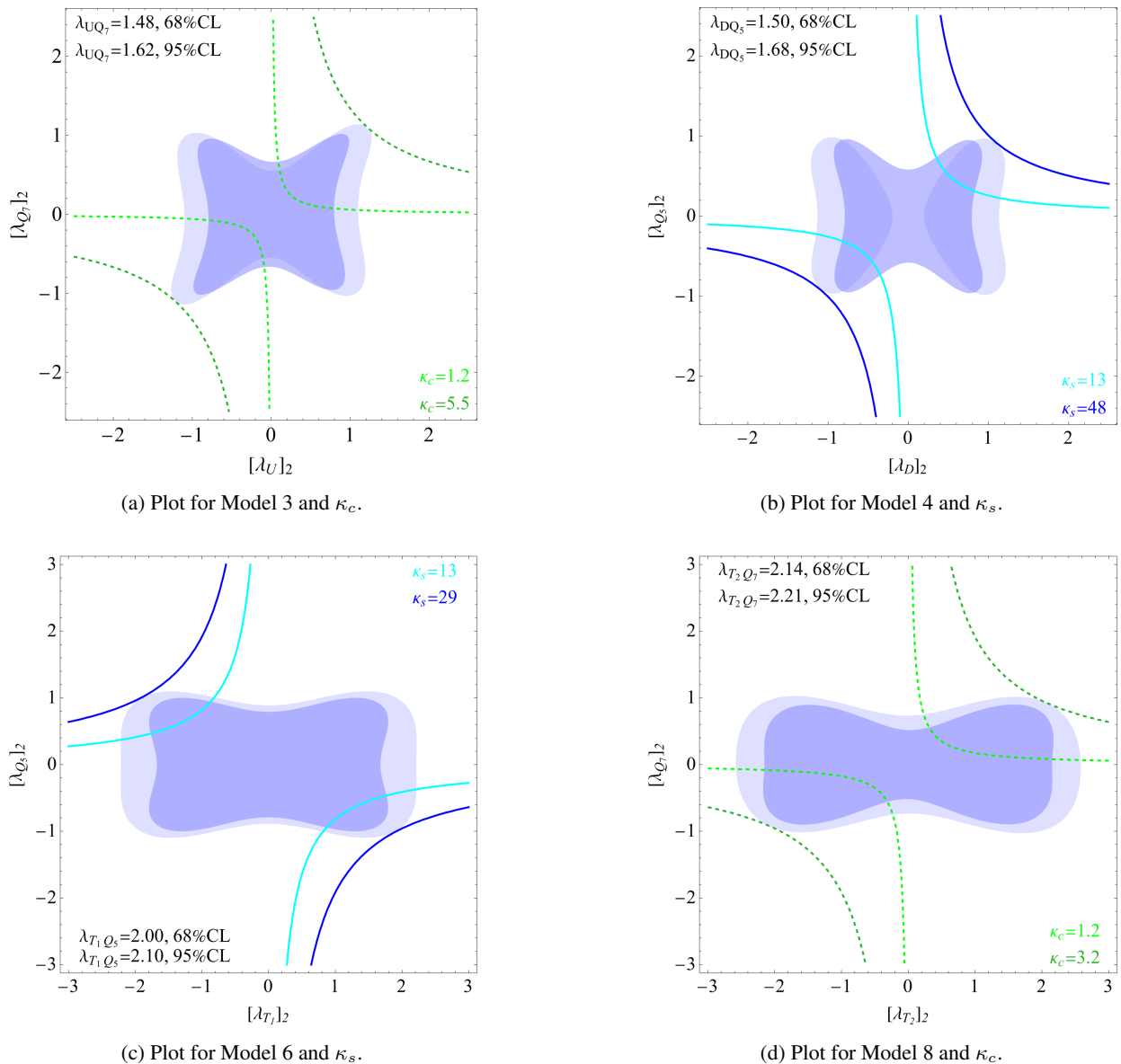


Figure 6.8: 68% and 95% CL regions plots for the models 3, 4, 6 and 8 in which the VLQs are coupled to the second generation SM quarks.

to realise the plots, as was done for the first generation. The conventions for colour and line styles are the following: the curves for the strange quark coupling modifier are solid, in blue for the largest value found in the thesis and cyan the reference $\kappa_s = 13$; the curves for the charm modifier are dashed, green for the reference $\kappa_c = 1.2$ and teal for the largest allowed value.

The simpler case is provided by the models without Q_1 , with results presented in Figure 6.8. The largest enhancements are provided by Model 3 for the charm (Figure 6.8a) and by Model 4 for the strange (Figure 6.8b), they are:

$$\kappa_c < 5.5, \quad \kappa_s < 48. \quad (6.31)$$

The approximate factor 10 difference between the two upper bounds is related to the fact that the charm quark is about 10 times more massive than the strange.

Before moving on to the other models, one should notice that in the case of Model 3 and, especially, Model 4 the 68% CL region is not entirely contained in the 95% CL one, in contrast with the other two models in Figure 6.8 and also those that will be shown in Figures 6.9 and 6.10. This is due to the fact that, while for most models the two different

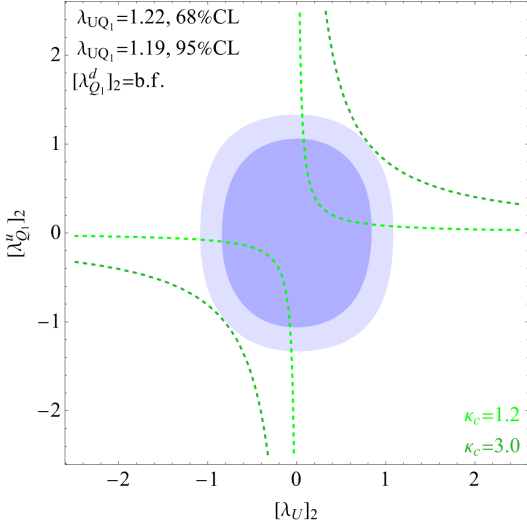
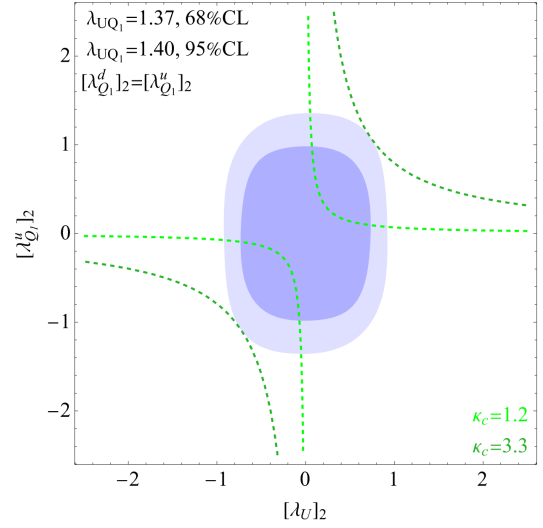
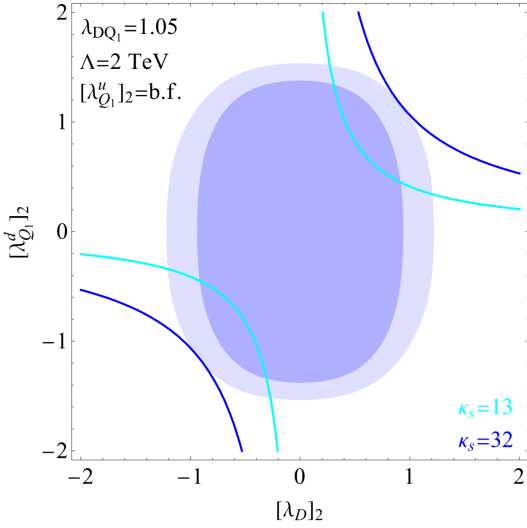
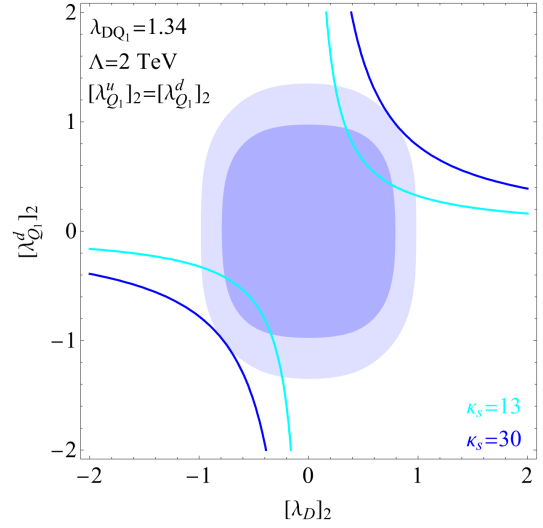
(a) Plot for model 1 with $[\lambda_{Q_1}^d]_2$ set to the best-fit value.(b) Plot for Model 1 with $[\lambda_{Q_1}^d]_2 = [\lambda_{Q_1}^u]_2$.(c) Plot for Model 2 with $[\lambda_{Q_1}^u]_2$ set to the best-fit value.(d) Plot for Model 2 where $[\lambda_{Q_1}^d]_2 = [\lambda_{Q_1}^u]_2$.

Figure 6.9: Plots for the models involving the doublet Q_1 and one of the singlets (either U or D) coupled to the second generation of the SM quarks. On the left there are the plots in which one of Q_1 's coupling has been set to the best-fit value, on the right the two couplings are set to be the same.

values found for the VLQ-VLQ coupling are very close, having therefore limited impact on the χ^2 function once they are substituted, for Models 3 and 4 there is an approximate 10% difference between the two.

Considering now the models that contain the Q_1 doublet, the same two scenarios considered for the first generation are constructed. While in the previous section the two cases were treated separately, here they are set side-by-side for each model.

In Figure 6.9, the plots for the models involving Q_1 and one of the VLQ singlets are shown: having the two scenarios close clearly shows that once again there is only a slight difference between the two. The literature projections for κ_c and κ_s intersect the allowed parameter space, though the allowed values for the modifiers found here are more constrained than those obtained by Models 3 and 4.

In Figure 6.10 the plots for the models containing the Q_1 doublet and one of the triplets are presented. In this case, the two scenarios are very different: if the two couplings of Q_1 are set to be the same, both κ_c and κ_s can be probed (Figures 6.10b and Figures 6.10d). If instead one of the two couplings is fixed to its best-fit value, then only one of the two coupling modifiers remains a function of two couplings, the other instead will only depend on one coupling, as can be concluded by replacing the first family indices with those of the second family in Equations (6.29) and (6.30).

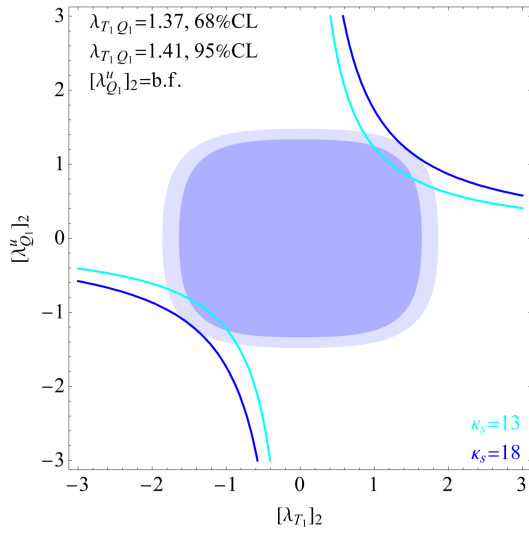
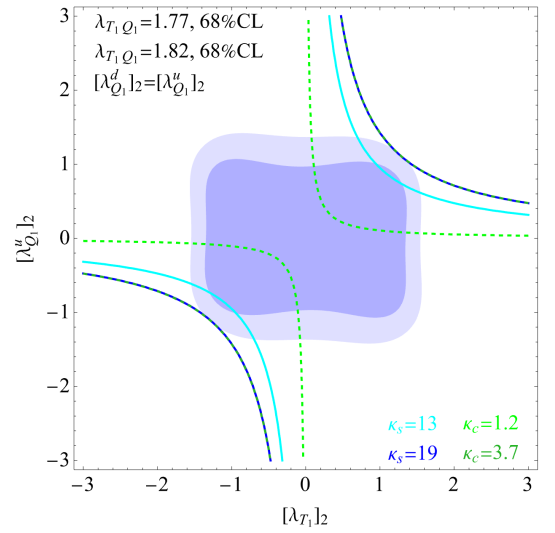
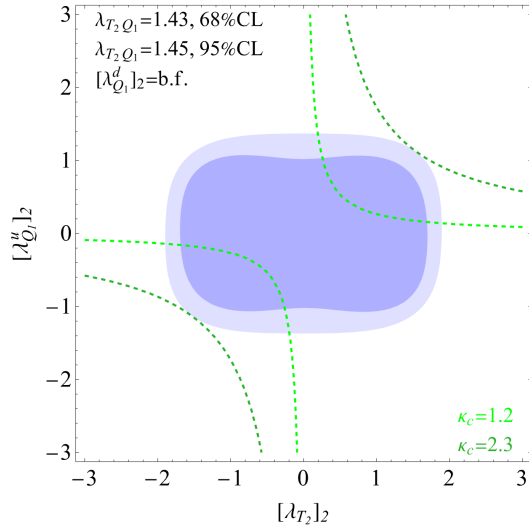
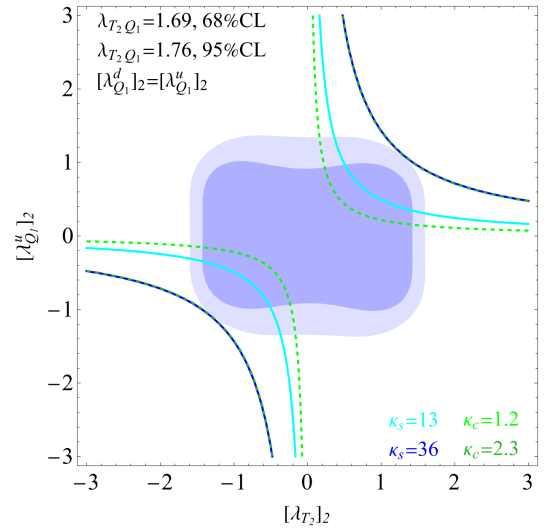

 (a) Plot for Model 5 with $[\lambda_{Q_1}^d]_2 = \text{b.f.}$ and κ_c .

 (b) Plot for Model 5 with $[\lambda_{Q_1}^d]_2 = [\lambda_{Q_1}^u]_2$.

 (c) Plot for Model 7 with $[\lambda_{Q_1}^u]_2 = \text{b.f.}$ and κ_s .

 (d) Plot for Model 7 with $[\lambda_{Q_1}^d]_2 = [\lambda_{Q_1}^u]_2$.

Figure 6.10: Plots for the models involving the doublet Q_1 and one of the triplets (either T_1 or T_2) coupled to the second generation of the SM quarks. On the left the either $[\lambda_{Q_1}^u]_2$ or $[\lambda_{Q_1}^d]_2$ is set to the best-fit value, on the right $[\lambda_{Q_1}^u]_2 = [\lambda_{Q_1}^d]_2$.

In this scenario Model 5 allows for large deviations with respect to the SM in κ_s (Figure 6.10a) while Model 7 for large deviation in κ_c (Figure 6.10c). The graphically omitted κ enhancements are $\kappa_c^{M5} = 1.4$ and $\kappa_s^{M7} = 20$. Also in this case, larger enhancements were found by considering Models 3 and 4.

For the second generation quarks, VLQs with order one couplings to the SM second-generation quarks can be admitted. The largest enhancement for the Yukawa couplings was provided by Model 4 for the strange and by Model 3 for the charm, Equation (6.31). Interestingly, the upper bound found for the charm couplings modifier κ_c is comparable with the 95% CL interval found by [12], which is

$$1.1 < |\kappa_c^{CMS}| < 5.5. \quad (6.32)$$

This result was derived considering the associated production of the Higgs boson with a vector boson, under the assumption that only one quark Yukawa coupling is modified (which is exactly the case of Model 3) and the production

cross-section is unaffected. This allows to rewrite the signal strength defined in Equation (6.21) as

$$\mu_{h \rightarrow \bar{c}c} = \frac{\kappa_c^2}{1 + (\kappa_c^2 - 1)\text{BR}^{SM}(h \rightarrow \bar{c}c)}, \quad (6.33)$$

from which the value of $|\kappa_c|$ is derived once the signal strength is experimentally determined. This result motivates the interest in the continued improvements in the charm coupling measurements.

Chapter 7

Direct Searches

The experimental searches for VLQs are performed in various final states, involving a SM quark and either a massive gauge boson or the Higgs boson¹. The VLQs are considered to be produced either individually or in pairs.

The production of a single VLQ is a model-dependent electroweak process that requires the knowledge of the VLQ coupling to the W^\pm and Z bosons and on the VLQ mass [76–78]. This type of production is expected to dominate for larger VLQ masses compared to the pair production; however, the searches that have so far been performed consider the VLQs to be coupled only to the third generation SM quarks. The final states for these searches therefore involve only the top or the bottom quark. Given that in the models considered in this thesis the VLQs are coupled only to the lighter quark generations, the results for the single production cannot be used.

Having excluded the single production searches, VLQ pair production is considered (Figure 7.1). This is a QCD process whose cross-section depends solely on the mass of the VLQs and is therefore model independent. However, for large VLQ masses the energy required to produce two on-shell VLQs is quite large, leading to a phase space suppression. Pair production has been studied both considering the VLQs coupled to the third generation SM quarks [79–83] and in the case the VLQs are coupled to the lighter quarks [26], which is exactly what is being studied here. The latter search is based on the data collected during Run 2 at LHC, its results will be used in this chapter to find the appropriate value to which the VLQ mass Λ should be set for the study in the previous chapter.

Figure 7.1 also shows the available decay channels for the VLQs, as mentioned involving a boson (the Higgs boson or the massive gauge bosons) and a light quark.

To perform the analysis, the ATLAS collaboration had to select a decay channel and make an assumption on the



Figure 7.1: Example Feynman diagrams for VLQ pair production via gluon fusion and subsequent possible decays.

¹In the context of experimental searches, the name "Higgs boson" h refers to the degree of freedom of the Higgs doublet ϕ that appears as a physical particle in the broken phase.

corresponding branching ratio (BR): the two different choices and the consequent bounds on the VLQ masses are reported in Section 7.1. After that, theoretical predictions of the branching ratios for the VLQs in the models considered in this thesis are derived and then compared to those assumed by ATLAS. When the BRs for the models are different from the ones assumed by ATLAS, the bounds from the ATLAS search can be rescaled. Model 1 is studied explicitly, whereas for the study of the decays in the remaining models a generalised description is developed and employed. Several formulae and intermediate steps are required for this study; to guarantee readability many intermediate steps and results are only presented in Appendix G.

7.1 ATLAS Search

The decay channel chosen by ATLAS sees both the VLQs of the pair decaying into a SM quark and a W^\pm boson. Of the two resulting W bosons, one is selected to decay leptonically (e.g. $W^- \rightarrow l_r \nu_r$, $l_r = e, \mu$) and the other hadronically. The final state is, therefore, characterised by the presence of at least three jets, a charged lepton (electron² or muon³) and missing transverse momentum which is associated with neutrino production.

To perform the analysis an assumption had to be made on the branching ratio for the decay channel of the VLQs into a quark+ W final state; ATLAS considers two scenarios and reports the corresponding lower bounds. In the following let ψ be the VLQ and q the SM quark.

1. In the first scenario, $\text{BR}(\psi \rightarrow qW) = 1$ was assumed and led to $\Lambda > 1.530$ TeV at 95% Confidence Level (CL);
2. In the second case, a 95% CL lower bound of $\Lambda > 1.150$ TeV was found in the limit $\text{BR}(\psi \rightarrow qW : qZ : qh) = 0.5 : 0.25 : 0.25$.

7.2 Decays in Model 1

The calculation of branching ratios requires knowledge of the partial and the total decay widths of the VLQs, which in turn need the appropriate interaction vertices to be identified. In the original Lagrangian \mathcal{L}_{NP} before SSB there is no interaction of the VLQs with gauge bosons and SM quarks: in the following, it is shown how these interactions arise after SSB and moving to a basis in which the quark mass matrix is diagonal.

The relevant Lagrangian terms are labelled as follows: \mathcal{L}_W contains quark interaction with the massive W boson, \mathcal{L}_Z involves the quarks and the neutral Z boson, \mathcal{L}^{H+VLQ} contains the Yukawa interactions of the Higgs with the quarks (both SM and vector-like) and the VLQ mass term, finally the Lagrangian component \mathcal{L}_h contains the interactions of the quarks with the Higgs h in the broken phase.

The starting point is \mathcal{L}^{H+VLQ} after SSB, this Lagrangian contribution can be split into two parts: mass term and interaction with the Higgs h term. From the mass term, non-diagonal mass matrices can be identified and can be put into diagonal form through bi-unitary rotations of the quark fields. The determination of the transformations will be performed by a perturbative diagonalisation procedure and is valid up to higher-order corrections. The required rotation has to be performed also in \mathcal{L}_W and \mathcal{L}_Z , thus affecting the interactions of the VLQs not only with the Higgs h but also with the massive gauge bosons. The different interaction vertices and the associated couplings can then be determined and the decay amplitudes be computed.

7.2.1 Gauge and Higgs sector before and after Spontaneous Symmetry Breaking

Starting from the gauge sector, the interactions of the VLQs with W_μ^j and B_μ are picked up from the VLQ covariant derivative term. This is the same as what was seen in Subsection 2.4.3 for the SM particles (except for the absence of

²Detected in the electromagnetic calorimeter.

³Detected in the muon chamber, the outermost layer in detectors. The schematics for the ATLAS detector are reported in Appendix F.

projectors to left or right-handed fields)

$$-\mathcal{L}_{NP}^{gauge} = \bar{Q}_1 \left(\frac{g_L}{2} \sigma^J \mathcal{W}^J + g_Y Y_{Q_1} \mathcal{B} \right) Q_1 + \bar{U} (g_Y Y_u \mathcal{B}) U. \quad (7.1)$$

Including the SM quarks and using Equations (2.13) and (2.14) to rewrite W_μ^J and B_μ in terms W_μ^\pm and Z_μ :

$$-\mathcal{L}_W = \frac{g_L}{\sqrt{2}} \left(\bar{q}_L \sigma^+ \mathcal{W}^+ q_L + \bar{Q}_1 \sigma^+ \mathcal{W}^+ Q_1 + \bar{q}_L \sigma^- \mathcal{W}^- q_L + \bar{Q}_1 \sigma^- \mathcal{W}^- Q_1 \right), \quad (7.2)$$

$$\begin{aligned} -\mathcal{L}_Z = & \frac{g_L}{\cos \theta_W} \bar{q}_L \left(\frac{1}{2} \sigma^3 - Q_q \sin^2 \theta_W \right) \mathcal{Z} q_L + \frac{g_L}{\cos \theta_W} \bar{Q}_1 \left(\frac{1}{2} \sigma^3 - Q_{Q_1} \sin^2 \theta_W \right) \mathcal{Z} Q_1 + \\ & - \frac{g_L}{\cos \theta_W} \left(\bar{U} Q_U \sin^2 \theta_W \mathcal{Z} U + \bar{u}_R Q_u \sin^2 \theta_W \mathcal{Z} u_R + \bar{d}_R Q_d \sin^2 \theta_W \mathcal{Z} d_R \right). \end{aligned} \quad (7.3)$$

As for the term involving the Yukawa interactions and the VLQ mass terms, setting $M_U = M_{Q_1} = \Lambda$,

$$\begin{aligned} -\mathcal{L}^{H+VLQ} = & y_u \bar{q}_L \tilde{\phi} u_R + y_d \bar{q}_L \phi d_R + \lambda_{Q_1}^u \bar{Q}_{1L} \tilde{\phi} u_R + \lambda_{Q_1}^d \bar{Q}_{1L} \phi d_R + \lambda_U \bar{q}_L \tilde{\phi} U_R + \lambda_{UQ_1} \bar{Q}_{1L} \tilde{\phi} U_R + \text{h.c.} + \\ & + \Lambda \bar{U}_L U_R + \Lambda \bar{Q}_{1L} Q_{1R} + \text{h.c.} . \end{aligned} \quad (7.4)$$

Accounting for SSB, recalling $q_L = \begin{pmatrix} u_L & d_L \end{pmatrix}^T$ and $Q_1 = \begin{pmatrix} T & B \end{pmatrix}^T$, the above Lagrangian term can be recast as

$$\begin{aligned} -\mathcal{L}^{H+VLQ} = & \left(\bar{u}_L \quad \bar{T}_L \quad \bar{U}_L \right) \underbrace{\begin{pmatrix} y_u \frac{v}{\sqrt{2}} & 0 & \lambda_U \frac{v}{\sqrt{2}} \\ \lambda_{Q_1}^u \frac{v}{\sqrt{2}} & \Lambda & \lambda_{UQ_1} \frac{v}{\sqrt{2}} \\ 0 & 0 & \Lambda \end{pmatrix}}_{M_u} \begin{pmatrix} u_R \\ T_R \\ U_R \end{pmatrix} + \frac{h}{\sqrt{2}} \left(\bar{u}_L \quad \bar{T}_L \quad \bar{U}_L \right) \begin{pmatrix} y_u & 0 & \lambda_U \\ \lambda_{Q_1}^u & 0 & \lambda_{UQ_1} \\ 0 & 0 & 0 \end{pmatrix} \begin{pmatrix} u_R \\ T_R \\ U_R \end{pmatrix} + \\ & + \left(\bar{d}_L \quad \bar{B}_L \right) \underbrace{\begin{pmatrix} y_d \frac{v}{\sqrt{2}} & 0 \\ \lambda_{Q_1}^d \frac{v}{\sqrt{2}} & \Lambda \end{pmatrix}}_{M_d} \begin{pmatrix} d_R \\ B_R \end{pmatrix} + \frac{h}{\sqrt{2}} \left(\bar{d}_L \quad \bar{B}_L \right) \begin{pmatrix} y_d \frac{v}{\sqrt{2}} & 0 \\ \lambda_{Q_1}^d \frac{v}{\sqrt{2}} & 0 \end{pmatrix} \begin{pmatrix} d_R \\ B_R \end{pmatrix} + \text{h.c.} . \end{aligned} \quad (7.5)$$

The mass matrices for the up (M_u) and down (M_d) sectors are identified.

As for the gauge sector after SSB, the expressions for \mathcal{L}_W and \mathcal{L}_Z are reported in Appendix G.1.

7.2.2 Perturbative diagonalisation of the Mass matrices

Having identified the non-diagonal matrices M_u and M_d and setting the two Yukawa couplings y_d and y_u to zero, they are diagonalised perturbatively. The difference between perturbative and exact diagonalisation is that the latter is written in terms of an expansion parameter, in this case v/Λ , and is required to hold up to a given order in this parameter (the second).

Similarly to what was shown in Subsection 2.4.4 for the change of basis for the Yukawa matrices, the quark rotation has to be performed in all sectors of the Lagrangian density. Each rotation involves only one VLQ Yukawa-like coupling at a time; this is included in the notation by giving the rotation matrices an upper index identifying the row and column where the coupling appears in the mass matrix. So, for example, U_{Lup}^{13} acts on the left-handed up-type quarks and contains the couplings λ_U . The explicit expressions of the transformation matrices are reported in Appendix G.1.

Using a prime to denote the quarks in the rotated basis, the rotations that diagonalise the mass matrices are:

$$M_u^{diag} = U_{Lup}^{23} U_{Lup}^{13} M_u U_{Rup}^{21\dagger} U_{Rup}^{23\dagger} \quad \& \quad M_d^{diag} = \mathbb{1}_{2 \times 2} M_d U_{Rdown}^{21\dagger}; \quad (7.6)$$

$$\begin{pmatrix} u'_L \\ T'_L \\ U'_L \end{pmatrix} = U_{Lup}^{23} U_{Lup}^{13} \begin{pmatrix} u_L \\ T_L \\ U_L \end{pmatrix}, \quad \begin{pmatrix} u'_R \\ T'_R \\ U'_R \end{pmatrix} = U_{Rup}^{23} U_{Rup}^{21} \begin{pmatrix} u_R \\ T_R \\ U_R \end{pmatrix} \quad \& \quad \begin{pmatrix} d'_L \\ B'_L \end{pmatrix} = \begin{pmatrix} d_L \\ B_L \end{pmatrix}, \quad \begin{pmatrix} d'_R \\ B'_R \end{pmatrix} = U_{Rdown}^{21} \begin{pmatrix} d_R \\ B_R \end{pmatrix}. \quad (7.7)$$

The diagonalised matrices turn out to be:

$$M_u^{diag} = \Lambda \left[\begin{pmatrix} 0 & 0 & 0 \\ 0 & 1 - \frac{\lambda_{UQ_1} v}{2\sqrt{2} \Lambda} & 0 \\ 0 & 0 & 1 + \frac{\lambda_{UQ_1} v}{2\sqrt{2} \Lambda} \end{pmatrix} + O\left(\frac{v^2}{\Lambda^2}\right) \right] \quad \& \quad M_d^{diag} = \Lambda \left[\begin{pmatrix} 0 & 0 \\ 0 & 1 \end{pmatrix} + O\left(\frac{v^2}{\Lambda^2}\right) \right] \quad (7.8)$$

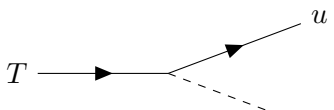
7.2.3 Effects of the rotation on the interactions

To lighten the notation, the primes on the rotated quarks are dropped. The explicit expressions for \mathcal{L}_W , \mathcal{L}_Z and \mathcal{L}_h after the rotation turn out to be quite cumbersome; they are reported in Appendix G.1. The Feynman rules can be read off the appropriate Lagrangian terms. In the following, only those relevant for the computation of the decays are reported.

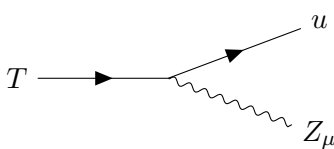
7.2.4 Decay widths and branching ratios

The decay widths for two-body decays are a known result [84], the branching ratios for a particular decay channel is defined as the ratio between the decay width for that particular channel and the total decay width of the particle.

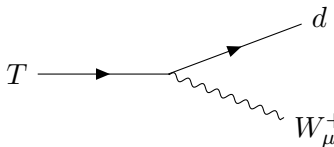
Considering the VLQ T , simply by looking at charge conservation one can identify the following decay modes: $T \rightarrow u + h$ (7.9), $T \rightarrow u + Z$ (7.10) and $T \rightarrow d + W^+$ (7.11). For each of these models, the interaction vertex and the final decay width are reported, assuming that the VLQs are much heavier than the SM quarks and the Higgs boson, whose can therefore be neglected. The generation index of the couplings is dropped.



$$T \longrightarrow \begin{matrix} u \\ h \end{matrix} \quad -i \frac{\lambda_U}{2} P_R + i \frac{\lambda_{Q_1}^u}{2} P_L \quad \Rightarrow \quad \Gamma_{T \rightarrow uh} = \frac{1}{128\pi} (\lambda_U^2 + (\lambda_{Q_1}^u)^2) \Lambda; \quad (7.9)$$



$$T \longrightarrow \begin{matrix} u \\ Z_\mu \end{matrix} \quad i \frac{M_Z}{2\Lambda} \gamma^\mu (\lambda_U P_L + \lambda_{Q_1}^u P_R) \quad \Rightarrow \quad \Gamma_{T \rightarrow uZ} = \frac{1}{128\pi} (\lambda_U^2 + (\lambda_{Q_1}^u)^2) \Lambda; \quad (7.10)$$



$$T \longrightarrow \begin{matrix} d \\ W_\mu^+ \end{matrix} \quad i \frac{M_W}{\sqrt{2}\Lambda} \gamma^\mu (\lambda_U P_L + \lambda_{Q_1}^d P_R) \quad \Rightarrow \quad \Gamma_{T \rightarrow dW} = \frac{1}{64\pi} (\lambda_U^2 + (\lambda_{Q_1}^d)^2) \Lambda; \quad (7.11)$$

Having these results, the total decay width for the T Vector-like Quark is

$$\Gamma_T = \frac{1}{64\pi} \left((\lambda_{Q_1}^u)^2 + (\lambda_{Q_1}^d)^2 + 2\lambda_U^2 \right), \quad (7.12)$$

from which three branching functions can be derived:

$$\text{BR}(T \rightarrow Zu) = \text{BR}(T \rightarrow hu) = \frac{1}{2} \frac{\lambda_U^2 + (\lambda_{Q_1}^u)^2}{2\lambda_U^2 + (\lambda_{Q_1}^u)^2 + (\lambda_{Q_1}^d)^2}, \quad (7.13)$$

$$\text{BR}(T \rightarrow W^+d) = \frac{\lambda_U^2 + (\lambda_{Q_1}^d)^2}{(\lambda_{Q_1}^u)^2 + (\lambda_{Q_1}^d)^2 + 2\lambda_U^2}. \quad (7.14)$$

The graphs shown in Figures 7.2a and 7.2b were made by leaving $\lambda_{Q_1}^d$ and $\lambda_{Q_1}^u$ free to vary while the third coupling is set to its best-fit value (from the combined fit in the previous Chapter): $\lambda_U = -0.210$.

In the limit of same squared couplings of the Q_1 doublet to the u_R and d_R quarks, the branching ratios are found to be:

$$\text{BR}(T \rightarrow W^+d) \xrightarrow{(\lambda_{Q_1}^d)^2 \rightarrow (\lambda_{Q_1}^u)^2} 0.5, \quad \text{BR}(T \rightarrow Zu) \xrightarrow{(\lambda_{Q_1}^d)^2 \rightarrow (\lambda_{Q_1}^u)^2} 0.25 \quad \text{BR}(T \rightarrow hu) \xrightarrow{\lambda_{Q_1}^{d2} \rightarrow \lambda_{Q_1}^{u2}} 0.25. \quad (7.15)$$

This reproduces exactly ATLAS' second scenario, which excludes masses $\Lambda < 1.15$ TeV with a 95% CL. However, it comes at the cost of assuming that the two couplings have the same modulus, which is not something expected a priori.

Turning to the other two VLQ components, U turns out to have the same decay widths as T ; for B , instead, the branching ratios, shown in Figures 7.2c and 7.2d, are:

$$\text{BR}(B \rightarrow hd) = \text{BR}(B \rightarrow Zd) = \frac{1}{2} \frac{(\lambda_{Q_1}^d)^2}{(\lambda_{Q_1}^u)^2 + (\lambda_{Q_1}^d)^2} \xrightarrow{(\lambda_{Q_1}^d)^2 \rightarrow (\lambda_{Q_1}^u)^2} 0.25, \quad (7.16)$$

$$\text{BR}(B \rightarrow W^-u) = \frac{(\lambda_{Q_1}^u)^2}{(\lambda_{Q_1}^u)^2 + (\lambda_{Q_1}^d)^2} \xrightarrow{(\lambda_{Q_1}^d)^2 \rightarrow (\lambda_{Q_1}^u)^2} 0.5. \quad (7.17)$$

Again, ATLAS' second scenario is found in the same squared-coupling limit. Assumption 1, instead, is not recovered.

In conclusion, this affects the fits performed in the previous chapter for Model 1 in the following manner:

1. For the first scenario in which $\lambda_{Q_1}^d = \lambda_{Q_1}^u$ was used, one had to set $\Lambda > 1.150$ TeV;
2. For the second scenario the coupling $\lambda_{Q_1}^d$ was set to its best-fit value. In this case the bound could be avoided.

7.3 Generalisation to all models

Table 4.3 of Chapter 4 contained the electromagnetic charges associated to the different VLQ components. Keeping in mind the particular case of Model 1, the goal is to organise the particle content in multiplets based on their electromagnetic charge. Then the \mathcal{L}_W , \mathcal{L}_Z and \mathcal{L}_h Lagrangian contributions can be written as a series of matrices and particle multiplets. From the mass matrices, recognised in the Higgs sector, it is possible to identify and perform the rotations that put them in diagonal form, thus affecting all the other interactions.

The generalisation is achieved by consistently introducing all the possible charged particles, with the addition of auxiliary couplings and variables. The specific models are uniquely extracted using replacement rules for such auxiliary couplings and variables.

The available particle content can be organised in categories as follows:

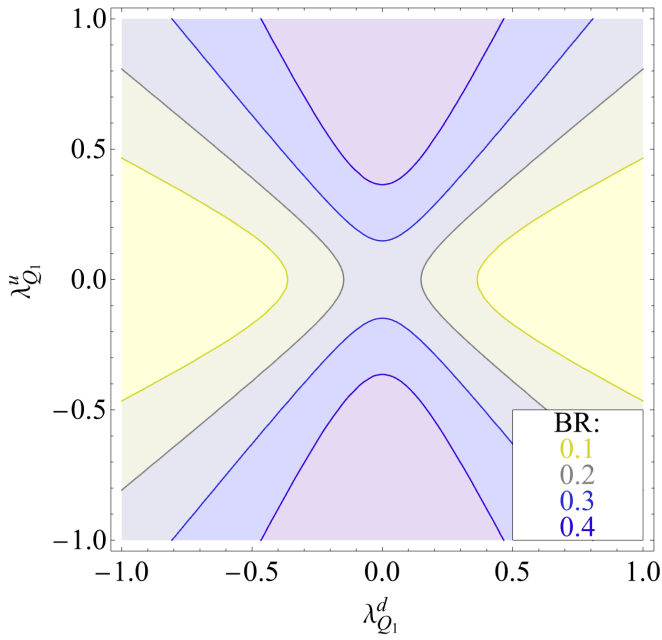
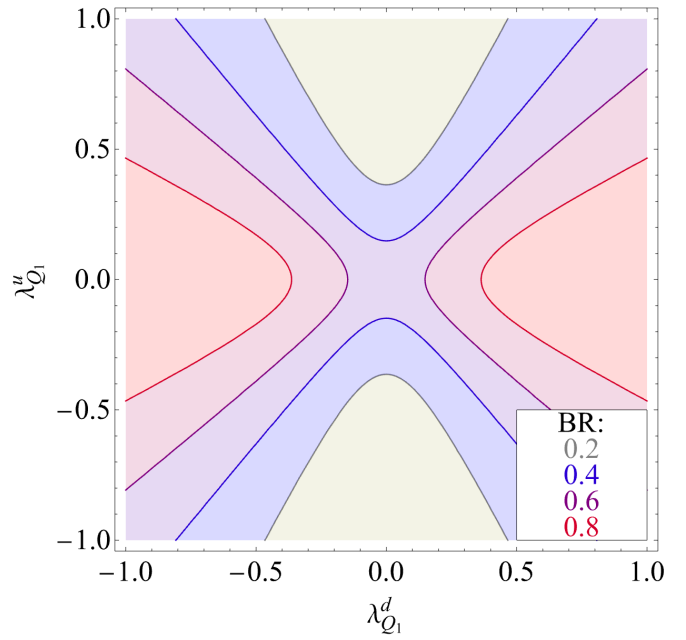
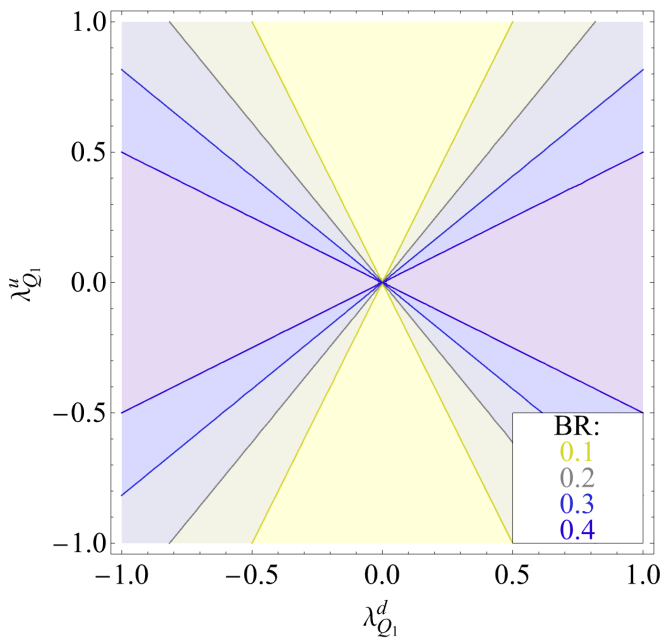
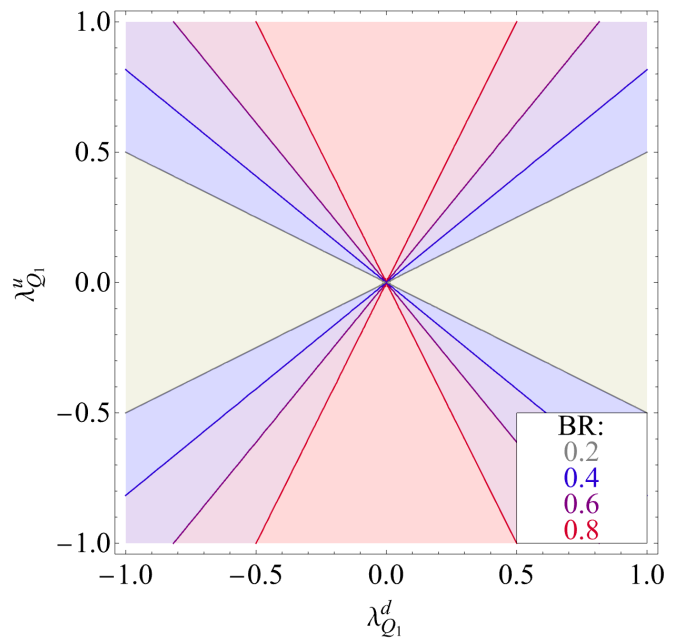
(a) BRs for the T and U decays into hu or Zu .(b) BRs for the T and U decays into W^+d .(c) BRs for the B decays into hd or Zd .(d) BRs for the B decays into W^-u .

Figure 7.2: Contour plots for the BRs for the decays of U , T and B as described by Model 1. For all three cases, the BRs for the final state involving a SM quark and either the Z or the Higgs boson are the same, so only one plot is shown (plots on the left). Additionally, the T and U decays have the same final states and associated BRs, hence the plots are shown only once (upper plots).

charge 2/3 : five different particles have this charge. They are the SM up quark u , the T component of the doublets Q_1 and Q_7 , the U singlet and the $T_{1,2}^{2/3}$ component from the triplets. Noticing that U , $T_1^{2/3}$ and $T_2^{2/3}$ never appear in the same model, they are denoted by a common symbol Su ;

charge -1/3 : again there are five particles satisfying the requirement. They are the SM down quark d , the B component of Q_1 and Q_5 , the D singlet and $T_{1,2}^{-1/3}$. Also in this case, since the singlet and the triplets are never simultaneously present, they are grouped into Sd ;

charge -4/3 : charge carried by the Y , associated with Q_5 , and $T_1^{-4/3}$;

charge 5/3 : corresponds to X from Q_7 and $T_2^{5/3}$.

This means that the following multiplets can be built:

$$\mathcal{U} = \begin{pmatrix} u \\ T \\ Su \end{pmatrix} \quad \text{where } Su \in \{U, T_1^{2/3}, T_2^{2/3}\}, \quad (7.18)$$

$$\mathcal{D} = \begin{pmatrix} d \\ B \\ Sd \end{pmatrix} \quad \text{where } Sd \in \{D, T_1^{-1/3}, T_2^{-1/3}\}, \quad (7.19)$$

$$\mathcal{X} = \begin{pmatrix} X \\ T_2^{5/3} \end{pmatrix}, \quad \mathcal{Y} = \begin{pmatrix} Y \\ T_1^{-4/3} \end{pmatrix} \quad (7.20)$$

The "Higgs+VLQ mass" term in the Lagrangian can be written as

$$-\mathcal{L}^{H+VLQ} = \bar{\mathcal{U}}_L M_{\mathcal{U}} \mathcal{U}_R + \bar{\mathcal{D}}_L M_{\mathcal{D}} \mathcal{D}_R + \bar{\mathcal{X}}_L M_{\mathcal{X}} \mathcal{X}_R + \bar{\mathcal{Y}}_L M_{\mathcal{Y}} \mathcal{Y}_R + \\ + h (\bar{\mathcal{U}}_L C_{\mathcal{U}} \mathcal{U}_R + \bar{\mathcal{D}}_L C_{\mathcal{D}} \mathcal{D}_R + \bar{\mathcal{X}}_L C_{\mathcal{X}} \mathcal{X}_R + \bar{\mathcal{Y}}_L C_{\mathcal{Y}} \mathcal{Y}_R). \quad (7.21)$$

The first line contains the mass matrices, defined below, and the second the interactions of the quarks with the Higgs boson h , where the coupling matrices are defined as $C_{\alpha} = \frac{\partial}{\partial v} M_{\alpha}$. The mass matrices are:

$$M_{\mathcal{U}} = \begin{pmatrix} y_u \frac{v}{\sqrt{2}} & 0 & \lambda_{Su} \frac{v}{\sqrt{2}} \\ \lambda_Q^u \frac{v}{\sqrt{2}} & M & \lambda_{SuQ} \frac{v}{\sqrt{2}} \\ 0 & 0 & M \end{pmatrix}, \quad M_{\mathcal{X}} = \begin{pmatrix} M & \lambda_{XQ} \frac{v}{\sqrt{2}} \\ 0 & M \end{pmatrix}, \quad (7.22)$$

$$M_{\mathcal{D}} = \begin{pmatrix} y_d \frac{v}{\sqrt{2}} & 0 & \lambda_{Sd} \frac{v}{\sqrt{2}} \\ \lambda_Q^d \frac{v}{\sqrt{2}} & M & \lambda_{SdQ} \frac{v}{\sqrt{2}} \\ 0 & 0 & M \end{pmatrix}, \quad M_{\mathcal{Y}} = \begin{pmatrix} M & \lambda_{YQ} \frac{v}{\sqrt{2}} \\ 0 & M \end{pmatrix}. \quad (7.23)$$

The replacement rules for the auxiliary coupling constants introduced before are given for each model in Table 7.1. The auxiliary variables mentioned above needed for the construction of the generalised rotations to the mass basis and of the generalised \mathcal{L}_W and \mathcal{L}_Z Lagrangian terms are given in Appendix G.2 together with the model specific replacement rules.

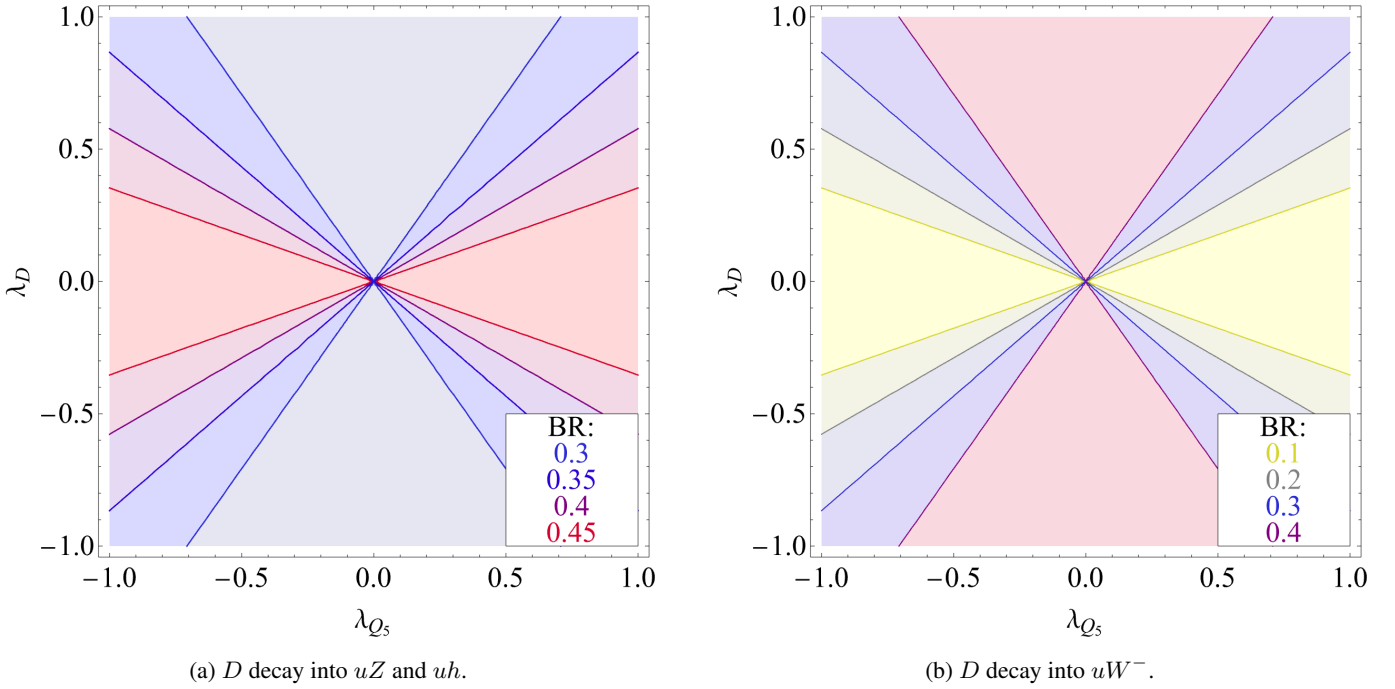
7.3.1 Generalised decay widths

Having the generalised description, the decays as described by other models can now be studied.

Starting from the components bearing the same charges as the SM quarks, there is no further insight: ATLAS's second scenario can be recovered by taking the appropriate limit in the VLQ doublet couplings to the SM singlets. Consider

Model	λ_{Su}	λ_Q^u	λ_{SuQ}	λ_{XQ}	λ_{Sd}	λ_Q^d	λ_{SdQ}	λ_{YQ}
1	λ_U	$\lambda_{Q_1}^u$	λ_{UQ_1}	0	0	$\lambda_{Q_1}^d$	0	0
2	0	$\lambda_{Q_1}^u$	0	0	λ_D	$\lambda_{Q_1}^d$	λ_{DQ_1}	0
3	λ_U	λ_{Q_7}	λ_{UQ_7}	0	0	0	0	0
4	0	0	0	0	λ_D	λ_{Q_5}	λ_{DQ_5}	0
5	$\frac{1}{\sqrt{2}}\lambda_{T_1}$	$\lambda_{Q_1}^u$	$\frac{1}{\sqrt{2}}\lambda_{T_1Q_1}$	0	$-\frac{1}{2}\lambda_{T_1}$	$\lambda_{Q_1}^d$	$-\frac{1}{2}\lambda_{T_1Q_1}$	0
6	$\frac{1}{\sqrt{2}}\lambda_{T_1}$	0	0	0	$-\frac{1}{2}\lambda_{T_1}$	λ_{Q_5}	$\frac{1}{2}\lambda_{T_1Q_5}$	$\frac{1}{\sqrt{2}}\lambda_{T_1Q_5}$
7	$\frac{1}{2}\lambda_{T_2}$	$\lambda_{Q_1}^u$	$\frac{1}{2}\lambda_{T_2Q_1}$	0	$\frac{1}{\sqrt{2}}\lambda_{T_2}$	$\lambda_{Q_1}^d$	$\frac{1}{\sqrt{2}}\lambda_{T_2Q_1}$	0
8	$\frac{1}{2}\lambda_{T_2}$	λ_{Q_7}	$-\frac{1}{2}\lambda_{T_2Q_7}$	$\frac{1}{\sqrt{2}}\lambda_{T_2Q_7}$	$\frac{1}{\sqrt{2}}\lambda_{T_2}$	0	0	0

Table 7.1: Coupling substitutions to obtain the particular model starting from the generalisation.

Figure 7.3: Plots showing the different values the branching ratios for the decays of D as described by Model 4. The decay channels involving the neutral Z and h have the same branching ratio.

for example the decays of the D VLQ in Model 4 (whose New Physics particle content consists in D and Q_5), the resulting branching ratios are shown in Figure 7.3 and are expressed as:

$$\text{BR}(D \rightarrow hd) = \text{BR}(D \rightarrow Zd) = \frac{1}{2} \frac{\lambda_D^2 + \lambda_{Q_5}^2}{2\lambda_D^2 + \lambda_{Q_5}^2} \xrightarrow{\lambda_{Q_5} \rightarrow 0} 0.25, \quad (7.24)$$

$$\text{BR}(D \rightarrow W^-u) = \frac{\lambda_D^2}{2\lambda_D^2 + \lambda_{Q_5}^2} \xrightarrow{\lambda_{Q_5} \rightarrow 0} 0.5. \quad (7.25)$$

While in the presence of the Q_1 doublet there are two couplings $\lambda_{Q_1}^d$ and $\lambda_{Q_1}^u$ and the scenario is recovered in the limit they become the same, Q_5 can only couple to d_R and the coupling λ_{Q_5} has to be set to zero.

The overall conclusion is that, as long as the VLQs being studied have SM charges, an appropriate choice of the couplings can provide Assumption 2, while scenario 1 in the ATLAS analysis does not appear. In the presence of a SM-charged particle, all three decay channels are available.

The situation is different once the particles with new charges are introduced, which happens in all models except for

the first two. In this case, the only possible decays are:

$$X \rightarrow u W^+ \quad \text{and} \quad T_2^{5/3} \rightarrow u W^+, \quad (7.26)$$

$$Y \rightarrow d W^- \quad \text{and} \quad T_1^{-4/3} \rightarrow d W^-. \quad (7.27)$$

Without requiring calculations, the scenario $\text{BR}(\psi \rightarrow qW) = 1$ is automatically recovered.

Considering the assumption that the VLQs have the same mass Λ , the take-away message from this study is that the lower mass bounds can only be avoided for the first two models with the requirement $\lambda_{Q_1}^d \neq \lambda_{Q_1}^u$. If $\lambda_{Q_1}^d = \lambda_{Q_1}^u$, or if a VLQ with charge $-4/3$ or $5/3$ is present, then the bounds from scenarios 1 and 2 respectively have to be applied.

To treat all the models equally but still be consistent with the ATLAS result, in the previous Chapter $\Lambda = 2 \text{ TeV}$ was picked.

Chapter 8

Conclusions and Future Studies

Knowing that the Standard Model is not the final theory for our understanding of Particle Physics, many new models have been developed, each trying to address at least one of the questions left unanswered by the Standard Model. Some of these models introduce new hypothetical particles known as vector-like quarks, which can couple to the Higgs boson via Yukawa-like couplings but that do not require the Higgs mechanism to gain a mass term. Simplified models were considered in this thesis: vector-like quarks were studied in the context of producing enhancements to the couplings of the two lighter quark generations to the Higgs boson, without referring to any of the specific models that address open problems in the Standard Model by introducing vector-like quarks.

With the assumption that the vector-like quarks can couple only to one generation of Standard Model quarks at a time, that they appear in only one generation and can have a coupling amongst themselves, eight different models involving pairs of vector-like quarks can be built.

The New Physics models were matched onto the dimension-six SMEFT Lagrangian in the Warsaw basis. The SMEFT provides a model-independent framework to study the departure of observables from the Standard Model predictions; in particular, the correspondence between SMEFT operator and its effect on an observable has been extensively documented in the literature. This allows the construction of χ^2 functions written entirely out of the SMEFT coefficients that, after the matching results have been substituted, allow the translation of experimental bounds on the New Physics parameters. For the models considered in this thesis, the parameters are the Yukawa-like couplings of vector-like quarks to the Higgs bosons and their masses; the experimental bounds are taken from ElectroWeak Precision Tests and Higgs Physics.

Accounting for the recent experimental searches for pair-produced vector-like quarks with couplings to the lighter generation quarks performed by the ATLAS collaboration, the values of the masses were all set to be $\Lambda = 2 \text{ TeV}$. In this case, the models considered in this thesis could produce values for the ratio between the New Physics prediction for the Yukawa coupling and its Standard Model value for the first generation quarks up to

$$\kappa_u < 940, \quad (8.1)$$

$$\kappa_d < 520, \quad (8.2)$$

while still being compatible with ElectroWeak Precision Tests and Higgs Physics measurements.

As for the second generation quarks, the models can have values up to

$$\kappa_c < 5.5, \quad (8.3)$$

$$\kappa_s < 48. \quad (8.4)$$

The result for the charm quark coupling enhancement is consistent with the one found by the CMS collaboration at 95% CL interval, which is $1.1 < |\kappa_c^{CMS}| < 5.5$; such result motivates to improve on these searches since they are starting to probe realistic parameter space.

Models involving vector-like quarks have therefore been shown to generate considerable enhancements of the light quark Yukawa couplings. Dedicated searches for the charm quark coupling are already being performed and promising proposals have been put forward for the other three quarks: the measurements of their enhancements could be within the reach of future experimental searches.

Throughout the work, several future directions have been identified:

- In Chapter 4 a different type of New Physics model which can generate quark-Yukawa enhancements was identified: it consists in adding one vector-like quark and one heavy scalar to the Standard Model description. Also in this case the number of possible pairs that can be made is finite and can be studied in complete analogy with what was done in this thesis;
- In light of the community effort to identify future collider experiments, these eight models can be a case study. Since in particular ElectroWeak precision measurements were found to lead to important constraints, the study of how a future FCC-ee run at the Z pole would impact the parameter space of these models is motivated;
- Still regarding the study of the parameter space, other ways to reduce the number of variables in the χ^2 functions to two should be investigated. For example, marginalisation with respect to a variable, instead of associating to it a numerical value, could provide interesting results;
- The assumption that the vector-like quarks can only couple to one generation of Standard Model quarks at a time can be relaxed. This would allow to exploit Flavour Physics as a source of bounds for the couplings;
- The effects of higher dimension operators can also be considered. In this thesis only deviations due to the dimension-six Warsaw basis operators were accounted for, which cause deviations in the observables proportional to Λ^{-2} . However, in the construction of the Higgs Physics χ^2 -function, terms proportional to κ_q^2 and $(1 - \kappa_q)^2$ were introduced: this implies that Λ^{-4} suppressed terms are expected to have a non-negligible effect. Given that Λ^{-4} is associated, in the tower expansion of the Effective Field Theory, to the dimension-eight operators, such operators could also meaningfully contribute.
- For the Higgs Physics study, the only observables considered were total rates. However, differential measurements are also available, which could potentially provide better constraints on the parameter space.

Appendix A

Group Theory

In this appendix, relevant group theory results are presented. Several works describing the use of group theory for particle physics can be found in the literature. For this section [85, 86] were used as references.

Groups which often appear in Physics are the Lie groups $SU(N)$, $N \geq 2$, and $U(1)$. Such groups are identified by their generators T^a (where $a \in \{1, \dots, N^2 - 1\}$) and the commutation relations of such generators. The generators are normalised so that

$$\text{Tr}[T^a T^b] = \frac{1}{2} \delta^{ab}. \quad (\text{A.1})$$

A group is said to be Abelian if its generators commute, if not the group is said to be non-Abelian. The commutation relations between the generators of a given group are written as

$$[T^a, T^b] = i f^{abc} T^c. \quad (\text{A.2})$$

The f^{abc} factors are known as structure constants, they are by definition antisymmetric under permutations of the indices. The previous definition of Abelian group implies that such groups have vanishing structure constants. The structure constants are also used to characterise the group in the adjoint representation.

The only groups that appear in this thesis are the SM ones: the Abelian $U(1)$ and the non-Abelian $SU(N)$, with $N = 2, 3$.

Starting from $U(1)$, its generator is the identity matrix $\mathbb{1}$. The generators for $SU(3)$ and $SU(2)$ are presented below.

A.1 Gell-Mann Matrices

The $SU(3)$ gauge group is associated to the Gell-Mann matrices defined below. To guarantee the normalisation requirement in Equation (A.1), the group generators are defined to the $T^A = \frac{1}{2} \lambda^A$.

$$\begin{aligned} \lambda_1 &= \begin{pmatrix} 0 & 1 & 0 \\ 1 & 0 & 0 \\ 0 & 0 & 0 \end{pmatrix}, & \lambda_2 &= \begin{pmatrix} 0 & -i & 0 \\ i & 0 & 0 \\ 0 & 0 & 0 \end{pmatrix}, & \lambda_3 &= \begin{pmatrix} 1 & 0 & 0 \\ 0 & -1 & 0 \\ 0 & 0 & 0 \end{pmatrix}, & \lambda_4 &= \begin{pmatrix} 0 & 0 & 1 \\ 0 & 0 & 0 \\ 1 & 0 & 0 \end{pmatrix}, \\ \lambda_5 &= \begin{pmatrix} 0 & 0 & -i \\ 0 & 0 & 0 \\ i & 0 & 0 \end{pmatrix}, & \lambda_6 &= \begin{pmatrix} 0 & 0 & 0 \\ 0 & 0 & 1 \\ 0 & 1 & 0 \end{pmatrix}, & \lambda_7 &= \begin{pmatrix} 0 & 0 & 0 \\ 0 & 0 & -i \\ 0 & i & 0 \end{pmatrix}, & \lambda_8 &= \frac{1}{\sqrt{3}} \begin{pmatrix} 1 & 0 & 0 \\ 0 & 1 & 0 \\ 0 & 0 & -2 \end{pmatrix}. \end{aligned} \quad (\text{A.3})$$

The non-zero structure constants are listed below. The others are either null or obtained by permuting the indices.

$$\begin{aligned}
 f^{123} &= 1, \\
 f^{147} &= f^{156} = f^{246} = f^{345} = -f^{257} = -f^{367} = \frac{1}{2}, \\
 f^{458} &= f^{678} = \frac{\sqrt{3}}{2}.
 \end{aligned} \tag{A.4}$$

A.2 Pauli Matrices

The SU(2) group generators consists in the rescaled Pauli matrices $\tau^J = \frac{1}{2}\sigma^J$. The Pauli matrices are:

$$\sigma^1 = \begin{pmatrix} 0 & 1 \\ 1 & 0 \end{pmatrix}, \quad \sigma^2 = \begin{pmatrix} 0 & -i \\ i & 0 \end{pmatrix}, \quad \sigma^3 = \begin{pmatrix} 1 & 0 \\ 0 & -1 \end{pmatrix}. \tag{A.5}$$

The structure constant in this case is the Levi-Civita tensor: $f^{JJK} = \epsilon^{JJK}$.

Appendix B

Triplet Interactions with the W^\pm and Z Bosons

Some more detail on the VLQs in triplet presentations of $SU(2)$, namely $T_1 \sim (3, 3)_{-\frac{1}{3}}$ and $T_2 \sim (3, 3)_{\frac{2}{3}}$, are provided. The interaction terms for the VLQs with the electroweak gauge bosons are picked up from the covariant derivative in the fermionic kinetic term. In the presence of an $SU(2)$ triplet, this has the form (explicating all the indices):

$$D_\mu T_\alpha^{aJ} = \partial_\mu T_1^{aJ} + ig_S \frac{\lambda_{ab}^A}{2} G_\mu^A T_\alpha^{bJ} + ig_L (T_{adj}^J)^{\beta\gamma} W_\mu^\beta T_\alpha^{a\gamma} + ig_Y B_\mu T_\alpha^{aJ}, \quad \alpha = 1, 2. \quad (\text{B.1})$$

The W^\pm and Z appear in the broken symmetry phase, as shown in Subsection 2.4.1. For $T_1 \sim (3, 3)_{-\frac{1}{3}}$ three charge states can be build out of $T_1 = \begin{pmatrix} T_1^1 & T_1^2 & T_1^3 \end{pmatrix}^T$; the same can be done for $T_2 \sim (3, 3)_{\frac{2}{3}}$, with $T_2 = \begin{pmatrix} T_2^1 & T_2^2 & T_2^3 \end{pmatrix}^T$. The charge states are defined in Tables B.1 and B.2 respectively.

The Lagrangian terms describing T_1 's interaction with the W and Z boson are, respectively,

$$-\frac{1}{g_L} \mathcal{L}_W = \left(-\bar{T}_1^{-4/3} \not{W}^- T_1^{-1/3} + \bar{T}_1^{-1/3} \not{W}^- T_1^{2/3} + \text{h.c.} \right), \quad (\text{B.2})$$

$$\begin{aligned} -\frac{\cos \theta_W}{g_L} \mathcal{L}_Z &= \left(1 - \frac{2}{3} \sin^2 \theta_W \right) \bar{T}_1^{2/3} \not{Z} T_1^{2/3} + \left(-1 + \frac{4}{3} \sin^2 \theta_W \right) \bar{T}_1^{-4/3} \not{Z} T_1^{-4/3} + \\ &+ \left(0 + \frac{1}{3} \sin^2 \theta_W \right) \bar{T}_1^{-1/3} \not{Z} T_1^{-1/3}. \end{aligned} \quad (\text{B.3})$$

Similarly, for T_2 one can write

$$-\frac{1}{g_L} \mathcal{L}_W = \left(-\bar{T}_2^{-1/3} \not{W}^- T_2^{2/3} + \bar{T}_2^{2/3} \not{W}^- T_2^{5/3} + \text{h.c.} \right), \quad (\text{B.4})$$

$$\begin{aligned} -\frac{\cos \theta_W}{g_L} \mathcal{L}_Z &= \left(1 - \frac{5}{3} \sin^2 \theta_W \right) \bar{T}_2^{5/3} \not{Z} T_2^{5/3} + \left(-1 + \frac{1}{3} \sin^2 \theta_W \right) \bar{T}_2^{-1/3} \not{Z} T_2^{-1/3} + \\ &+ \left(0 - \frac{2}{3} \sin^2 \theta_W \right) \bar{T}_2^{2/3} \not{Z} T_2^{2/3}. \end{aligned} \quad (\text{B.5})$$

Notice that T_1 and T_2 always introduce two particles with SM-singlet-like charges. For convenience, Table B.3

Notation	Definition	Charge
$T_1^{2/3}$	$\frac{T_1^1 - iT_1^2}{\sqrt{2}}$	$1 + Y_{T_1} = \frac{2}{3}$
$T_1^{-4/3}$	$\frac{T_1^1 + iT_1^2}{\sqrt{2}}$	$-1 + Y_{T_1} = -\frac{4}{3}$
$T_1^{-1/3}$	T_1^3	$0 + Y_{T_1} = -\frac{1}{3}$

Table B.1: Charge states from the Triplet T_1 .

Notation	Definition	Charge
$T_2^{5/3}$	$\frac{T_2^1 - iT_2^2}{\sqrt{2}}$	$1 + Y_{T_2} = \frac{5}{3}$
$T_2^{-1/3}$	$\frac{T_2^1 + iT_2^2}{\sqrt{2}}$	$-1 + Y_{T_2} = -\frac{1}{3}$
$T_2^{2/3}$	T_2^3	$0 + Y_{T_2} = \frac{2}{3}$

Table B.2: Charge states from the Triplet T_2 .

Field	Charges			
	$-\frac{4}{3}$	$-\frac{1}{3}$	$\frac{2}{3}$	$\frac{5}{3}$
Q_1	-	B	T	-
Q_5	Y	B	-	-
Q_7	-	-	T	X
T_1	$T_1^{-4/3}$	$T_1^{-1/3}$	$T_1^{2/3}$	-
T_2	-	$T_2^{-1/3}$	$T_2^{2/3}$	$T_2^{5/3}$

Table B.3: Charges introduced by the VLQs in models from 5 to 8.

contains all the possible charges introduced by the particles involved in Models 5 to 8.

Notice that, due to the presence of one of the triplets in each of these models, there will always be a new particle per sector. In particular, Models 5 and 7, which, besides one of the triplets, also contain the Q_1 doublet, introduce a total of four particles with SM-like charges and a fifth with a new one. Models 6 and 8, instead, add three SM-like particles and two new ones.

The interaction of the triplets with the other doublets (both SM and VLQ) contains a Pauli matrix, with the "adjoint" index contracted with the triplet and the "fundamental" one contracted with the doublet's $SU(2)$ index. Eg, for Model 5,

$$\begin{aligned}
 -\mathcal{L}_{NP}^{int} \supset \frac{\lambda_{T_1}}{2} \bar{T}_{1R}^j \phi^\dagger \sigma^j q_L &= \frac{\lambda_{T_1}}{2} \bar{T}_{1R}^j \phi^{i\dagger} \sigma_{ij}^j q_L \stackrel{\text{Eq. (B.7)}}{=} \frac{\lambda_{T_1}}{2} [\bar{T}_{1R}]_{ij} \phi^{i\dagger} q_L^j \\
 &\stackrel{\text{SSB.}}{=} \frac{\lambda_{T_1}}{2} (v+h) \left(\bar{T}_{1R}^{2/3} u_L - \frac{1}{\sqrt{2}} \bar{T}_{1R}^{-1/3} d_L \right). \tag{B.6}
 \end{aligned}$$

Where we defined

$$T_1 = T_1^j \sigma^j = \begin{pmatrix} T_1^3 & T_1^1 - iT_1^2 \\ T_1^1 + iT_1^2 & -T_1^3 \end{pmatrix} \stackrel{\text{Tab. B.1}}{=} \begin{pmatrix} T_1^{-1/3} & \sqrt{2} T_1^{2/3} \\ \sqrt{2} T_1^{-4/3} & -T_1^{-1/3} \end{pmatrix}, \tag{B.7}$$

$$T_2 = T_2^j \sigma^j = \begin{pmatrix} T_2^3 & T_2^1 - iT_2^2 \\ T_2^1 + iT_2^2 & -T_2^3 \end{pmatrix} \stackrel{\text{Tab. B.2}}{=} \begin{pmatrix} T_2^{2/3} & \sqrt{2} T_2^{5/3} \\ \sqrt{2} T_2^{-1/3} & -T_2^{2/3} \end{pmatrix}. \tag{B.8}$$

Appendix C

Feynman Rules

In this appendix, the Feynman rules for the VLQ interactions with the Higgs doublet ϕ and the gauge bosons G_μ^A , W_μ^J and B_μ are reported. The different indices that the quark q may have are specified as q_{ar}^i , where a is the colour index, r the flavour index and i the isospin index.

Additionally, the Feynman rules associated to the operators of the $\phi^2\psi^2D$ -class in the Warsaw SMEFT basis are summarised. These were employed in the course of Chapter 5.

C.1 VLQ Yukawa-like Interactions

The interactions of the VLQs with the Higgs doublet are generally shown in Figure C.1. While the the $SU(2)$ index of the Higgs doublet is explicated in the figures, the quarks are generically denoted by ψ_1 and ψ_2 .

In Table C.1 the Feynman rules for the interaction of one VLQ with a SM quark and the Higgs ϕ are specified. These are associated with the diagram on the left of Figure C.1. The rules associated with the Feynman diagram on the right of the same figure are found by hermitian conjugation: the roles of ψ_1 and ψ_2 are exchanged (hence changing the projector P involved), the complex conjugate of the couplings λ is taken and the indices of ϵ and δ are exchanged.

Instead, Table C.2 summarises the Feynman rules associated with the interaction of a pair of VLQs with the Higgs boson. Once again, the rules reported are associated with the Feynman diagram on the left of Figure C.1, while the rules for the diagram on the right are found by considering the hermitian conjugate.

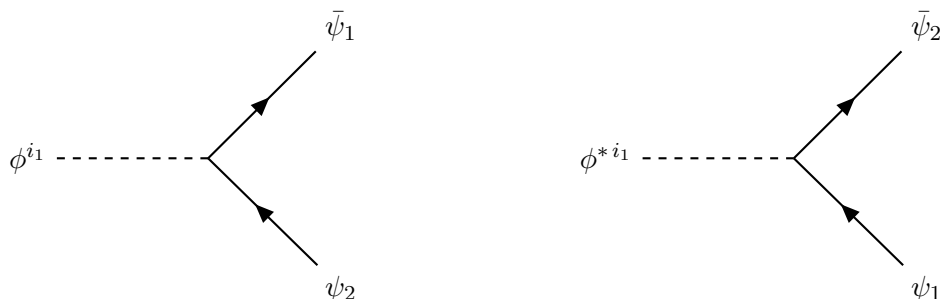


Figure C.1: Two possible diagrams for Yukawa interactions of the Higgs doublet with quarks, be them the SM quarks or the VLQs.

SU(2)	VLQ	ψ_1	ψ_2	Feynman Rule
Singlet	U	$U_{R a_2}$	$q_{L a_1 r}^{i_2}$	$i [\lambda_U]_r \epsilon_{i_1 i_2} \delta_{a_1 a_2} P_L$
	D	$q_{L a_1 r}^{i_2}$	$D_{R a_2}$	$-i [\lambda_D]_r^* \delta_{i_2 i_1} \delta_{a_1 a_2} P_R$
Doublet	Q_1	$u_{R a_1 r}$	$Q_{1 L a_2}^{i_2}$	$i [\lambda_{Q_1}^u]_r^* \epsilon_{i_1 i_2} \delta_{a_1 a_2} P_L$
		$Q_{1 L a_2}^{i_2}$	$d_{R a_1 r}$	$-i [\lambda_{Q_1}^d]_r \delta_{i_2 i_1} \delta_{a_1 a_2} P_R$
	Q_5	$d_{R a_1 r}$	$Q_{5 L a_2}^{i_2}$	$i [\lambda_{Q_5}]_r^* \epsilon_{i_1 i_2} \delta_{a_1 a_2} P_L$
	Q_7	$Q_{7 L a_2}^{i_2}$	$u_{R a_1 r}$	$-i [\lambda_{Q_7}]_r \delta_{i_2 i_1} \delta_{a_1 a_2} P_R$
Triplet	T_1	$q_{L a_2 r}^{i_2}$	$T_{1 R a_1}^J$	$-\frac{i}{2} \sigma_{i_2 i_1}^J [\lambda_{T_1}]_r^* \delta_{a_1 a_2} P_R$
	T_2	$q_{L a_2 r}^{i_2}$	$T_{2 R a_2}^J$	$-\frac{i}{2} \sigma_{i_2 j}^J \epsilon_{j i_1} [\lambda_{T_2}]_r^* \delta_{a_1 a_2} P_R$

Table C.1: Feynman rules for the interactions of the VLQs with a SM quark and the Higgs doublet.

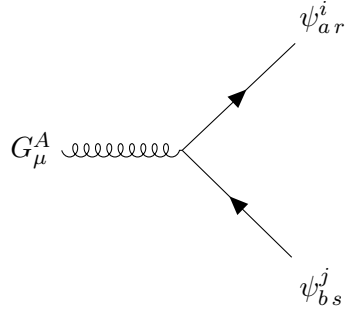
Model	ψ_1	ψ_2	Feynman Rule
1 ($U + Q_1$)	U_{a_2}	$Q_{1 a_1}^{i_2}$	$i \lambda_{U Q_1} \epsilon_{i_1 i_2} \delta_{a_1 a_2}$
2 ($D + Q_1$)	$q_{L a_1 r}^{i_2}$	$D_{R a_2}$	$-i \lambda_{D Q_1}^* \delta_{i_2 i_1} \delta_{a_1 a_2}$
3 ($U + Q_7$)	$Q_{7 a_1}^{i_2}$	U_{a_2}	$-i \lambda_{U Q_7}^* \delta_{i_2 i_1} \delta_{a_1 a_2}$
4 ($D + Q_5$)	\bar{D}_{a_2}	$Q_{5 a_1}^{i_2}$	$i \lambda_{D Q_5} \epsilon_{i_1 i_2} \delta_{a_1 a_2}$
5 ($T_1 + Q_1$)	$\bar{T}_{1 a_2}^J$	$Q_{1 a_1}^{i_2}$	$-\frac{i}{2} \lambda_{T_1 Q_1} \sigma_{i_1 i_2}^J \delta_{a_1 a_2}$
6 ($T_1 + Q_5$)	$T_{1 a_2}^J$	$Q_{5 a_1}^{i_2}$	$\frac{i}{2} \lambda_{T_1 Q_5} \epsilon_{i_1 j} \sigma_{j i_2}^J \delta_{a_1 a_2}$
7 ($T_2 + Q_1$)	$T_{2 a_2}^J$	$Q_{1 a_1}^{i_2}$	$\frac{i}{2} \epsilon_{i_1 j} \sigma_{j i_2}^J \lambda_{T_2 Q_1} \delta_{a_1 a_2}$
8 ($T_2 + Q_7$)	$\bar{T}_{2 a_1}^J$	$Q_{7 a_2}^{i_2}$	$-\frac{i}{2} \lambda_{T_2 Q_7} \sigma_{i_1 i_2}^J \delta_{a_1 a_2}$

Table C.2: Feynman rules for the interactions between a pair of VLQs and the Higgs doublet. Each interaction is uniquely associated with one of the models being studied.

C.2 Quark Interaction with the Gauge Bosons

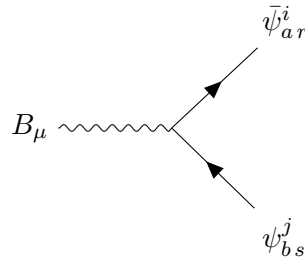
Here the Feynman rules for the interactions of the quark content of Model 1 with the gauge bosons in the unbroken phase are presented.

Starting from the interaction with the Gluons, we have:



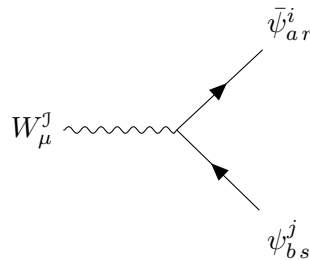
$$= -ig_s \gamma_\mu P_x \frac{\lambda_{ab}^A}{2} \delta^{ij} \delta_{rs}, \quad \begin{cases} P_x = P_L & \psi = q_L \\ P_x = P_R & \psi = u_R, d_R \\ P_x = \mathbb{1} \end{cases} . \quad (\text{C.1})$$

Next, the interactions with the $U(1)_Y$ associated gauge boson,

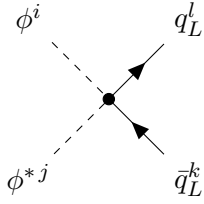
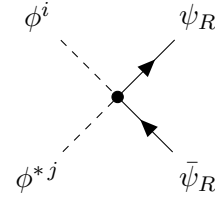


$$= -ig_Y Y_\psi \gamma_\mu P_X \delta_{ab} \delta^{ij} \delta_{rs}, \quad P_X = \begin{cases} P_L & \psi = q_L \\ P_R & \psi = u_R, d_R \\ \mathbb{1} & \psi = U, Q_1 \end{cases} . \quad (\text{C.2})$$

Finally, the interactions with the three W_μ^J gauge bosons,



$$= -ig_L \delta_{ab} \frac{\sigma_{ij}^J}{2} \delta_{rs} \gamma_\mu P_X, \quad P_X = \begin{cases} P_L & \psi = q_L \\ 0 & \psi = u_R, d_R, U \\ \mathbb{1} & \psi = Q_1 \end{cases} . \quad (\text{C.3})$$

(a) EFT vertex with the SM quark doublet q .(b) EFT vertex with one of the two SM singlets, $\psi = u, d$.Figure C.2: EFT tree level diagrams generated by the operators belonging to the $\psi^2\phi^2D$ -class operators, separated depending on whether the SM quark is the doublet or one of the singlets.

C.3 $\psi^2\phi^2D$ -class Operators

In Chapter 5, processes involving SMEFT operators were studied. The Feynman rules for the one-loop generated operators $\mathcal{Q}_{\phi\Box}$, $\mathcal{Q}_{\phi D}$, $\mathcal{Q}'_{\phi D}$ and $\mathcal{Q}''_{\phi D}$ were presented in Table 5.6. In this section the Feynman rules for the tree level-generated operators of the $\psi^2\phi^2D$ -class are presented.

For the operators $\mathcal{O}_{\phi u}$ and $\mathcal{O}_{\phi d}$, the Feynman Rules for the vertex in Figure C.2a read

$$i \mathcal{C}_{\phi u} \delta^{ij} (\not{p}_1 - \not{p}_2) P_R. \quad (\text{C.4})$$

Moving to the operators with the doublets, $\mathcal{O}_{\phi q}^{(1)}$ is associated with the Feynman Rule

$$i \mathcal{C}_{\phi q}^{(1)} \delta^{ij} (\not{p}_1 - \not{p}_2) P_L. \quad (\text{C.5})$$

Finally, the Feynman rule for $\mathcal{O}_{\phi q}^{(3)}$, keeping care of the weak index contractions, provides

$$i \mathcal{C}_{\phi q}^{(3)} (2\delta_{jl}\delta_{ik} - \delta_{ij}\delta_{kl}) (\not{p}_1 - \not{p}_2) P_L. \quad (\text{C.6})$$

For the Feynman rules associated to other operators in the Warsaw basis, a reference is [87].

Appendix D

Flavour Physics

In the SM there are no tree level Flavour Changing Neutral Current (FCNC) processes, which involve a change in flavour without a charge transfer. These processes start to appear at the one-loop level: for example, one can consider meson-antimeson oscillations like the one shown in Figure D.1. Besides the loop suppression, these processes are also suppressed by the GIM mechanism [88].

From the SMEFT point of view, Warsaw basis operators that can contribute to FCNC are defined in Table D.1. None of these operators is produced at the tree level in the models being considered here: one must therefore move to the one-loop level.

In [64, 89], FCNC processes involving VLQs were considered. In particular, [64] used the results reported in [90] to find lower bounds on the VLQ masses. Higher bounds were however found in this reference from the study of ElectroWeak Precision Observables and Higgs Physics. In both references [64, 89], the VLQs were allowed to couple to more than one generation of SM quarks at a time.

In this work, instead, the VLQs are allowed to couple to only either the first or the second generation SM quarks. Therefore a VLQ cannot be used, for example, to connect a first generation SM quark to a second generation one unsuppressed by the CKM matrix. From the effective field theory point of view, an effective vertex involving different flavours cannot arise if the particle being integrated out can only couple to one flavour.

Given this assumption, the bounds to be obtained from the study of Flavour Physics are expected to be weak compared to those from Electroweak Precision Observables and Higgs Physics, hence they will not be considered in this thesis. However, in future works in which the assumption is relaxed it could be of interest to investigate the bounds from Flavour Physics as well.

Category	Name	Definition	Name	Definition
$(\bar{L}L)(\bar{L}L)$	$[\mathcal{O}_{qq}^{(1)}]_{prst}$	$(\bar{q}_{Lp}\gamma_\mu q_{Lr})(\bar{q}_{Ls}\gamma^\mu q_{Lt})$	$[\mathcal{O}_{qq}^{(3)}]_{prst}$	$(\bar{q}_{Lp}\gamma_\mu\sigma^J q_{Lr})(\bar{q}_{Ls}\gamma^\mu\sigma^J q_{Lt})$
$(\bar{L}L)(\bar{R}R)$	$[\mathcal{O}_{qd}^{(1)}]_{prst}$	$(\bar{q}_{Lp}\gamma_\mu q_{Lr})(\bar{d}_{Rs}\gamma^\mu d_{Rt})$	$[\mathcal{O}_{qu}^{(1)}]_{prst}$	$(\bar{q}_{Lp}\gamma_\mu q_{Lr})(\bar{u}_{Rs}\gamma^\mu u_{Rt})$
	$[\mathcal{O}_{qd}^{(8)}]_{prst}$	$(\bar{q}_{Lp}\gamma_\mu\frac{\lambda^A}{2}q_{Lr})(\bar{d}_{Rs}\gamma^\mu\frac{\lambda^A}{2}d_{Rt})$	$[\mathcal{O}_{qu}^{(8)}]_{prst}$	$(\bar{q}_{Lp}\gamma_\mu\frac{\lambda^A}{2}q_{Lr})(\bar{u}_{Rs}\gamma^\mu\frac{\lambda^A}{2}u_{Rt})$
$(\bar{R}R)(\bar{R}R)$	$[\mathcal{O}_{dd}]_{prst}$	$(\bar{d}_{Rp}\gamma_\mu d_{Rr})(\bar{d}_{Rs}\gamma^\mu d_{Rt})$	$[\mathcal{O}_{uu}]_{prst}$	$(\bar{u}_{Rp}\gamma_\mu u_{Rr})(\bar{u}_{Rs}\gamma^\mu u_{Rt})$

Table D.1: Four-fermion operators in the Warsaw basis which contribute to FCNC processes.

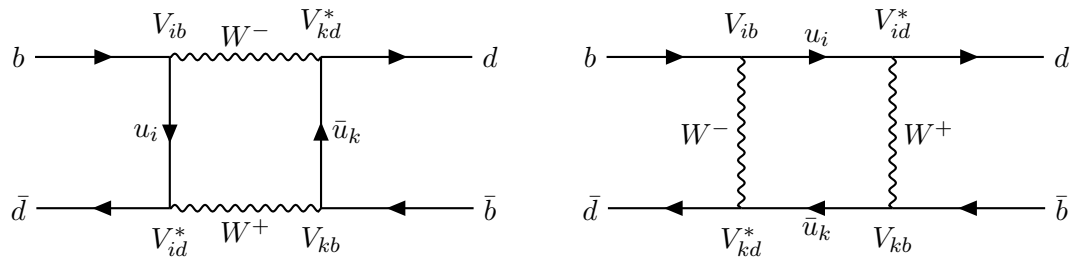


Figure D.1: Feynman diagrams described the loop induced $B_d^0 \leftrightarrow \bar{B}_d^0$ oscillation in the Standard Model.

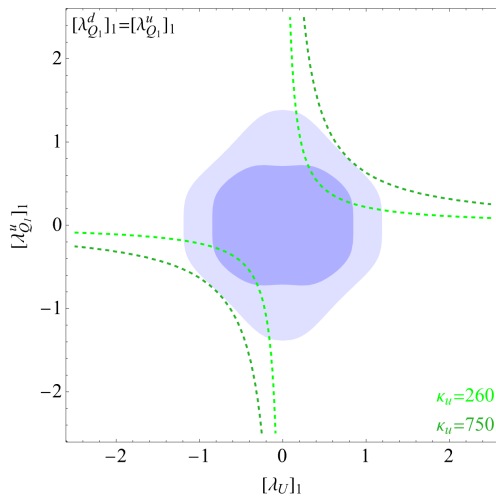
Appendix E

Additional Parameter Space Plots

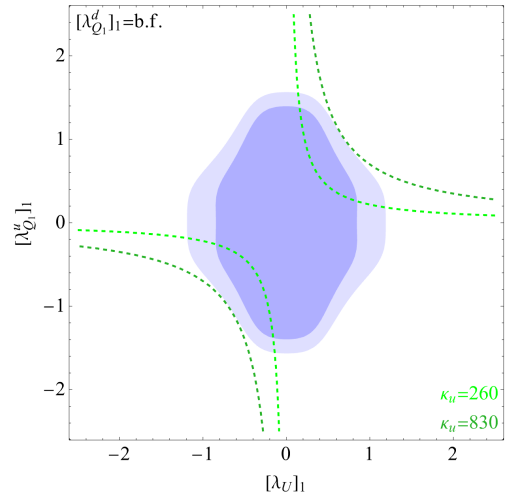
In Sections 6.3 and 6.4, the allowed parameter space for the VLQ Yukawa-like couplings was studied by taking into account constraints for ElectroWeak and Higgs Physics. Since each model introduces three or four couplings, to perform two-dimensional plots assumptions had to be made in order to reduce the number of free parameters in the χ^2 function and κ_q to two. In particular, it was chosen to fix the VLQ-VLQ coupling to the value that maximises the contribution to the coupling modifier at the two selected CLs. In this Appendix, an alternative choice of setting such coupling to 1 in the solution of the inequalities in Equation (6.4) is investigated.

The resulting plots for both the first and second generations are shown in the following pages. The colour and line style conventions used in Sections 6.3 and 6.4 are respected; unsurprisingly, since 1 is smaller than any of the values used in the main text, the upper bounds turn out to be smaller. The maximal allowed enhancements are $\kappa_u = 830$ from Model 1 (Figure E.1b), $\kappa_d = 470$ from Model 4 (Figure E.9b), $\kappa_s = 40$ from Model 4 (Figure E.9b) and $\kappa_c = 3.9$ from Model 3 (Figure E.9a). While the possible values for the allowed coupling modifiers become smaller, their order of magnitude stays the same and doesn't change the conclusion that the searches for light quark Yukawa deviations at the HL-LHC is motivated also from a UV perspective.

The 68% CL region is always contained in the 95% CL one; this confirms the idea that Models 3 and 4 in Section 6.4 deviated from such expectation due to the non-negligible difference between the 68% and 95% CL values used for the VLQ-VLQ coupling. More details are provided in the captions of the plots.



(a) Same coupling limit for the Q_1 couplings.



(b) $[\lambda_{Q_1}^d]_1$ set to the best-fit value from the χ^2 minimisation.

Figure E.1: These two plots show the allowed parameter space for the VLQs in Model 1 coupled to first generation SM quarks. The two different scenarios for the treatment of the fourth VLQ coupling are both considered.

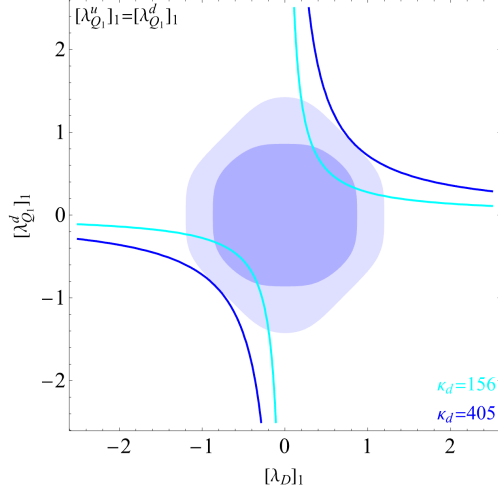
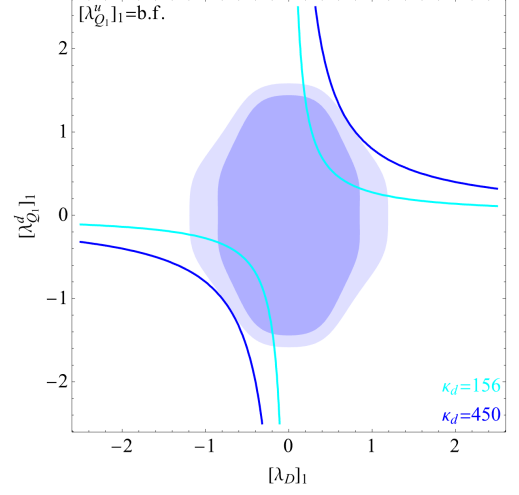
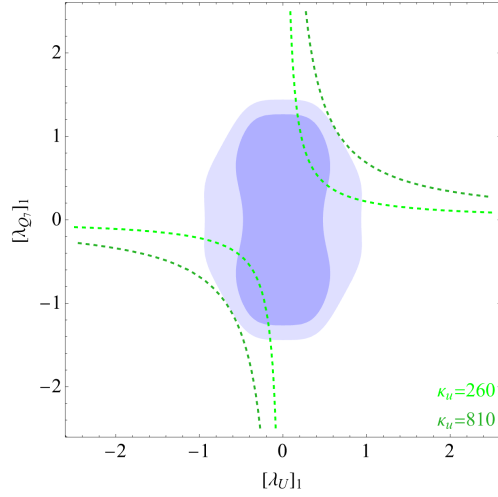
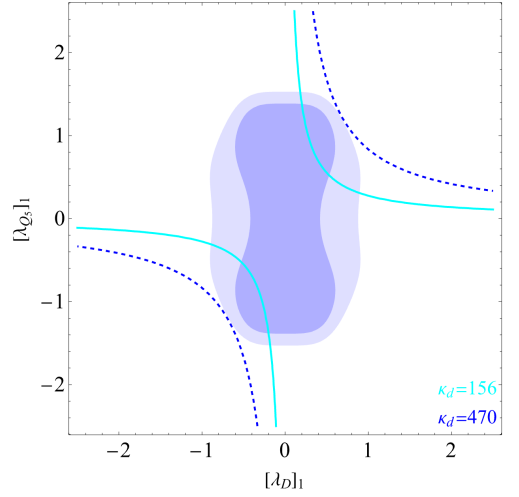

 (a) Same coupling limit for the Q_1 couplings.

 (b) $[\lambda_{Q_1}^u]_1$ set to the best-fit value from the χ^2 minimisation.

Figure E.2: Allowed parameter space for the VLQs in Model 2 coupled to first generation SM quarks.



(a) Model 3.



(b) Model 4.

Figure E.3: Parameter space and coupling modifiers for Models 3 and 4.

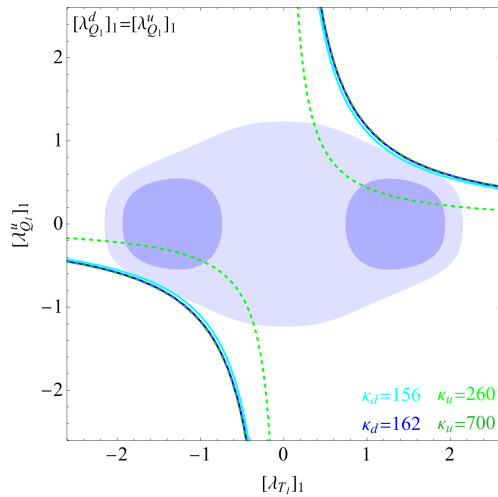
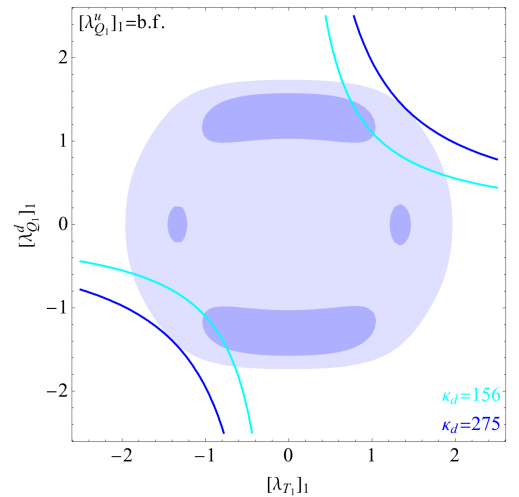
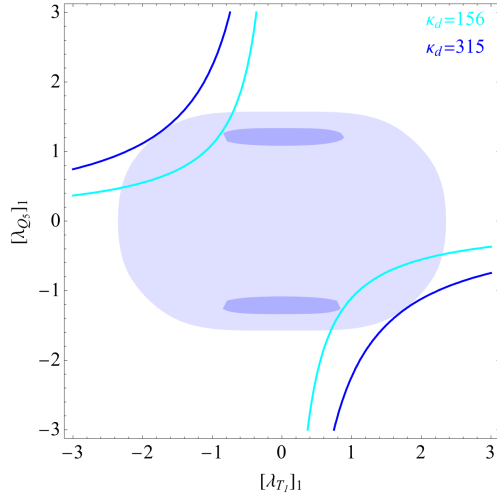
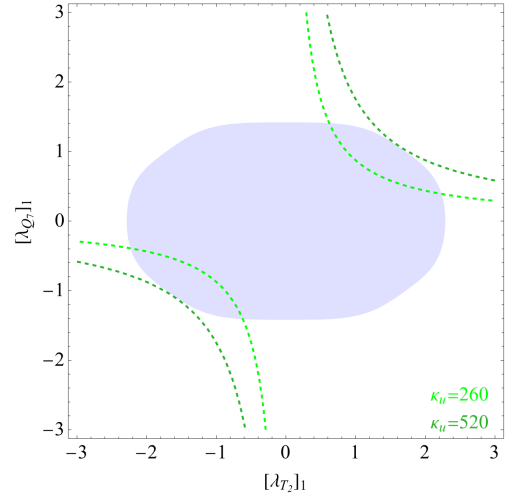

 (a) Scenario in which $[\lambda_{Q_1}^d]_1 = [\lambda_{Q_1}^u]_1$.

 (b) Scenario where $[\lambda_{Q_1}^u]_1$ is set to the best-fit value.

 Figure E.4: Model 5 parameter spaces for the first generation according to the two different treatments of the Q_1 couplings.



(a) Model 6.



(b) Model 8.

Figure E.5: Model 6 and Model 8 parameter space, with VLQs coupled to the first generation SM quarks.

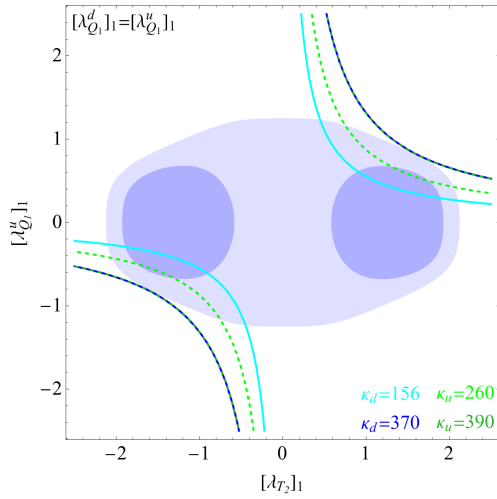
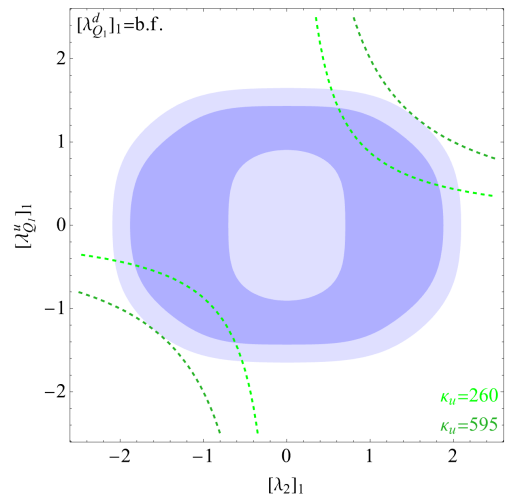

 (a) Scenario in which $[\lambda_{Q_1}^d]_1 = [\lambda_{Q_1}^u]_1$.

 (b) $[\lambda_{Q_1}^u]_1$ set to the best-fit value.

Figure E.6: Allowed parameter space for Model 7 according to the two different treatments for the fourth VLQ coupling.

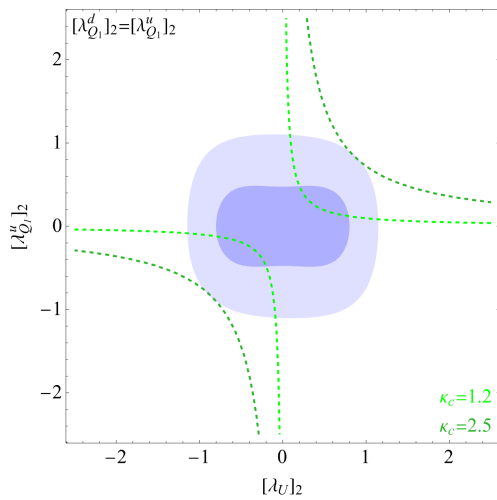
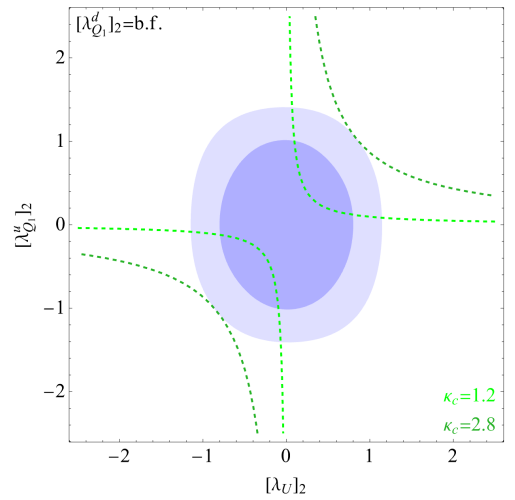

 (a) Same coupling limit for the Q_1 couplings.

 (b) $[\lambda_{Q_1}^d]_2$ set to the best-fit value from the χ^2 minimisation.

Figure E.7: Parameter space for the VLQs in Model 1 coupled to second generation SM quarks according to the two different choices for the fourth coupling.

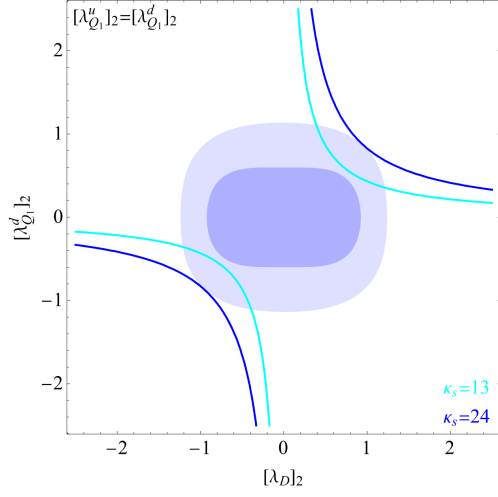
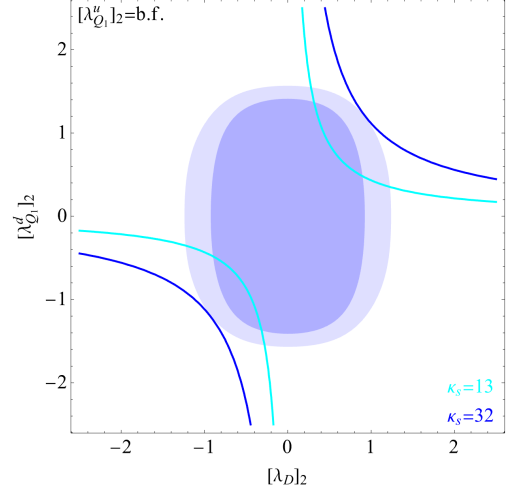
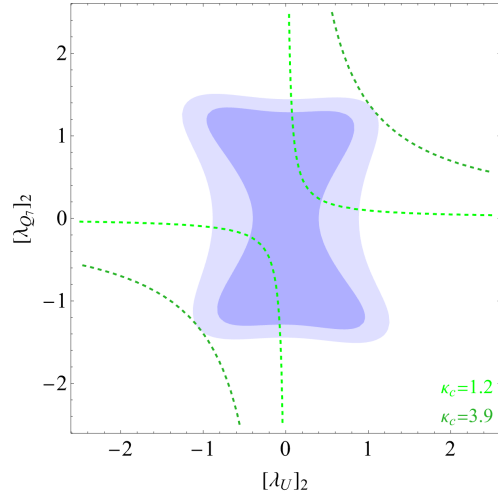
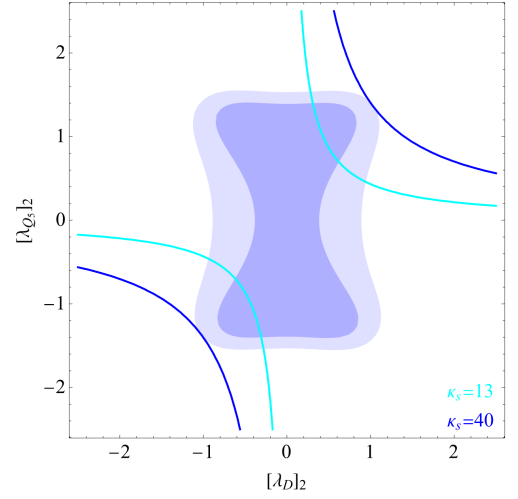

 (a) Same coupling limit for the Q_1 couplings.

 (b) $[\lambda_{Q_1}^u]_2$ set to the best-fit value from the χ^2 minimisation.

Figure E.8: Allowed parameter space for the VLQs in Model 2 coupled to second generation SM quarks.



(a) Model 3.



(b) Model 4.

Figure E.9: Parameter space and coupling modifiers for Models 3 and 4 coupled to second generation quarks.

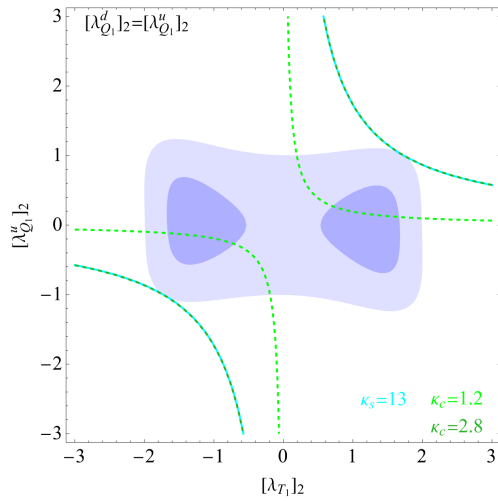
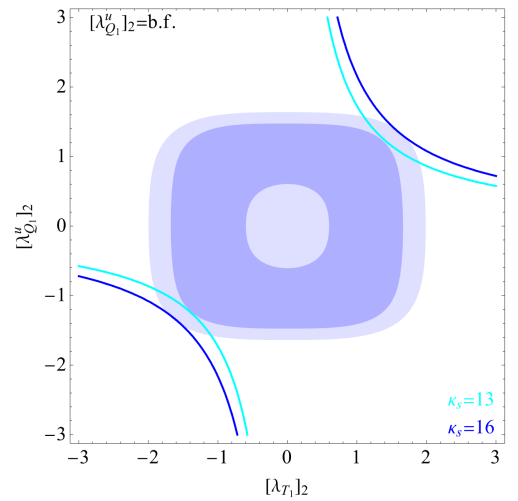

 (a) Scenario in which $[\lambda_{Q_1}^d]_2 = [\lambda_{Q_1}^u]_2$.

 (b) Scenario where $[\lambda_{Q_1}^u]_2$ is set to the best-fit value.

Figure E.10: Parameter space for Model 5 with VLQs coupled to the strange and charm quarks. Notice that in the same coupling limit the largest allowed value coincides with the result found in the literature [23].

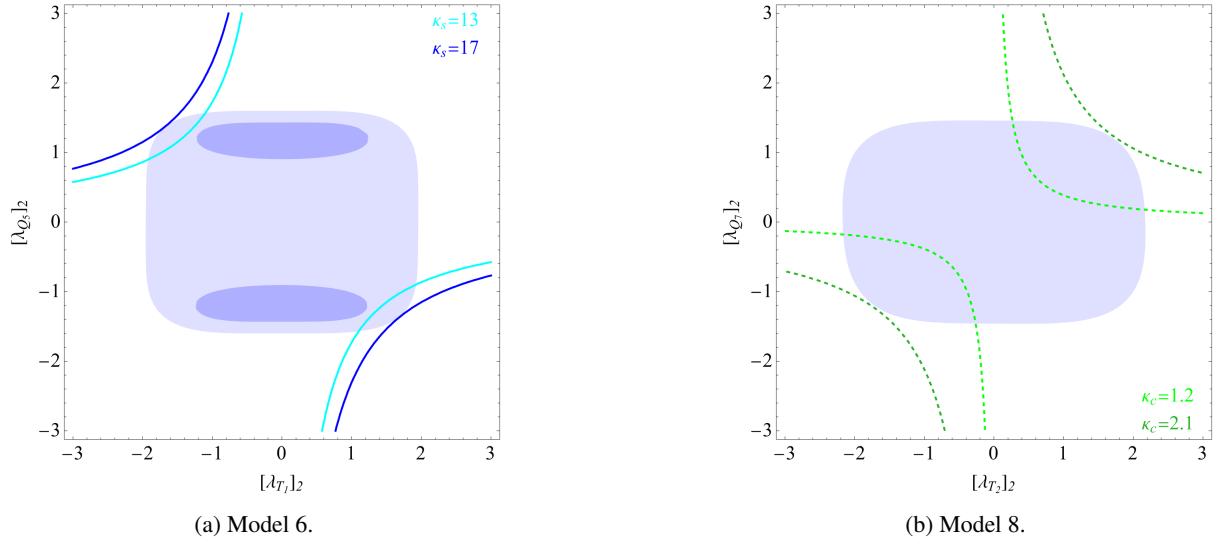


Figure E.11: Model 6 and Model 8 parameter space, with VLQs coupled to the second generation SM quarks.

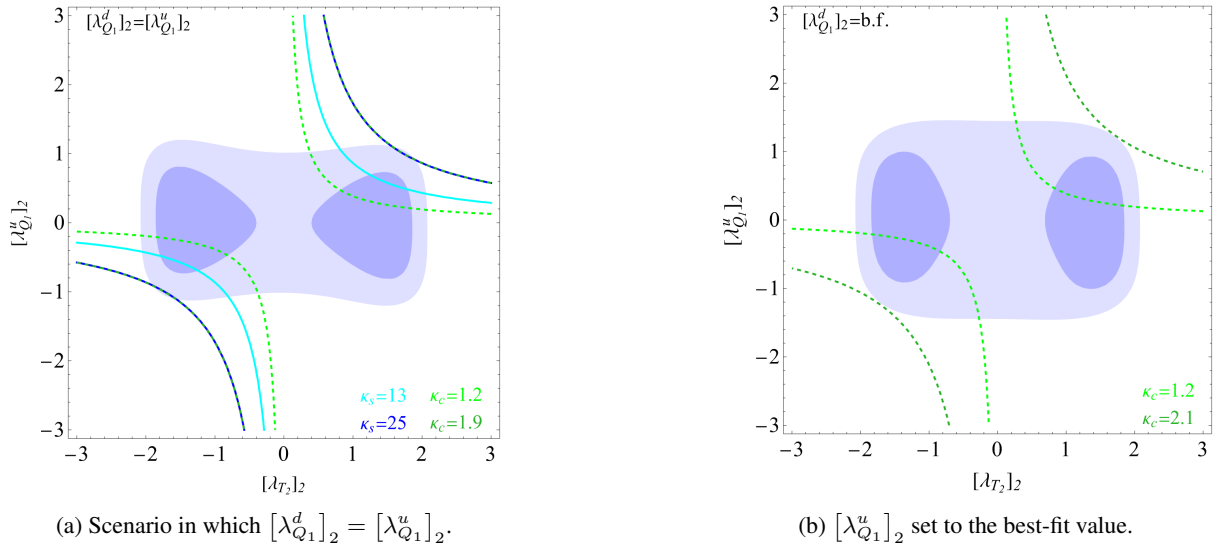


Figure E.12: Allowed parameter space for Model 7 according to the two different treatments for the fourth VLQ coupling.

Appendix F

Detector Schematics

At many points throughout this thesis, the results of experiments performed at the Large Hadron Collider (LHC), located at CERN (Conseil Européen pour la Recherche Nucléaire), were mentioned. In this appendix, a few details concerning the LHC and two of the experiments around its accelerator ring, ATLAS and CMS, are reported.

The Large Hadron Collider, whose accelerator ring has a circumference of 27 km, was designed in the 1990s to study the Standard Model (in particular, the search for the Higgs boson) and Beyond the Standard Model Physics [91]. The two beams being collided both consist of protons¹ and intersect in four different locations. In each of these points, an experiment is set up: ALICE, ATLAS, CMS and LHCb.

ATLAS (A Toroidal LHC Apparatus) and CMS (Compact Muon Solenoid) are two general-purpose experiments at LHC, both are cylindrical detectors which almost cover the entire solid angle except for the beam's track.

Both have a solenoid providing a magnetic field equal to 2 T for ATLAS and 3.8 T for CMS. Going from the innermost to the outermost layer, the two experiments have silicon trackers for particle trajectory reconstruction, calorimeters for energy measurements and muon chambers. There are two types of calorimeters: electromagnetic and hadronic. The former allows the study of electrons and photons, the latter of hadrons. The muons are the last detected particles since they present the least interactions with the rest of the detectors.

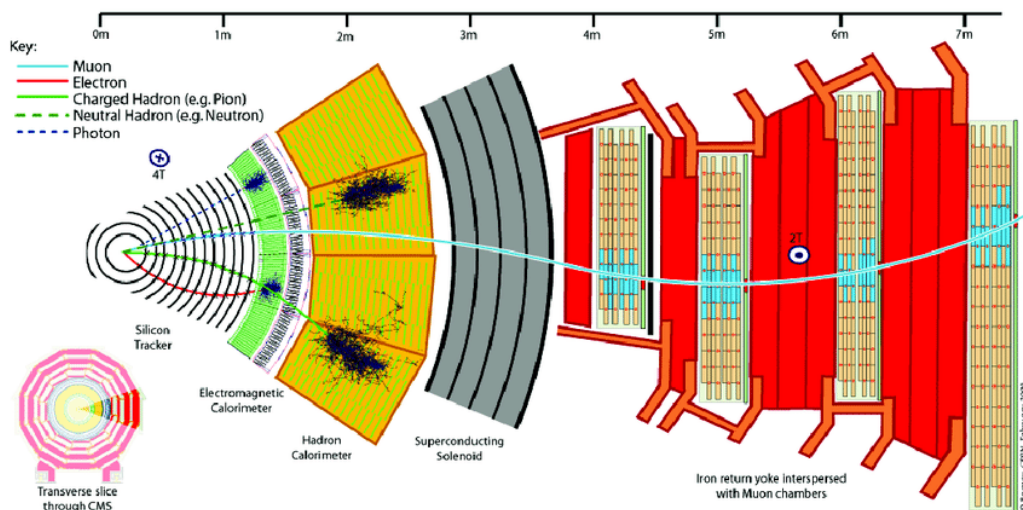


Figure F.1: CMS transverse section showing the internal structure of the detector going from left to right. In particular, the silicon trackers for the trajectory reconstruction, the electromagnetic followed by the hadronic calorimeter and finally the muon chambers can be identified.

¹The Tevatron at the Fermi National Accelerator Laboratories, instead, was a proton-antiproton collider.

Figure F.1 shows what has just been stated. The difference between the study of neutral and charged particles is clear by observing the effect of the magnetic field on the trajectories: neutral particles are unaffected and move in a straight line, whereas the charged ones are deviated. The development of the particle showers inside the calorimeters is also shown.

The figures presented in this section were taken from the official webpages of ATLAS and CMS.

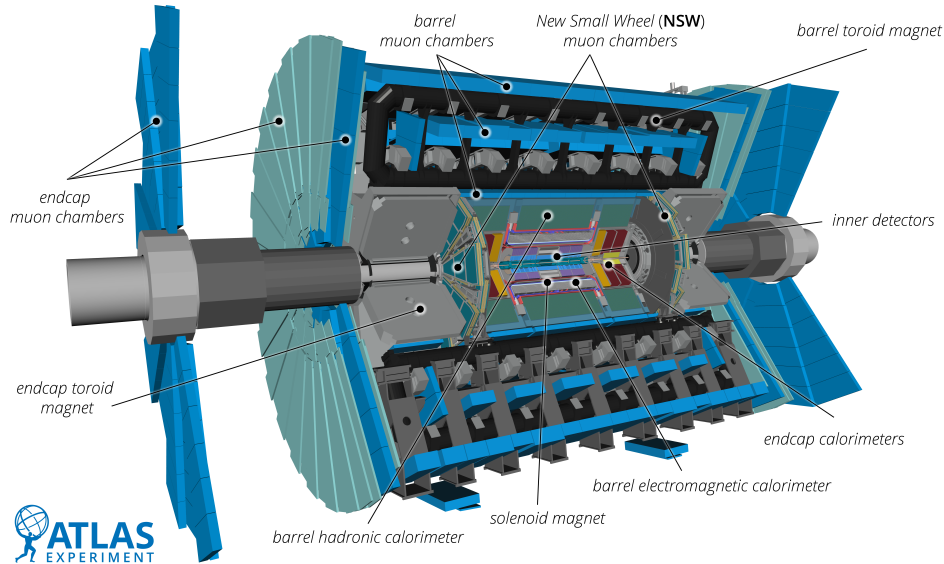


Figure F.2: ATLAS detector schematics.

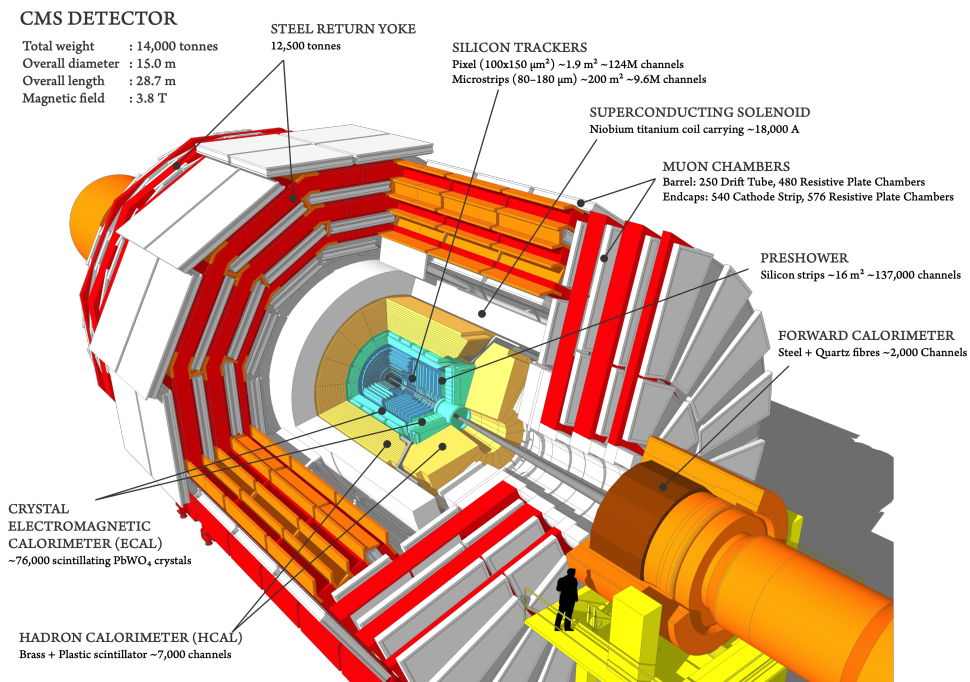


Figure F.3: CMS detector schematics.

Appendix G

Direct Searches

In this section, intermediate results for the Direct Searches (Chapter 7) are presented. For Model 1, these consist in the explicit expressions for the rotations matrices and the description of the interactions of the quarks (both the SM and the VLQs) with the final state bosons after the rotation into the mass basis has been performed.

Additionally, the details of the generalisation for the eight models are presented. In this case, the expressions for the generalised Lagrangian before and after the rotation are provided. Again, the rotation matrices are reported. For the generalisation to be made, some auxiliary functions have to be introduced. Their definitions and the set of replacement rules which uniquely identify the individual models are listed.

G.1 Model 1

The \mathcal{L}_W and \mathcal{L}_Z Lagrangians before the rotation into the mass basis are given by:

$$-\mathcal{L}_W = \frac{g_L}{\sqrt{2}} (\bar{u}_L \quad \bar{T}_L \quad \bar{U}_L) \mathcal{W}^+ \begin{pmatrix} 1 & 0 \\ 0 & 1 \\ 0 & 0 \end{pmatrix} \begin{pmatrix} d_L \\ B_L \end{pmatrix} + \frac{g_L}{\sqrt{2}} (\bar{u}_R \quad \bar{T}_R \quad \bar{U}_R) \mathcal{W}^+ \begin{pmatrix} 0 & 0 \\ 0 & 1 \\ 0 & 0 \end{pmatrix} \begin{pmatrix} d_R \\ B_R \end{pmatrix} + \text{h.c.} \quad (\text{G.1})$$

$$\begin{aligned} -\mathcal{L}_Z &= \frac{g_L}{\cos \theta_W} (\bar{u}_L \quad \bar{T}_L \quad \bar{U}_L) \mathcal{Z} \left[\frac{1}{2} \begin{pmatrix} 1 & 0 & 0 \\ 0 & 1 & 0 \\ 0 & 0 & 0 \end{pmatrix} - \frac{2}{3} \sin^2 \theta_W \mathbb{1}_{3 \times 3} \right] \begin{pmatrix} u_L \\ T_L \\ U_L \end{pmatrix} + \\ &+ \frac{g_L}{\cos \theta_W} (\bar{u}_R \quad \bar{T}_R \quad \bar{U}_R) \mathcal{Z} \left[\frac{1}{2} \begin{pmatrix} 0 & 0 & 0 \\ 0 & 1 & 0 \\ 0 & 0 & 0 \end{pmatrix} - \frac{2}{3} \sin^2 \theta_W \mathbb{1}_{3 \times 3} \right] \begin{pmatrix} u_R \\ T_R \\ U_R \end{pmatrix} + \\ &+ \frac{g_L}{\cos \theta_W} (\bar{d}_L \quad \bar{B}_L) \mathcal{Z} \left[-\frac{1}{2} + \frac{1}{3} \sin^2 \theta_W \right] \mathbb{1}_{2 \times 2} \begin{pmatrix} d_L \\ B_L \end{pmatrix} + \\ &+ \frac{g_L}{\cos \theta_W} (\bar{d}_R \quad \bar{B}_R) \mathcal{Z} \left[-\frac{1}{2} \begin{pmatrix} 0 & 0 \\ 0 & 1 \end{pmatrix} + \frac{1}{3} \sin^2 \theta_W \mathbb{1}_{2 \times 2} \right] \begin{pmatrix} d_R \\ B_R \end{pmatrix}. \end{aligned} \quad (\text{G.2})$$

The diagonalised matrices M_q^{diag} up to $O(v^2/M^2)$ corrections are obtained from M_q via the following rotations:

$$M_u^{diag} = U_{Lup}^{23} U_{Lup}^{13} M_u U_{Rup}^{21\dagger} U_{Rup}^{23\dagger}, \quad (\text{G.3})$$

$$M_d^{diag} = \mathbb{1}_{2 \times 2} M_d U_{Rdown}^{21\dagger}. \quad (\text{G.4})$$

The transformation matrices for the up sector are:

$$\begin{aligned}
U_{Lup}^{23} &= \begin{pmatrix} 1 & 0 & 0 \\ 0 & \frac{1}{\sqrt{2}} - \frac{\lambda_{UQ_1} v}{8M} & -\frac{1}{\sqrt{2}} - \frac{\lambda_{UQ_1} v}{8M} \\ 0 & \frac{1}{\sqrt{2}} + \frac{\lambda_{UQ_1} v}{8M} & \frac{1}{\sqrt{2}} - \frac{\lambda_{UQ_1} v}{8M} \end{pmatrix}, & U_{Rup}^{23} &= \begin{pmatrix} 1 & 0 & 0 \\ 0 & \frac{1}{\sqrt{2}} + \frac{\lambda_{UQ_1} v}{8M} & -\frac{1}{\sqrt{2}} + \frac{\lambda_{UQ_1} v}{8M} \\ 0 & \frac{1}{\sqrt{2}} - \frac{\lambda_{UQ_1} v}{8M} & \frac{1}{\sqrt{2}} + \frac{\lambda_{UQ_1} v}{8M} \end{pmatrix}, \\
U_{Lup}^{13} &= \begin{pmatrix} 1 & 0 & -\frac{\lambda_U v}{\sqrt{2}M} \\ 0 & 1 & 0 \\ \frac{\lambda_U v}{\sqrt{2}M} & 0 & 1 \end{pmatrix}, & U_{Rup}^{21} &= \begin{pmatrix} 1 & -\frac{\lambda_{Q_1}^u v}{2M} & 0 \\ \frac{\lambda_{Q_1}^u v}{\sqrt{2}M} & 1 & 0 \\ 0 & 0 & 1 \end{pmatrix}.
\end{aligned} \tag{G.5}$$

For the down sector, the transformation matrix is:

$$U_{Rdown}^{21} = \begin{pmatrix} 1 & -\frac{\lambda_{Q_1}^u v}{\sqrt{2}v} \\ \frac{\lambda_{Q_1}^u v}{\sqrt{2}v} & 1 \end{pmatrix}. \tag{G.6}$$

Having moved into the mass basis, we can rewrite the rotated interactions of the SM quarks and VLQs with the bosons h , W^\pm and Z . For more compact expressions, define the multiplets $\mathcal{U} = \begin{pmatrix} u & T & U \end{pmatrix}^T$ and $\mathcal{D} = \begin{pmatrix} d & B \end{pmatrix}^T$ containing quarks with same $U(1)_{EM}$ charge. The results are all truncated at $O(v^2/M^2)$ level.

Interaction with the Higgs the matrix entries present both an order zero and order one term in the expansion parameter are present. Only the order zero term is reported since it provides the dominant contribution.

$$-\mathcal{L}^h = h \bar{\mathcal{U}}_L \begin{pmatrix} 0 & -\frac{\lambda_U}{2} & \frac{\lambda_U}{2} \\ \frac{\lambda_{Q_1}^u}{2} & -\frac{\lambda_{UQ_1}}{2\sqrt{2}} & \frac{\lambda_{UQ_1}}{2\sqrt{2}} \\ \frac{\lambda_{Q_1}^u}{2} & -\frac{\lambda_{UQ_1}}{2\sqrt{2}} & \frac{\lambda_{UQ_1}}{2\sqrt{2}} \end{pmatrix} \mathcal{U}_R + h \bar{\mathcal{D}}_L \begin{pmatrix} 0 & 0 \\ \frac{\lambda_{Q_1}^d}{\sqrt{2}} & \frac{(\lambda_{Q_1}^d)^2 v}{2M} \end{pmatrix} \mathcal{D}_R + \text{h.c.} \tag{G.7}$$

Interaction with the W boson the interaction turns out to be

$$-\frac{\sqrt{2}}{g_L} \mathcal{L}_W = \bar{\mathcal{U}}_L W^+ \begin{pmatrix} 1 & 0 \\ -\frac{\lambda_U v}{2M} & \frac{1}{\sqrt{2}} \\ \frac{\lambda_U v}{2M} & \frac{1}{\sqrt{2}} \end{pmatrix} \mathcal{D}_L + \bar{\mathcal{U}}_R W^+ \begin{pmatrix} 0 & -\frac{\lambda_{Q_1}^u v}{\sqrt{2}M} \\ -\frac{\lambda_{Q_1}^d v}{2M} & \frac{1}{\sqrt{2}} \\ -\frac{\lambda_{Q_1}^d v}{2M} & \frac{1}{\sqrt{2}} \end{pmatrix} \mathcal{D}_R + \text{h.c.} \tag{G.8}$$

Interaction with the Z boson finally, the rotated Lagrangian contribution involving Z and the quarks is

$$\begin{aligned}
-\frac{\cos \theta_W}{g_L} \mathcal{L}_Z &= \bar{\mathcal{U}}_L Z \left(\frac{1}{2} \begin{pmatrix} 1 & -\frac{\lambda_U v}{2M} & \frac{\lambda_U v}{2M} \\ -\frac{\lambda_U v}{2M} & \frac{1}{2} & \frac{1}{2} \\ \frac{\lambda_U v}{2M} & \frac{1}{2} & \frac{1}{2} \end{pmatrix} - \frac{2}{3} \sin^2 \theta_W \mathbb{1}_{3 \times 3} \right) \mathcal{U}_L + \\
&+ \bar{\mathcal{U}}_R Z \left(\frac{1}{2} \begin{pmatrix} 1 & -\frac{\lambda_{Q_1}^u v}{2M} & -\frac{\lambda_{Q_1}^u v}{2M} \\ -\frac{\lambda_{Q_1}^u v}{2M} & \frac{1}{2} & \frac{1}{2} \\ -\frac{\lambda_{Q_1}^u v}{2M} & \frac{1}{2} & \frac{1}{2} \end{pmatrix} - \frac{2}{3} \sin^2 \theta_W \mathbb{1}_{3 \times 3} \right) \mathcal{U}_R + \\
&+ \bar{\mathcal{D}}_L Z \left(-\frac{1}{2} + \frac{1}{3} \sin^2 \theta_W \right) \mathbb{1}_{2 \times 2} \mathcal{D}_L + \\
&+ \bar{\mathcal{D}}_R Z \left(-\frac{1}{2} \begin{pmatrix} 0 & -\frac{\lambda_{Q_1}^d v}{\sqrt{2}M} \\ -\frac{\lambda_{Q_1}^d v}{\sqrt{2}M} & 0 \end{pmatrix} + \frac{1}{3} \sin^2 \theta_W \mathbb{1}_{2 \times 2} \right) \mathcal{D}_R.
\end{aligned} \tag{G.9}$$

G.2 Generalisation to all models

For the convenience of the reader, the VLQ components along with their charges are repeated in Table G.1 and the particle content of the various models are given in Table G.2. Noticing that in all models there is a doublet and either a singlet or a triplet, the notation $Su \in \{U, T_1^{2/3}, T_2^{2/3}\}$ and $Sd \in \{D, T_1^{-1/3}, T_2^{-1/3}\}$ was introduced. The multiplets containing quarks with the same charge are, therefore,

$$\mathcal{U} = \begin{pmatrix} u \\ T \\ Su \end{pmatrix}, \quad \mathcal{D} = \begin{pmatrix} d \\ B \\ Sd \end{pmatrix}, \quad \mathcal{X} = \begin{pmatrix} X \\ T_2^{5/3} \end{pmatrix} \quad \& \quad \mathcal{Y} = \begin{pmatrix} Y \\ T_1^{-4/3} \end{pmatrix}. \quad (\text{G.10})$$

G.2.1 Generalised initial Lagrangian

The generalised Higgs sector was already reported in Chapter 7.

For the W^\pm interactions two auxiliary parameters have to be introduced, let them be:

$$\mathbb{F} = \begin{cases} 0 & \text{Model with } U \text{ or } D \\ 1 & \text{Model with } T_1 \\ -1 & \text{Model with } T_2 \end{cases}, \quad (\text{G.11})$$

$$\Theta(q) = \begin{cases} 1 & \text{if the particle } q \text{ is present} \\ 0 & \text{else} \end{cases}. \quad (\text{G.12})$$

The first accounts for the fact that the singlets do not couple to the W bosons, while the triplets do interact but with different signs (see Appendix B). The second auxiliary variable instead deals with the possibility offered by the presence of the triplets to create the multiplets \mathcal{X} and \mathcal{Y} of quarks with non-SM charges. Indeed, in the model involving singlets and doublets, there can be at most one particle with non-SM charge, provided either by Q_5 or by Q_7 . Once the triplets are included, this is no longer the case (Models 6 and 8).

Field	Charges			
	$-\frac{4}{3}$	$-\frac{1}{3}$	$\frac{2}{3}$	$\frac{5}{3}$
U	-	-	U	-
D	-	D	-	-
Q_1	-	B	T	-
Q_5	Y	B	-	-
Q_7	-	-	T	X
T_1	$T_1^{-4/3}$	$T_1^{-1/3}$	$T_1^{2/3}$	-
T_2	-	$T_2^{-1/3}$	$T_2^{2/3}$	$T_2^{5/3}$

Table G.1: Charge assignments for the VLQ components.

Singlet + Doublet		Doublet + Triplet	
Model 1	$U + Q_1$	Model 5	$T_1 + Q_1$
Model 2	$D + Q_1$	Model 6	$T_1 + Q_5$
Model 3	$U + Q_7$	Model 7	$T_2 + Q_1$
Model 4	$D + Q_5$	Model 8	$T_2 + Q_7$

Table G.2: Summary of the models' particle content.

The Lagrangian describing the interaction before the rotation is identified to be:

$$\begin{aligned}
-\frac{\sqrt{2}}{g_L}\mathcal{L}_W &= \bar{u}_L W^+ \begin{pmatrix} 1 & 0 & 0 \\ 0 & 1 & 0 \\ 0 & 0 & \sqrt{2}f \end{pmatrix} \mathcal{D}_L + \bar{u}_R W^+ \begin{pmatrix} 0 & 0 & 0 \\ 0 & 1 & 0 \\ 0 & 0 & \sqrt{2}f \end{pmatrix} \mathcal{D}_R + \\
&+ \bar{x}_L W^+ \begin{pmatrix} 0 & 1 & 0 \\ 0 & 0 & -\sqrt{2}f\Theta(T_2) \end{pmatrix} \mathcal{U}_L + \bar{x}_R W^+ \begin{pmatrix} 0 & 1 & 0 \\ 0 & 0 & -\sqrt{2}f\Theta(T_2) \end{pmatrix} \mathcal{U}_R + \\
&+ \bar{D}_L W^+ \begin{pmatrix} 0 & 0 \\ 1 & 0 \\ 0 & \sqrt{2}f\Theta(T_1) \end{pmatrix} \mathcal{Y}_L + \bar{D}_R W^+ \begin{pmatrix} 0 & 0 \\ 1 & 0 \\ 0 & \sqrt{2}f\Theta(T_1) \end{pmatrix} \mathcal{Y}_R + \text{h.c.} . \quad (\text{G.13})
\end{aligned}$$

Finally, for the Z part of the New Physics Lagrangian, a further auxiliary parameter is needed. Let it be defined as

$$x = \begin{cases} 1 & \text{if the VLQ doublet is } Q_1 \\ -1 & \text{if the VLQ doublet is either } Q_5 \text{ or } Q_7 \end{cases} . \quad (\text{G.14})$$

Its role is to account for the doublets' isospin. Consider the action of σ^3 on the doublets:

$$\sigma^3 Q_1 = \begin{pmatrix} T \\ -B \end{pmatrix}, \quad \sigma^3 Q_5 = \begin{pmatrix} B \\ -Y \end{pmatrix}, \quad \sigma^3 Q_7 = \begin{pmatrix} X \\ T \end{pmatrix}. \quad (\text{G.15})$$

From this, one can notice how T and B pick up different signs depending on which doublet introduces them.

With x and $\Theta(q)$, one can therefore write:

$$\begin{aligned}
-\frac{\cos\theta_W}{g_L}\mathcal{L}_Z &= \bar{u}_L Z \left(\frac{1}{2} \begin{pmatrix} 1 & 0 & 0 \\ 0 & x & 0 \\ 0 & 0 & 2\Theta(T_1) \end{pmatrix} - \frac{2}{3} \sin^2\theta_W \mathbb{1}_{3\times 3} \right) \mathcal{U}_L + \\
&+ \bar{u}_R Z \left(\frac{1}{2} \begin{pmatrix} 0 & 0 & 0 \\ 0 & x & 0 \\ 0 & 0 & 2\Theta(T_1) \end{pmatrix} - \frac{2}{3} \sin^2\theta_W \mathbb{1}_{3\times 3} \right) \mathcal{U}_R + \\
&+ \bar{D}_L Z \left(-\frac{1}{2} \begin{pmatrix} 1 & 0 & 0 \\ 0 & x & 0 \\ 0 & 0 & 2\Theta(T_2) \end{pmatrix} + \frac{1}{3} \sin^2\theta_W \mathbb{1}_{3\times 3} \right) \mathcal{D}_L + \\
&+ \bar{D}_R Z \left(-\frac{1}{2} \begin{pmatrix} 0 & 0 & 0 \\ 0 & x & 0 \\ 0 & 0 & 2\Theta(T_2) \end{pmatrix} + \frac{1}{3} \sin^2\theta_W \mathbb{1}_{3\times 3} \right) \mathcal{D}_R . \quad (\text{G.16})
\end{aligned}$$

G.2.2 Rotation to mass basis

The rotation matrices for M_U and M_D are of the same form of the ones in Equation (G.18), as long as the appropriate substitutions are performed.

However, special care must be placed in the rotations that affect only VLQs. Indeed, while the other two matrices reduce to the identity once the NP coupling has been set to 0, a generalisation of U_{Lu}^{23} and U_{Fu}^{23} would retain an extra $1/\sqrt{2}$ factor and some off-diagonal entries. Therefore, to achieve generalisation it is necessary to introduce two more

Model	aux_u	aux_d	aux_χ	aux_γ	\mathbb{f}	x	$\Theta(T_1)$	$\Theta(T_2)$
1	1	$\sqrt{2}$	$\sqrt{2}$	$\sqrt{2}$	0	1	0	0
2	$\sqrt{2}$	1	$\sqrt{2}$	$\sqrt{2}$	0	1	0	0
3	1	$\sqrt{2}$	$\sqrt{2}$	$\sqrt{2}$	0	-1	0	0
4	$\sqrt{2}$	1	$\sqrt{2}$	$\sqrt{2}$	0	-1	0	0
5	1	1	$\sqrt{2}$	$\sqrt{2}$	1	1	1	0
6	1	1	$\sqrt{2}$	1	1	-1	1	0
7	1	1	$\sqrt{2}$	$\sqrt{2}$	-1	1	0	1
8	1	1	1	$\sqrt{2}$	-1	-1	0	1

Table G.3: Auxiliary function substitutions to recover the particular model of interest.

auxiliary functions:

$$aux_{\alpha,\beta} = \begin{cases} 1 & \text{if } \lambda_{S\alpha,\beta Q} \neq 0 \\ \sqrt{2} & \text{if } \lambda_{S\alpha,\beta Q} = 0 \end{cases} \quad \alpha = u, d \text{ and } \beta = \chi, \gamma. \quad (\text{G.17})$$

$$U_{L\alpha}^{13} = \begin{pmatrix} 1 & 0 & -\frac{\lambda_{S\alpha} v}{\sqrt{2}M} \\ 0 & 1 & 0 \\ \frac{\lambda_{\alpha} v}{\sqrt{2}M} & 0 & 1 \end{pmatrix}, \quad U_{L\alpha}^{23} = \begin{pmatrix} 1 & 0 & 0 \\ 0 & \frac{aux_{\alpha}}{\sqrt{2}} - \frac{\lambda_{S\alpha} Q v}{8M} & -\frac{(2-aux_{\alpha}^2)}{\sqrt{2}} - \frac{\lambda_{S\alpha} Q v}{8M} \\ 0 & \frac{(2-aux_{\alpha}^2)}{\sqrt{2}} + \frac{\lambda_{S\alpha} Q v}{8M} & \frac{aux_{\alpha}}{\sqrt{2}} - \frac{\lambda_{S\alpha} Q v}{8M} \end{pmatrix},$$

$$U_{R\alpha}^{21} = \begin{pmatrix} 1 & -\frac{\lambda_{\alpha}^v}{\sqrt{2}M} & 0 \\ \frac{\lambda_{\alpha}^v}{\sqrt{2}M} & 1 & 0 \\ 0 & 0 & 1 \end{pmatrix}, \quad U_{R\alpha}^{23} = \begin{pmatrix} 1 & 0 & 0 \\ 0 & \frac{aux_{\alpha}}{\sqrt{2}} + \frac{\lambda_{S\alpha} Q v}{8M} & -\frac{(2-aux_{\alpha}^2)}{\sqrt{2}} + \frac{\lambda_{S\alpha} Q v}{8M} \\ 0 & \frac{(2-aux_{\alpha}^2)}{\sqrt{2}} - \frac{\lambda_{S\alpha} Q v}{8M} & \frac{aux_{\alpha}}{\sqrt{2}} + \frac{\lambda_{S\alpha} Q v}{8M} \end{pmatrix}. \quad (\text{G.18})$$

As for the diagonalisation of the 2×2 matrices for the non-SM charged quarks, the following matrices can be used:

$$U_{L\beta}^{21} = \begin{pmatrix} \frac{aux_{\beta}}{\sqrt{2}} - \frac{\lambda_{S\beta} Q v}{8M} & -\frac{(2-aux_{\beta}^2)}{\sqrt{2}} - \frac{\lambda_{S\beta} Q v}{8M} \\ \frac{(2-aux_{\beta}^2)}{\sqrt{2}} + \frac{\lambda_{S\beta} Q v}{8M} & \frac{aux_{\beta}}{\sqrt{2}} - \frac{\lambda_{S\beta} Q v}{8M} \end{pmatrix}, \quad U_{R\beta}^{21} = \begin{pmatrix} \frac{aux_{\beta}}{\sqrt{2}} + \frac{\lambda_{S\beta} Q v}{8M} & -\frac{(2-aux_{\beta}^2)}{\sqrt{2}} + \frac{\lambda_{S\beta} Q v}{8M} \\ \frac{(2-aux_{\beta}^2)}{\sqrt{2}} - \frac{\lambda_{S\beta} Q v}{8M} & \frac{aux_{\beta}}{\sqrt{2}} + \frac{\lambda_{S\beta} Q v}{8M} \end{pmatrix}. \quad (\text{G.19})$$

The transformations required to diagonalise the matrices for the SM-like charged particles are:

$$M_{\alpha}^{diag} = U_{L\alpha}^{23} U_{L\alpha}^{13} M_{\alpha} U_{R\alpha}^{21 \dagger} U_{R\alpha}^{23 \dagger}, \quad (\text{G.20})$$

while the 2×2 matrices involving "new-charged" particles are diagonalised via:

$$M_{X/Y} = U_{LX/Y}^{23} M_{X/Y} U_{RX/Y}^{23 \dagger}. \quad (\text{G.21})$$

Hence the multiplets transform in the following manner:

$$\begin{aligned} \mathcal{U}'_L &= U_{Lu}^{23} U_{Lu}^{13} \mathcal{U}_L, & \mathcal{U}'_R &= U_{Ru}^{23} U_{Ru}^{21} \mathcal{U}_R, \\ \mathcal{D}'_L &= U_{Ld}^{23} U_{Ld}^{13} \mathcal{D}_L, & \mathcal{D}'_R &= U_{Rd}^{23} U_{Rd}^{21} \mathcal{D}_R, \\ \mathcal{X}'_L &= U_{L\chi}^{23} \mathcal{X}_L, & \mathcal{X}'_R &= U_{R\chi}^{23} \mathcal{X}_R, \\ \mathcal{Y}'_L &= U_{Ly}^{23} \mathcal{Y}_L, & \mathcal{Y}'_R &= U_{Ry}^{23} \mathcal{Y}_R. \end{aligned} \quad (\text{G.22})$$

G.2.3 After the rotation

After the rotation, the three Lagrangian contributions can be compactly written as

$$-\mathcal{L}^h = h \bar{u}_L C_{uL}^r u_R + h \bar{D}_L C_{D_L}^r \mathcal{D}_R + \text{h.c.}, \quad (\text{G.23})$$

$$\begin{aligned} -\frac{\sqrt{2}}{g_L} \mathcal{L}_W = & \bar{u}_L W^+ M_{1L}^{Wr} \mathcal{D}_L + \bar{u}_R W^+ M_{1R}^{Wr} \mathcal{D}_R + \bar{x}_L W^+ M_{2L}^{Wr} u_L + \bar{x}_R W^+ M_{2R}^{Wr} u_R + \\ & + \bar{D}_L W^+ M_{3L}^{Wr} y_L + \bar{D}_R W^+ M_{3R}^{Wr} y_R + \text{h.c.}, \end{aligned} \quad (\text{G.24})$$

$$-\frac{\cos \theta_W}{g_L} \mathcal{L}_Z = \bar{u}_L Z M_{uL}^{Zr} u_L + \bar{u}_R Z M_{uR}^{Zr} u_R + \bar{D}_L Z M_{D_L}^{Zr} \mathcal{D}_L + \bar{D}_R Z M_{D_R}^{Zr} \mathcal{D}_R. \quad (\text{G.25})$$

Given the great number of auxiliary couplings and variables introduced, the results are not easy to read and, therefore, will not be explicitly written out. However, let us point out that, once the initial interaction matrices for the different sectors and the rotation matrices have been identified, all the remaining calculations for the branching ratios can be easily implemented in a MATHEMATICA notebook. The only operations that have to be performed are matrix multiplications and substitutions, using the replacements in Tables 7.1 and G.3.

Appendix H

Bibliography

- [1] P. W. Higgs, “Broken Symmetries and the Masses of Gauge Bosons,” *Phys. Rev. Lett.* **13** (1964) 508–509.
- [2] F. Englert and R. Brout, “Broken Symmetry and the Mass of Gauge Vector Mesons,” *Phys. Rev. Lett.* **13** (1964) 321–323.
- [3] G. S. Guralnik, C. R. Hagen, and T. W. B. Kibble, “Global Conservation Laws and Massless Particles,” *Phys. Rev. Lett.* **13** (1964) 585–587.
- [4] ATLAS Collaboration, G. Aad *et al.*, “Observation of a new particle in the search for the Standard Model Higgs boson with the ATLAS detector at the LHC,” *Phys. Lett. B* **716** (2012) 1–29, [arXiv:1207.7214 \[hep-ex\]](#).
- [5] CMS Collaboration, S. Chatrchyan *et al.*, “Observation of a New Boson at a Mass of 125 GeV with the CMS Experiment at the LHC,” *Phys. Lett. B* **716** (2012) 30–61, [arXiv:1207.7235 \[hep-ex\]](#).
- [6] CMS Collaboration, A. Tumasyan *et al.*, “A portrait of the Higgs boson by the CMS experiment ten years after the discovery,” *Nature* **607** no. 7917, (2022) 60–68, [arXiv:2207.00043 \[hep-ex\]](#).
- [7] ATLAS Collaboration, G. Aad *et al.*, “A detailed map of Higgs boson interactions by the ATLAS experiment ten years after the discovery,” *Nature* **607** no. 7917, (2022) 52–59, [arXiv:2207.00092 \[hep-ex\]](#). [Erratum: *Nature* 612, E24 (2022)].
- [8] Y. Nir, “The three jewels in the crown of the LHC,” *CERN Cour.* **60** (2020) 41–45, [arXiv:2010.13126 \[hep-ph\]](#).
- [9] CMS Collaboration, A. M. Sirunyan *et al.*, “Evidence for Higgs boson decay to a pair of muons,” *JHEP* **01** (2021) 148, [arXiv:2009.04363 \[hep-ex\]](#).
- [10] ATLAS Collaboration, G. Aad *et al.*, “A search for the dimuon decay of the Standard Model Higgs boson with the ATLAS detector,” *Phys. Lett. B* **812** (2021) 135980, [arXiv:2007.07830 \[hep-ex\]](#).
- [11] H. Davoudiasl and P. P. Giardino, “Electron $g-2$ foreshadowing discoveries at FCC-ee,” *Phys. Rev. D* **109** no. 7, (2024) 075037, [arXiv:2311.12112 \[hep-ph\]](#).
- [12] CMS Collaboration, A. Tumasyan *et al.*, “Search for Higgs Boson Decay to a Charm Quark-Antiquark Pair in Proton-Proton Collisions at $\sqrt{s}=13$ TeV,” *Phys. Rev. Lett.* **131** no. 6, (2023) 061801, [arXiv:2205.05550 \[hep-ex\]](#).

- [13] **ATLAS** Collaboration, G. Aad *et al.*, “Direct constraint on the Higgs-charm coupling from a search for Higgs boson decays into charm quarks with the ATLAS detector,” *Eur. Phys. J. C* **82** (2022) 717, [arXiv:2201.11428 \[hep-ex\]](#).
- [14] G. T. Bodwin, F. Petriello, S. Stoynev, and M. Velasco, “Higgs boson decays to quarkonia and the $H\bar{c}c$ coupling,” *Phys. Rev. D* **88** no. 5, (2013) 053003, [arXiv:1306.5770 \[hep-ph\]](#).
- [15] **ATLAS** Collaboration, M. Aaboud *et al.*, “Searches for exclusive Higgs and Z boson decays into $J/\psi\gamma$, $\psi(2S)\gamma$, and $\Upsilon(nS)\gamma$ at $\sqrt{s} = 13$ TeV with the ATLAS detector,” *Phys. Lett. B* **786** (2018) 134–155, [arXiv:1807.00802 \[hep-ex\]](#).
- [16] **CMS** Collaboration, A. Tumasyan *et al.*, “Search for Higgs boson decays into Z and J/ψ and for Higgs and Z boson decays into J/ψ or Y pairs in pp collisions at $s=13$ TeV,” *Phys. Lett. B* **842** (2023) 137534, [arXiv:2206.03525 \[hep-ex\]](#).
- [17] J. Duarte-Campderros, G. Perez, M. Schlaffer, and A. Soffer, “Probing the Higgs–strange-quark coupling at e^+e^- colliders using light-jet flavor tagging,” *Phys. Rev. D* **101** no. 11, (2020) 115005, [arXiv:1811.09636 \[hep-ph\]](#).
- [18] L. Alasfar, R. Corral Lopez, and R. Gröber, “Probing Higgs couplings to light quarks via Higgs pair production,” *JHEP* **11** (2019) 088, [arXiv:1909.05279 \[hep-ph\]](#).
- [19] Y. Soreq, H. X. Zhu, and J. Zupan, “Light quark Yukawa couplings from Higgs kinematics,” *JHEP* **12** (2016) 045, [arXiv:1606.09621 \[hep-ph\]](#).
- [20] G. Bonner and H. E. Logan, “Constraining the Higgs couplings to up and down quarks using production kinematics at the CERN Large Hadron Collider,” [arXiv:1608.04376 \[hep-ph\]](#).
- [21] J. A. Aguilar-Saavedra, J. M. Cano, and J. M. No, “More light on Higgs flavor at the LHC: Higgs boson couplings to light quarks through $h + \gamma$ production,” *Phys. Rev. D* **103** no. 9, (2021) 095023, [arXiv:2008.12538 \[hep-ph\]](#).
- [22] **CMS** Collaboration, A. Hayrapetyan *et al.*, “Observation of $WW\gamma$ production and search for $H\gamma$ production in proton-proton collisions at $\sqrt{s} = 13$ TeV,” *Phys. Rev. Lett.* **132** no. 12, (2024) 121901, [arXiv:2310.05164 \[hep-ex\]](#).
- [23] J. de Blas *et al.*, “Higgs Boson Studies at Future Particle Colliders,” *JHEP* **01** (2020) 139, [arXiv:1905.03764 \[hep-ph\]](#).
- [24] Y. Zhou, “Constraining the Higgs boson coupling to light quarks in the $H \rightarrow ZZ$ final states,” *Phys. Rev. D* **93** no. 1, (2016) 013019, [arXiv:1505.06369 \[hep-ph\]](#).
- [25] E. Balzani, R. Gröber, and M. Vitti, “Light-quark Yukawa couplings from off-shell Higgs production,” *JHEP* **10** (2023) 027, [arXiv:2304.09772 \[hep-ph\]](#).
- [26] **ATLAS** Collaboration, G. Aad *et al.*, “Search for pair-produced vector-like quarks coupling to light quarks in the lepton plus jets final state using 13 TeV pp collisions with the ATLAS detector,” [arXiv:2405.19862 \[hep-ex\]](#).
- [27] S. L. Glashow, “Partial-symmetries of weak interactions,” *Nuclear Physics* **22** no. 4, (1961) 579–588. <https://www.sciencedirect.com/science/article/pii/0029558261904692>.
- [28] S. Weinberg, “A model of leptons,” *Phys. Rev. Lett.* **19** (Nov, 1967) 1264–1266. <https://link.aps.org/doi/10.1103/PhysRevLett.19.1264>.

- [29] M. D. Schwartz, *Quantum Field Theory and the Standard Model*. Cambridge University Press, 3, 2014.
- [30] D. Tong, “Lectures on particle physics,”
<http://www.damtp.cam.ac.uk/user/tong/particle.html>.
- [31] **Particle Data Group** Collaboration, R. L. Workman and Others, “Review of Particle Physics,” *PTEP* **2022** (2022) 083C01.
- [32] P. Higgs, “Broken symmetries, massless particles and gauge fields,” *Physics Letters* **12** no. 2, (1964) 132–133.
<https://www.sciencedirect.com/science/article/pii/0031916364911369>.
- [33] E. Fermi, “An attempt of a theory of beta radiation. 1.,” *Z. Phys.* **88** (1934) 161–177.
- [34] R. P. Feynman and M. Gell-Mann, “Theory of the fermi interaction,” *Phys. Rev.* **109** (Jan, 1958) 193–198.
<https://link.aps.org/doi/10.1103/PhysRev.109.193>.
- [35] C. Cheung, P. Creminelli, A. L. Fitzpatrick, J. Kaplan, and L. Senatore, “The Effective Field Theory of Inflation,” *JHEP* **03** (2008) 014, [arXiv:0709.0293](https://arxiv.org/abs/0709.0293) [hep-th].
- [36] D. Baumann, “Inflation,” in *Theoretical Advanced Study Institute in Elementary Particle Physics: Physics of the Large and the Small*, pp. 523–686. 2011. [arXiv:0907.5424](https://arxiv.org/abs/0907.5424) [hep-th].
- [37] S. Weinberg, “Effective chiral Lagrangians for nucleon - pion interactions and nuclear forces,” *Nucl. Phys. B* **363** (1991) 3–18.
- [38] D. B. Kaplan, “Five lectures on effective field theory,” 10, 2005. [arXiv:nucl-th/0510023](https://arxiv.org/abs/nucl-th/0510023).
- [39] E. E. Jenkins, A. V. Manohar, and P. Stoffer, “Low-Energy Effective Field Theory below the Electroweak Scale: Operators and Matching,” *JHEP* **03** (2018) 016, [arXiv:1709.04486](https://arxiv.org/abs/1709.04486) [hep-ph]. [Erratum: *JHEP* **12**, 043 (2023)].
- [40] E. E. Jenkins, A. V. Manohar, and M. Trott, “Renormalization Group Evolution of the Standard Model Dimension Six Operators I: Formalism and lambda Dependence,” *JHEP* **10** (2013) 087, [arXiv:1308.2627](https://arxiv.org/abs/1308.2627) [hep-ph].
- [41] E. E. Jenkins, A. V. Manohar, and M. Trott, “Renormalization Group Evolution of the Standard Model Dimension Six Operators II: Yukawa Dependence,” *JHEP* **01** (2014) 035, [arXiv:1310.4838](https://arxiv.org/abs/1310.4838) [hep-ph].
- [42] R. Alonso, E. E. Jenkins, A. V. Manohar, and M. Trott, “Renormalization Group Evolution of the Standard Model Dimension Six Operators III: Gauge Coupling Dependence and Phenomenology,” *JHEP* **04** (2014) 159, [arXiv:1312.2014](https://arxiv.org/abs/1312.2014) [hep-ph].
- [43] B. Henning, X. Lu, and H. Murayama, “How to use the Standard Model effective field theory,” *JHEP* **01** (2016) 023, [arXiv:1412.1837](https://arxiv.org/abs/1412.1837) [hep-ph].
- [44] C. P. Burgess, *Introduction to Effective Field Theory: Thinking Effectively about Hierarchies of Scale*. Cambridge University Press, 1, 2021.
- [45] S. Weinberg, “Baryon and Lepton Nonconserving Processes,” *Phys. Rev. Lett.* **43** (1979) 1566–1570.
- [46] V. Gherardi, D. Marzocca, and E. Venturini, “Matching scalar leptoquarks to the SMEFT at one loop,” *JHEP* **07** (2020) 225, [arXiv:2003.12525](https://arxiv.org/abs/2003.12525) [hep-ph]. [Erratum: *JHEP* **01**, 006 (2021)].
- [47] B. Grzadkowski, M. Iskrzynski, M. Misiak, and J. Rosiek, “Dimension-Six Terms in the Standard Model Lagrangian,” *JHEP* **10** (2010) 085, [arXiv:1008.4884](https://arxiv.org/abs/1008.4884) [hep-ph].

- [48] J. M. Cano, *Illuminating the Dark Side of the Higgs: Yukawa Couplings, Exotic Decays and Baryogenesis*. PhD thesis, Universidad Autónoma de Madrid, 2023.
- [49] **LHC Higgs Cross Section Working Group** Collaboration, A. David, A. Denner, M. Duehrssen, M. Grazzini, C. Grojean, G. Passarino, M. Schumacher, M. Spira, G. Weiglein, and M. Zanetti, “LHC HXSWG interim recommendations to explore the coupling structure of a Higgs-like particle,” [arXiv:1209.0040](#) [hep-ph].
- [50] **CMS** Collaboration, A. M. Sirunyan *et al.*, “A search for the standard model Higgs boson decaying to charm quarks,” *JHEP* **03** (2020) 131, [arXiv:1912.01662](#) [hep-ex].
- [51] J. de Blas, J. C. Criado, M. Perez-Victoria, and J. Santiago, “Effective description of general extensions of the Standard Model: the complete tree-level dictionary,” *JHEP* **03** (2018) 109, [arXiv:1711.10391](#) [hep-ph].
- [52] O. Eberhardt, G. Herbert, H. Lacker, A. Lenz, A. Menzel, U. Nierste, and M. Wiebusch, “Impact of a Higgs boson at a mass of 126 GeV on the standard model with three and four fermion generations,” *Phys. Rev. Lett.* **109** (2012) 241802, [arXiv:1209.1101](#) [hep-ph].
- [53] G. C. Branco and M. N. Rebelo, “Vector-like Quarks,” *PoS DISCRETE2020-2021* (2022) 004, [arXiv:2208.07235](#) [hep-ph].
- [54] J. a. M. Alves, G. C. Branco, A. L. Cherchiglia, C. C. Nishi, J. T. Penedo, P. M. F. Pereira, M. N. Rebelo, and J. I. Silva-Marcos, “Vector-like singlet quarks: A roadmap,” *Phys. Rept.* **1057** (2024) 1–69, [arXiv:2304.10561](#) [hep-ph].
- [55] D. B. Kaplan, H. Georgi, and S. Dimopoulos, “Composite Higgs Scalars,” *Phys. Lett. B* **136** (1984) 187–190.
- [56] K. Agashe, R. Contino, and A. Pomarol, “The Minimal composite Higgs model,” *Nucl. Phys. B* **719** (2005) 165–187, [arXiv:hep-ph/0412089](#).
- [57] P. Lodone, “Vector-like quarks in a ‘composite’ Higgs model,” *JHEP* **12** (2008) 029, [arXiv:0806.1472](#) [hep-ph].
- [58] N. Arkani-Hamed, A. G. Cohen, E. Katz, and A. E. Nelson, “The Littlest Higgs,” *JHEP* **07** (2002) 034, [arXiv:hep-ph/0206021](#).
- [59] S. Chakdar, K. Ghosh, S. Nandi, and S. K. Rai, “Collider signatures of mirror fermions in the framework of a left-right mirror model,” *Phys. Rev. D* **88** no. 9, (2013) 095005, [arXiv:1305.2641](#) [hep-ph].
- [60] C. T. Hill, “Topcolor assisted technicolor,” *Phys. Lett. B* **345** (1995) 483–489, [arXiv:hep-ph/9411426](#).
- [61] B. A. Dobrescu and C. T. Hill, “Electroweak symmetry breaking via top condensation seesaw,” *Phys. Rev. Lett.* **81** (1998) 2634–2637, [arXiv:hep-ph/9712319](#).
- [62] A. E. Nelson, “Naturally Weak CP Violation,” *Phys. Lett. B* **136** (1984) 387–391.
- [63] L. Bento, G. C. Branco, and P. A. Parada, “A Minimal model with natural suppression of strong CP violation,” *Phys. Lett. B* **267** (1991) 95–99.
- [64] S. Ziviani, “Enhanced light quark yukawa couplings,” Master’s thesis, Università degli Studi di Padova, Dipartimento di Fisica e Astronomia ‘Galileo Galilei’, 2022. <https://hdl.handle.net/20.500.12608/56234>.

- [65] W. R. Inc., “Mathematica, Version 14.0,” <https://www.wolfram.com/mathematica>. Champaign, IL, 2024.
- [66] J. Fuentes-Martín, M. König, J. Pagès, A. E. Thomsen, and F. Wilsch, “A proof of concept for matchete: an automated tool for matching effective theories,” *Eur. Phys. J. C* **83** no. 7, (2023) 662, [arXiv:2212.04510](https://arxiv.org/abs/2212.04510) [hep-ph].
- [67] G. Guedes, P. Olgoso, and J. Santiago, “Towards the one loop IR/UV dictionary in the SMEFT: One loop generated operators from new scalars and fermions,” *SciPost Phys.* **15** no. 4, (2023) 143, [arXiv:2303.16965](https://arxiv.org/abs/2303.16965) [hep-ph].
- [68] M. E. Peskin and T. Takeuchi, “Estimation of oblique electroweak corrections,” *Phys. Rev. D* **46** (1992) 381–409.
- [69] J. Erler, “Global fits of the SM parameters,” *PoS LHCP2019* (2019) 105, [arXiv:1908.07327](https://arxiv.org/abs/1908.07327) [hep-ph].
- [70] L. Allwicher, G. Isidori, J. M. Lizana, N. Selimovic, and B. A. Stefanek, “Third-family quark-lepton Unification and electroweak precision tests,” *JHEP* **05** (2023) 179, [arXiv:2302.11584](https://arxiv.org/abs/2302.11584) [hep-ph].
- [71] I. Brivio, T. Corbett, and M. Trott, “The Higgs width in the SMEFT,” *JHEP* **10** (2019) 056, [arXiv:1906.06949](https://arxiv.org/abs/1906.06949) [hep-ph].
- [72] M. Loretì, *Teoria degli Errori e Fondamenti di Statistica*. Private edition out of print, 2006.
- [73] V. Bresó-Pla, A. Falkowski, and M. González-Alonso, “ A_{FB} in the SMEFT: precision Z physics at the LHC,” *JHEP* **08** (2021) 021, [arXiv:2103.12074](https://arxiv.org/abs/2103.12074) [hep-ph].
- [74] I. Brivio, S. Dawson, J. de Blas, G. Durieux, P. Savard, A. Denner, A. Freitas, C. Hays, B. Pecjak, and A. Vicini, “Electroweak input parameters,” [arXiv:2111.12515](https://arxiv.org/abs/2111.12515) [hep-ph].
- [75] M. Spira, “Higgs Boson Production and Decay at Hadron Colliders,” *Prog. Part. Nucl. Phys.* **95** (2017) 98–159, [arXiv:1612.07651](https://arxiv.org/abs/1612.07651) [hep-ph].
- [76] J. A. Aguilar-Saavedra, R. Benbrik, S. Heinemeyer, and M. Pérez-Victoria, “Handbook of vectorlike quarks: Mixing and single production,” *Phys. Rev. D* **88** no. 9, (2013) 094010, [arXiv:1306.0572](https://arxiv.org/abs/1306.0572) [hep-ph].
- [77] A. Atre, G. Azuelos, M. Carena, T. Han, E. Ozcan, J. Santiago, and G. Unel, “Model-Independent Searches for New Quarks at the LHC,” *JHEP* **08** (2011) 080, [arXiv:1102.1987](https://arxiv.org/abs/1102.1987) [hep-ph].
- [78] M. Buchkremer, G. Cacciapaglia, A. Deandrea, and L. Panizzi, “Model Independent Framework for Searches of Top Partners,” *Nucl. Phys. B* **876** (2013) 376–417, [arXiv:1305.4172](https://arxiv.org/abs/1305.4172) [hep-ph].
- [79] CMS Collaboration, A. M. Sirunyan *et al.*, “Search for vector-like quarks in events with two oppositely charged leptons and jets in proton-proton collisions at $\sqrt{s} = 13$ TeV,” *Eur. Phys. J. C* **79** no. 4, (2019) 364, [arXiv:1812.09768](https://arxiv.org/abs/1812.09768) [hep-ex].
- [80] CMS Collaboration, A. Tumasyan *et al.*, “Search for pair production of vector-like quarks in leptonic final states in proton-proton collisions at $\sqrt{s} = 13$ TeV,” *JHEP* **07** (2023) 020, [arXiv:2209.07327](https://arxiv.org/abs/2209.07327) [hep-ex].
- [81] ATLAS Collaboration, G. Aad *et al.*, “Search for pair-production of vector-like quarks in pp collision events at $s=13$ TeV with at least one leptonically decaying Z boson and a third-generation quark with the ATLAS detector,” *Phys. Lett. B* **843** (2023) 138019, [arXiv:2210.15413](https://arxiv.org/abs/2210.15413) [hep-ex].

- [82] **ATLAS** Collaboration, G. Aad *et al.*, “Search for pair-produced vector-like top and bottom partners in events with large missing transverse momentum in pp collisions with the ATLAS detector,” *Eur. Phys. J. C* **83** no. 8, (2023) 719, [arXiv:2212.05263 \[hep-ex\]](#).
- [83] **ATLAS** Collaboration, G. Aad *et al.*, “Search for pair-production of vector-like quarks in lepton+jets final states containing at least one b-tagged jet using the Run 2 data from the ATLAS experiment,” *Phys. Lett. B* **854** (2024) 138743, [arXiv:2401.17165 \[hep-ex\]](#).
- [84] M. E. Peskin and D. V. Schroeder, *An Introduction to quantum field theory*. Addison-Wesley, Reading, USA, 1995.
- [85] H. Georgi, *Lie algebras in particle physics*, vol. 54. Perseus Books, Reading, MA, 2nd ed. ed., 1999.
- [86] A. Jain, “Notes on symmetries in particle physics,” [arXiv:2109.12087 \[hep-th\]](#).
- [87] A. Dedes, W. Materkowska, M. Paraskevas, J. Rosiek, and K. Suxho, “Feynman rules for the Standard Model Effective Field Theory in R_ξ -gauges,” *JHEP* **06** (2017) 143, [arXiv:1704.03888 \[hep-ph\]](#).
- [88] S. L. Glashow, J. Iliopoulos, and L. Maiani, “Weak Interactions with Lepton-Hadron Symmetry,” *Phys. Rev. D* **2** (1970) 1285–1292.
- [89] K. Ishiwata, Z. Ligeti, and M. B. Wise, “New Vector-Like Fermions and Flavor Physics,” *JHEP* **10** (2015) 027, [arXiv:1506.03484 \[hep-ph\]](#).
- [90] L. Silvestrini and M. Valli, “Model-independent Bounds on the Standard Model Effective Theory from Flavour Physics,” *Phys. Lett. B* **799** (2019) 135062, [arXiv:1812.10913 \[hep-ph\]](#).
- [91] A. Bettini, *Introduction to elementary particle physics*. 2008.